# Model Predictive Control of Induction Motor Drives

BY

**Mohamed Mamdouh Mohamed El Shormbably**

A Dissertation Presented to the

DEANSHIP OF GRADUATE STUDIES

**KING FAHD UNIVERSITY OF PETROLEUM & MINERALS**

DHAHRAN, SAUDI ARABIA

In Partial Fulfillment of the

Requirements for the Degree of

# DOCTOR OF PHILOSOPHY

**In**

**ELECTRICAL ENGINEERING DEPARTMENT**

**April 2018**

KING FAHD UNIVERSITY OF PETROLEUM & MINERALS

DHAHRAN- 31261, SAUDI ARABIA

**DEANSHIP OF GRADUATE STUDIES**

This thesis, written by Mohamed Mamdouh Mohamed El Shormbably under the direction of his thesis advisor and approved by his thesis committee, has been presented and accepted by the Dean of Graduate Studies, in partial fulfillment of the requirements for the degree of **DOCTOR OF PHILOSOPHY IN ELECTRICAL ENGINEERING.**

Dr. Mohammed Ali Abido
(Advisor)

Dr. Ali Al Shaikhi
Department Chairman

Dr. Zakariya Al Hamouz
(Co-Advisor)

Dr. Salam A. Zummo
Dean of Graduate Studies

Dr. Ibrahim El Amin
(Member)

23/7/2018
Date

Dr. Salim Ibrir
(Member)

Dr. Ralph Kennel
(Member)

This thesis is dedicated to my beloved parents and wife

# ACKNOWLEDGMENTS

First, I would like to thank God for his blessing and for providing me with the power and patience to complete this thesis. I want to acknowledge my parents whom no words will express my gratitude for their care, support and praying for me. I would like to thank my beloved wife for her encouragement, support and belief in me.

I would like to express my deep appreciation to my supervisor Prof. Mohamed Ali Abido for his continuous guidance and patience especially with many problems we faced to accomplish this work. He was always there for me welcoming discussions and suggestions. His advices and guidance not only the main reason for the success of this work but no doubt, they will affect my all career.

I would like to acknowledge King Fahd University of Petroleum and Minerals for the granted PhD scholarship. My gratitude to all the professors at KFUPM with whom I attended graduate courses. In addition, I would like to thank Prof. Raleph Kennel for giving me the opportunity to visit the institute of electric drive at Technical University of Munch during the summer of 2016. It was a fruitful experience and inspired me to upgrade my experimental setup and improve the outcomes of this work.

I would like to thank all my friends and colleagues at KFUPM for their company and support.

Finally, Special thanks to my instructors and professors during my undergraduate study. I was lucky to study under those great teachers from Tanta and Menoufia Universities. I would not be able to reach this point without there sincere efforts.

# TABLE OF CONTENT

# LIST OF TABLES

# LIST OF FIGURES

# LIST OF ABBREVIATIONS

| | | |
|---|---|---|
| **AOF** | **:** | **Aggregated Of Function** |
| **CONV** | **:** | **Conventional** |
| **DTC** | **:** | **Direct Torque Control** |
| **FCS-MPC** | **:** | **Finite Control Set Model Predictive Control** |
| **FOC** | **:** | **Field Oriented Control** |
| **FPTC** | **:** | **Fuzzy Predictive Torque Control** |
| **IM** | **:** | **Induction Motor** |
| **MPC** | **:** | **Model Predictive Control** |
| **MFPTC** | **:** | **Modified Fuzzy Predictive Torque Control** |
| **MMF** | **:** | **Magnetic Motive Force** |
| **PCC** | **:** | **Predictive Current Control** |
| **PI** | **:** | **Proportional Integral** |
| **PTC** | **:** | **Predictive Torque Control** |
| **PWM** | **:** | **Pulse Width Modulation** |
| **RSF** | **:** | **Reduced Switching Frequency** |

| | | |
|---|---|---|
| **THD** | **:** | **Total Harmonic Distortion** |
| **VSD** | **:** | **Voltage Space Decomposition** |
| **VV** | **:** | **Voltage Vector** |
| **WFE** | **:** | **Weighting Factor Elimination** |
| **WFS** | **:** | **Weighting Factor Selection** |
| **ZOH** | **:** | **Zero Order Hold** |

# ABSTRACT

Full Name : Mohamed Mamdouh Mohamed Saad El Shormbably

Thesis Title : Model Predictive Control of Induction Motor Drives

Major Field : ELECTRICAL ENGINEERING DEPARTMENT

Date of Degree : April, 2018

Electrical drive systems are widely used in many industries and automation systems. Recently model predictive control (MPC) gains a lot of interest in electric drives due to its simplicity and ability to deal with nonlinearity and constraints. In particular, finite control set MPC (FCS-MPC) is compatible with the discrete nature of different power converters. Regardless of its simplicity and high dynamic response, there are some challenges that need to be addressed for efficient implementation of MPC in electrical drive applications. These include difficulty in weighting factor selection (WFS), high computation burden, and extension to multi-phase drive systems.

In this thesis, five recent flux WFS methods are assessed based on different figure of merits. Multi-objective based methods found to be superior to the conventional offline method. An improvement of multi-objective fuzzy decision method is proposed which results in reduction in torque ripple. Aiming to reduce the computation burden of predictive torque control (PTC) algorithm, an efficient and simple technique is proposed which utilize only four voltage vectors instead of seven. The proposed method is validated using simulation and experimental results showing a reduction in the computation cost and the average switching frequency compared to the conventional method. For the sake of realization of MPC in multi-phase machines, the stator of a three-phase induction motor is rewound as asymmetric six-phase motor. Several tests are performed to accurately identify the new

motor parameters. Predictive current control (PCC) algorithm is designed and implemented in real time. The experimental results prove that PCC successfully tracks the flux and torque current component with complete decoupling. At the same time, it minimize the undesired circulating stator currents. All the proposed methods, for three and six phases motors, are verified experimentally using a flexible and efficient setup, developed for driving up to six-phase motors.

# ملخص الرسالة

**الاسم الكامل: محمد ممدوح محمد سعد الشرمبلى**

**عنوان الرسالة:**

**التخصص: الهندسة الكهربائية**

**تاريخ الدرجة العلمية: أبريل ٢٠١٨**

تنتشر أنظمة التسيير الكهربي ذات السرعات المتغيرة في كثير من التطبيقات الصناعية. وقد شهدت الفترة الأخيرة تطورا ونجاحا واسعا لطرق التحكم التنبؤى المعتمد على النماذج الرياضية للأنظمة مما سمح لها بالتنافس مع طرق التحكم التقليدية نظرا لبساطتها وقدرتها على التعامل مع الأنظمة غير الخطية والقيود. وعلى وجه الخصوص فإن التحكم التنبؤى ذات المجموعة المحددة يلائم طبيعة التشغيل المتقطعة لمحولات القوى المختلفة. ولكن على الرغم من بساطة وسرعة الاستجابة الديناميكية لهذا النوع من التحكم إلا أن هناك عدد من التحديات التي يجب مواجهتها كى تستخدم بشكل فعال في تطبيقات التسيير الكهربي. منها صعوبة اختيار معاملات الأهمية وزيادة الحسابات والوقت الازم للتنفيذ وكذلك تطبيقها على أنظمة التحريك متعددة الأوجه.

تتضمن هذه الأطروحة تقييم لخمس طرق مختلفة لتعيين معامل الأهمية وفقا لعدة معايير. حيث وجد أن الطرق المعتمدة على الأهداف المتعددة أكثر تفوقا من طريقة التعيين التقليدية المعتمدة على الحسابات المسبقة. وبالإضافة لذلك فقد تم اقتراح لتحسين أحد طرق تعيين معامل الأهمية المعتمد على الأهداف المتعددة باستخدام (fuzzy decision) والتي أدت إلى تقليل تذبذب العزم. وبهدف تقليل العبء الحسابي فقد تم اقتراح طريقة بسيطة وفعالة تعتمد على استخدام أربعة متجهات جهود فقط عوضا عن السبع المعتاد استخدامهم في الطريقة التقليدية. وقد تم التحقق من صحة الطريقة المقترحة باستخدام المحاكاة وبالتطبيق العملي مما أوضح أن العمليات الحسابية المطلوبة تم تقليصها وكذلك تقليل متوسط تردد تشغيل الموصلات الإلكترونية مقارنة بالطريقة التقليدية. ولتطبيق التحكم التنبؤى المعتمد على النماذج الرياضية على الآلات الكهربية متعددة الأوجه فقد تم إعادة لف للعضو الثابت لمحرك ثلاثي الوجه ليصبح محرك سداسي الوجه غير متماثل. وقد تم إجراء اختبارات عدة لتحديد خصائص وبناء نموذج رياضي للمحرك الجديد. اتبع ذلك تصميم وتنفيذ برنامج للتحكم التنبؤى في التيار للمحرك سداسي الوجه. حيث أظهرت التجارب العملية نجاح البرنامج في تتبع

مركبات التيار المؤثرة في العزم والفيض بشكل منفصل. كما أوضحت تقليل مركبة التيار الدوارة والغير مرغوب بها في المحرك. وقد تم اختبار كل الطرق المقترحة عمليا باستخدام نموذج معملي للتحكم ذو كفاءة ومرونة عالية تم تطويره ليتمكن من تسيير المحركات كهربية المتعددة الأوجه.

# CHAPTER 1

# INTRODUCTION

## 1.1 Background

Electrical drives systems are characterized by their ease of control compared to mechanical systems. They are available in a wide range of torque, speed and power. They are adaptable to almost any operating conditions such as explosive and radioactive environment, submerged in liquids, vertical mounting and so on. Compared to mechanical drive systems, they can be started instantly and can immediately be fully loaded. As a result, they invaded almost all automation industries. They are used in a large number of industrial and domestic applications like transportation systems, rolling mills, paper machines, textile mills, machine tools, fans, pumps, robots, elevator systems, and washing machines.

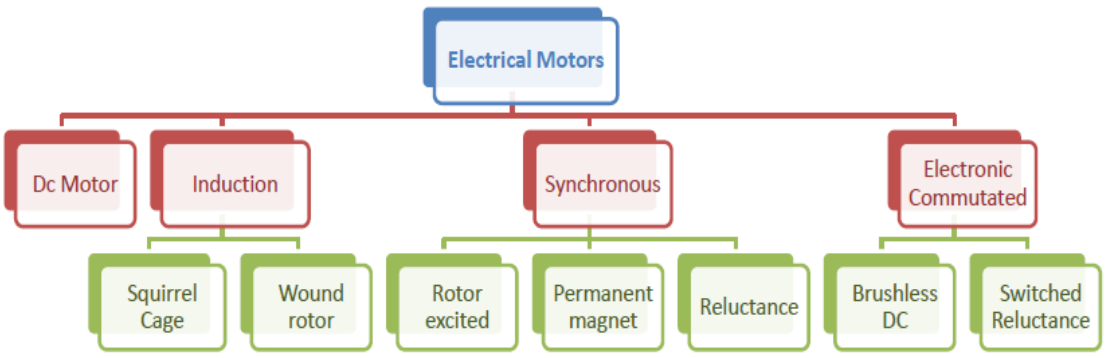


**Figure 1-1 Classification of electrical motors**

Figure 1-1illustrates different electrical motors utilized for electric drive system. DC motor was the first to be used in variable speed drive due to the simplicity of its control. Later, other motor types are emerged in electric drive system applications especially after the advances in power electronic converters. Among these motors, induction motors (IM) are the most commonly used for today electric drive systems. This is due to their robustness, cheap price, low maintenance, and ability to work safely in hazardous environment.

Variable speed control of induction motor evolved from scalar control method like V/f control to more sophisticated and efficient vector control methods as illustrated in Figure 1-2. Methods like field-oriented control (FOC) and direct torque control (DTC) are now very mature and widely used in many commercial inverters. FOC method is based on generating the torque and flux references using classical proportional integral (PI) controller. The field orientation theory is utilized to generate the required reference voltage to be applied. On the other hand, DTC works directly on the torque and flux. Based on the sign torque and flux errors and a lookup tables, the suitable voltage vector is selected and applied [1].

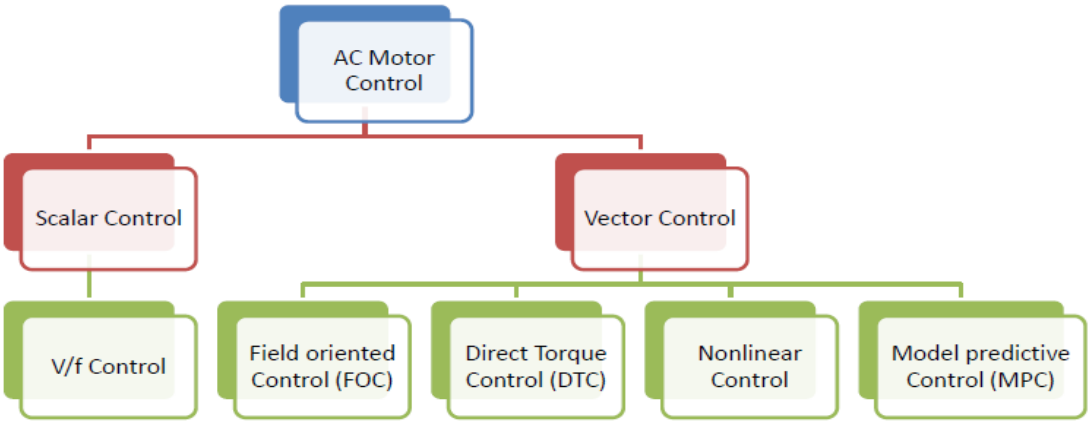


**Figure 1-2 Classification of different control algorithm used for AC Motor drives**

Since the power converter used are of discrete nature, suitable pulse width modulation (PWM) is used to generate the gating signal needed to drive these converters. The structure of this type of controller is based on cascade implementation of different control loops. For example, current inner control loop and outer speed loop are typically used for FOC. Using this cascade structure, sets limits on the bandwidth for each loop resulting in slow dynamic response for the outer loop especially for high power drive for which the switching frequency is limited to few hundred Hertz in order to reduce the power loss.

On the other hand, Model predictive control (MPC) techniques are characterized by their simple and intuitive concept. They are suitable for multivariable systems. Moreover constraints and nonlinearity could be easily handled. Unfortunately, it needs heavy calculations. Therefore, they have been used in application characterized by long time constant like chemical and some process control based industries [2], [3]. Recently, maturity of mathematical models of electrical machines and power converters along with the recent powerful microprocessors pave the way for implementations of various MPC methods in power electronics. For the last few years, MPC concept have been heavily utilized for power converters of different topologies [4] and [5].

## 1.2 Main concept and classifications of MPC based electric drives

Actually, the concept of MPC is very intuitive and can be inferred from many activities in our daily practice. Figure 1-3 illustrates an example of car driving. Based on the driver observations, dials readings and his knowledge of the car capability he should slow down a distance ahead before the road turns for safe and stable driving.

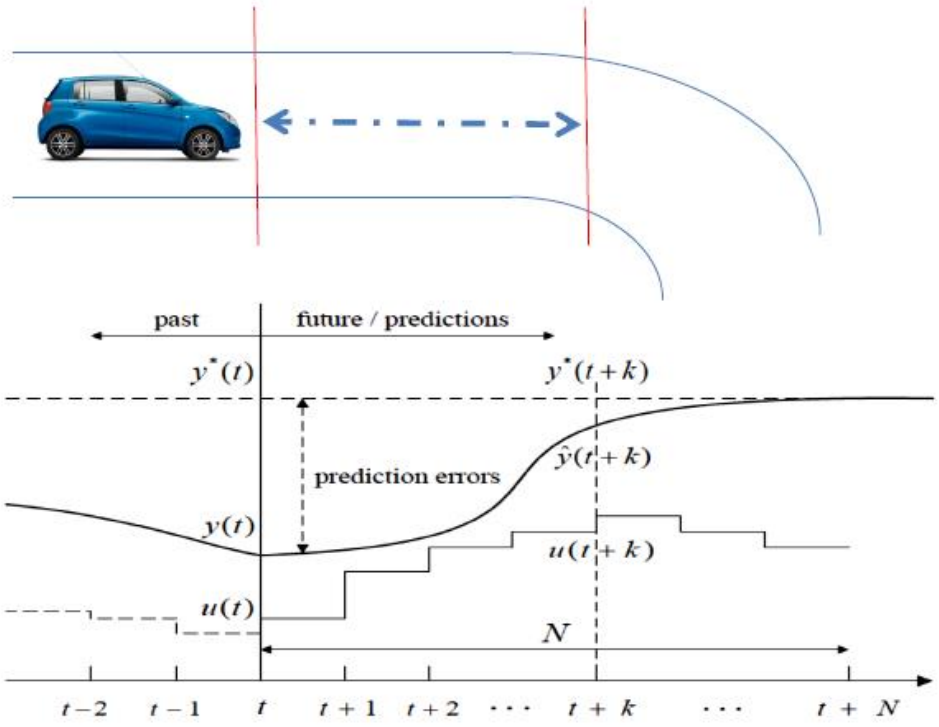


**Figure 1-3 Basics of Model predictive control**

Similarly, the main concept of MPC is to use the model of the system to predict few steps ahead in the future (Prediction horizon) based on the current states, which can be either measured or estimated. A predefined cost function is used to minimize the differences between the reference and predicted variables of interest. The output of this optimization step is an optimal control law of certain dimension (Control horizon). Only the first entry of this dimension will be applied at the next sample then the procedure is repeated (Receding Horizon) [3].

Several methods of MPC were reported in literature for power converter applications in general and for motor drives in particular [6], [7]. These methods can be categorized based on the optimization methodology, the predicted horizon, and the optimized variables. Based on the solution methodology of the optimization problem, the reported

approaches can be classified as continuous or classical MPC [8]–[10] and finite control set model predictive control (FCS-MPC) [11]. For the former, the solution of the optimization problem is the converter output voltage, which is modified to gating signals using suitable modulator. While the latter benefits from the discrete nature of power converters. Knowing the possible states of the converter switches, limited number of available output voltages are expected at each sample period and a cost function is tested against each possible output. Then, the output voltage associated with the optimum value of the cost function is selected.

For FCS-MPC two subcategories could be recognized depending on the length of the prediction horizon $Np$; long prediction horizon $Np > 2$ as presented in [12]–[14] and short prediction horizon for $Np = 1$ [15]–[17]. The latter is the most common since it offers less computation burden.

Another classification is based on the cost function used for the optimization process. Two main trends have been used widely in motor drive applications; Predictive Current Control (PCC) [11], [18]–[21] and Predictive Torque Control (PTC) [15], [16], [22], [23]. PCC is based on minimizing the error between the reference and predicted stator currents while the PTC aims at minimizing torque and flux errors. In addition, other terms could be added to the cost function to achieve certain goals like reducing the switching frequency, forcing certain frequency spectrum, and limiting the maximum value of machine variables for the sake of protection [21]. A comparison of the performance of induction motor drive under PCC and PTC can be found in [24].

Among the various categories of MPC, FS- MPC with short prediction horizon ($Np$ =1) is found to be more suitable for the discrete nature of power converters. Discrete model

is used to predict the values of the system for all the possible combination of actuation states. These possible outcomes are compared to the reference to choose the best one optimizing certain objective functions [25].

Recently published results in the field of MPC based IM drive, illustrate that it have a high potential in the variable speed drive area and is suitable for sophisticated power converters such as those used for multi-level converters and multi-phase machines. Comparing to classical (PWM) methods, MPC techniques can accomplish the same goals but with reduced complexity.

## 1.3 Thesis motivations

The field of power electronics and drives witnesses a rise in the number of publication related to MPC applications. Figure 1-4 illustrates the growth in publication for the last five years obtained from search about the word 'predictive control' in IEEE database only. As it can be noted the number of published papers almost tripled in 2017 compared to 2013.

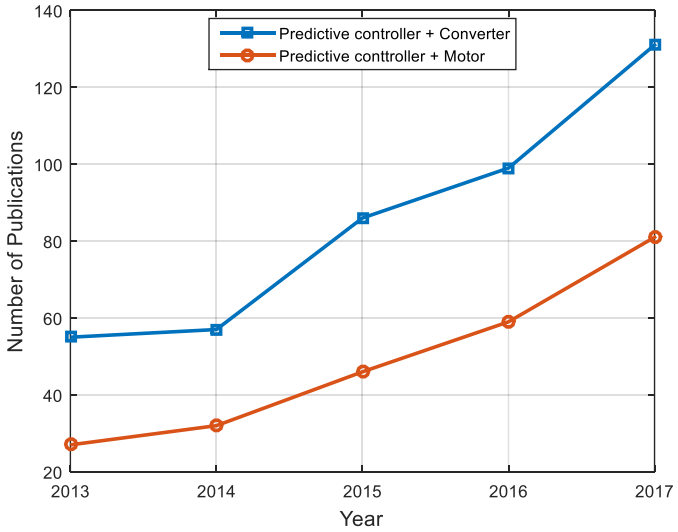


**Figure 1-4 Growth of publications number for MPC applications as obtained from IEEE database search**

On the other hand, the implementation of MPC based controller in the field of electric drives rise many challenges especially with the diversity of MPC techniques proposed [6], [7]. In this thesis the following problems will be investigated

### 1.3.1 Weighting factor calculation

As mentioned earlier, MPC techniques involve an optimization step where a predefined cost function is minimized. This cost function may consist of homogeneous components like the case of PCC or it may include variables of different nature. PTC is an example of the latter case for which minimization of torque and flux errors is considered. Therefore, the cost function should fairly represent all the objectives and in some cases to be capable of controlling the relative importance of each [26]. Since these objectives could be of different nature (units and magnitudes), weighting factor should be assigned to each of them in order to guarantee fair optimization. Setting of weighting factors is not an easy task, especially if the objective functions are of equal importance. Moreover, it turns out that the values of these weighting factors depend on the operating point [22]. As a result, tedious offline tuning is required if the operating point changes. This motivates many researchers to propose new methods, which consider the weighting factor calculation as a part of MPC algorithm [22], [23], [27]–[30]. Still the problem of weighting factor selection is an open question.

### 1.3.2 Computation Cost

Even with the recent advances in microprocessors, implementation of MPC technique requires heavy computation cost compared to conventional methods like FOC and DTC. This high computation cost is related to the prediction and optimization steps of the algorithm, which grows rapidly if the number of admissible voltage vectors increase.

This is typically the case for multi-phases and multi-level converters [31] and [6]. Therefore, for these systems, even if a short prediction horizon is used, a long sampling period is unavoidable for the algorithm to select the optimal voltage vector among all the available ones. Increasing the sampling period is reflected negatively on the quality of the controlled variable (torque, flux, and current).

### 1.3.3 MPC for multi-phase drive system

Multi-phase machines gain a lot of interest lately especially after the recent advances of power electronic devices. They are characterized by higher reliability, lower current per phase and higher power density compared to three phase counterparts. These advantages make multi-phase machines perfect candidates to be used in ships and aircrafts [32].

Many researches investigate different characteristics of multi-phase drives using FOC and DTC methods. The concept used in these method are similar to the one utilized with the three phase counterparts but other consideration is to be considered for minimizing low harmonic current. This in return complicates the controller design. MPC have been proposed recently as an alternative for classical controller in multi-phase IM drives. It avoids the need for PWM technique and different objectives can be simply considered in the cost function. Even though issues like accurate modeling of the machines and the effect of different weighting factor required in the cost function, still under investigation.

## 1.4 Thesis objectives

This research aims at proposing and developing a new controller for induction motor drives based on MPC techniques to improve the performance and reliability of the system. The specific objectives are as follows.

- Developing an improved weighting factor selection method fairly compromising between torque and flux ripple minimization.
- Developing a new approach for PTC to enhance three-phase IM drive performance by reducing flux and torque ripples yet maintaining simplicity and reduced computation cost.
- Developing an accurate predictive current control method for multi- phase induction motors under healthy conditions.
- Building an experimental test bench for three and six phases IM drives validating the proposed controllers experimentally

## 1.5 Thesis contributions

The research work results in the following contributions:

- An improved multi-objective fuzzy decision making method has been proposed and validated experimentally resulting in reduced torque ripple of predictive torque control of three-phase induction motor
- A computationally efficient predictive torque control algorithm is proposed for three-phase induction motor without sacrificing the performance compared to the conventional predictive torque control algorithm.
- Asymmetric six-phase induction motor is designed and implemented
- Predictive current control of six-phase induction motor base on accurate model by considering the effect of stator leakage mutual inductance is implemented in real time.

- Flexible and efficient experimental setup is developed for testing and validation of the proposed techniques.

## 1.6 Thesis organization

This thesis is organized as follows:

Chapter two discusses in details the different components of PTC algorithm. This includes modelling for the three-phase motor, the inverter, the estimation procedure and different weighting factor selection techniques. Moreover, a detailed description of the developed experimental setup is provided.

Chapter three investigates the flux weighting factor design problem. Five recently reported weighting factor selection approaches are compared. The performance of the three-phase IM under PTC algorithm is assessed for all the methods considering torque ripple, flux ripple, current THD and average switching frequency as figure of merits. Based on this study, a modification for one of the weighting factor design method is proposed. The original method suffers from high torque ripple at some operating points. The reason for this is explained and a remedy is introduced and validated experimentally.

In chapter four, an efficient PTC algorithm is proposed. Simple and fast execution time is the main feature of the proposed method yet good performance regarding torque and flux ripple is guaranteed.

Chapter five introduce different modeling methods of six-phase induction motor and the voltage source inverter followed by an accurate parameter identification for the six-phase machine.

Chapter six explores the potential of MPC based controller for six-phase IM. Principle of PCC of six-phase IM is discussed in details. PCC of six-phase IM is implemented successfully and validated using simulation and experimental results.

Chapter seven gives the final conclusions and discusses ideas for future work.

# CHAPTER 2

# FUNDAMENTALS of MPC FOR INDUCTION MOTOR DRIVES

This chapter discusses the different components of MPC algorithm. Specifically, predictive torque control (PTC) will be discussed in details.

## 2.1 Main steps of MPC

Figure 2-1 demonstrates the main steps required for MPC of IM drive. These steps are repeated in each control sample. In the following subsection, the details of each steps will be explained. Modelling of the motor and the converter will be presented in continuous and discrete versions, as they are essential for estimation and prediction steps of PTC.

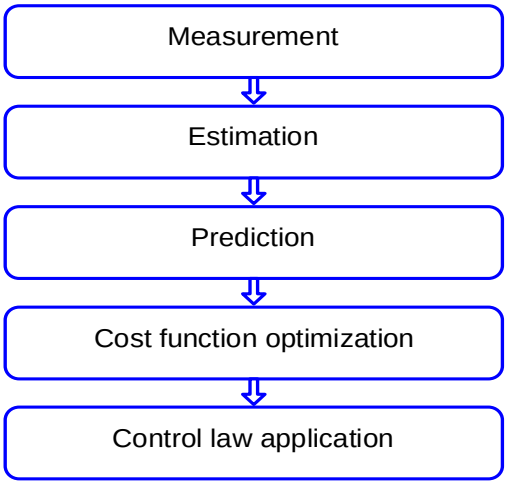


**Figure 2-1 Execution steps of MPC based algorithm**

A detailed discussion about different weighting factor selection (WFS) methods is provided which represents the main challenge for reaching fair optimization.

### 2.1.1 Three phase induction motor model

The dynamic model of IM can be expressed using different representations depending on the reference frame used [33]. If the stator reference frame is utilized and the direct and quadrature components of stator current $i_s$ and rotor flux $\psi_r$ are considered as the state variables, the dynamic equations can be expressed using complex vector notation as follows [34].

$$\left.\begin{aligned} v_s &= R_s\, i_s + p\, \psi_s \\ 0 &= R_r\, i_r + p\, \psi_r - j\, \omega_r\, \psi_r \end{aligned}\right\} \tag{2.1}$$

$$\left.\begin{aligned} \psi_s &= L_s\, i_s + L_m i_r \\ \psi_r &= L_r\, i_r + +L_m\, i_s \end{aligned}\right\} \tag{2.2}$$

Which can be represented in state space format as follows:

$$\dot{x}(\mathrm{t}) = A\big(\omega\,(t)\big)\, x(t) + B\, u(t) \tag{2.3}$$

where $x = [i_{ds}\, i_{qs}\, \psi_{dr}\ \psi_{qr}\,]^T$ are the state variables, $u = \left[v_{\alpha s}\, v_{\beta s}\right]^T$ represents the direct and quadrature components of the stator voltages, and matrices $A$ and $B$ are defined as follows:

$$A = \begin{bmatrix} \frac{-1}{\tau_\sigma} & 0 & \frac{k_r}{R_\sigma \tau_\sigma \tau_r} & \frac{k_r}{R_\sigma \tau_\sigma}\omega_r \\ 0 & \frac{-1}{\tau_\sigma} & -\frac{k_r}{R_\sigma \tau_\sigma}\omega_r & \frac{k_r}{R_\sigma \tau_\sigma \tau_r} \\ \frac{L_m}{\tau_r} & 0 & \frac{-1}{\tau_r} & -\omega_r \\ 0 & \frac{L_m}{\tau_r} & \omega_r & \frac{-1}{\tau_r} \end{bmatrix} \tag{2.4}$$

$$B = \begin{bmatrix} \frac{1}{R_\sigma \tau_\sigma} & 0 \\ 0 & \frac{1}{R_\sigma \tau_\sigma} \\ 0 & 0 \\ 0 & 0 \end{bmatrix} \tag{2.5}$$

Here,

$R_s$ and $R_r$ are stator and rotor resistances, respectively.

$L_s, L_r,$ and $L_m$ are stator, rotor and mutual inductances, respectively.

$\omega_r$ is electrical rotor speed.

$k_r = \frac{L_m}{L_r}$ is the rotor coupling factor.

$R_\sigma = R_s + k_r^2 R_r$ represents the equivalent resistance.

$L_\sigma = L_s(1 - \frac{L_m^2}{L_r})$ is the leakage inductance of the machine.

$\tau_\sigma = \frac{L_\sigma}{R_\sigma}$ is the stator transient time constant.

$\tau_r = \frac{L_r}{R_r}$ is the rotor time constant.

The electromagnetic torque can be calculated as:

$$T = \frac{3}{2}\, n_p\, (\overrightarrow{\psi_s} \times \overrightarrow{i_s}) \tag{2.6}$$

where $n_p$ is the number of pole pairs.

The prediction step in MPC requires the knowledge of the discrete model of IM. Several discretization methods are available in literature. Euler forward method is the simplest but the less accurate. On the other hand, Cayley-Hamilton is the most accurate but with high computation cost. For the sake of compromising between simplicity and accuracy,

Taylor second order method will be used [35].The discrete state space model can be expressed using

$$x^{k+1} = A_d\ (\omega^k)x^k + B_d(\omega^k)u^k \tag{2.7}$$

It should be noted that the matrices $A\big(\omega(t)\big)$, $A_d\ (\omega^k)$ and $B_d(\omega^k)$ are time varying as they depend on rotor speed. Therefore, they should be calculated at each control sample based on rotor speed measurement. For simplicity, hereafter the notation will be used as $A$, $A_d$ and $B_d$. The discretized matrices $A_d$ and $B_d$ can be calculated as follows.

$$A_d = I + T_s A + \frac{T_s^2}{2} A^2 \tag{2.8}$$

$$B_d = T_s B + \frac{T_s}{2} AB \tag{2.9}$$

where $I$ is the identity matrix and $T_s$ is the sampling time.

### 2.1.2 Inverter model

As illustrated in Figure 2-2, the 2L-VSI has two switches per phase. Therefore, there are eight possible combinations of switching states, $S_{abc}$, for three phases resulting in eight voltage vectors as given in Table 2-1.

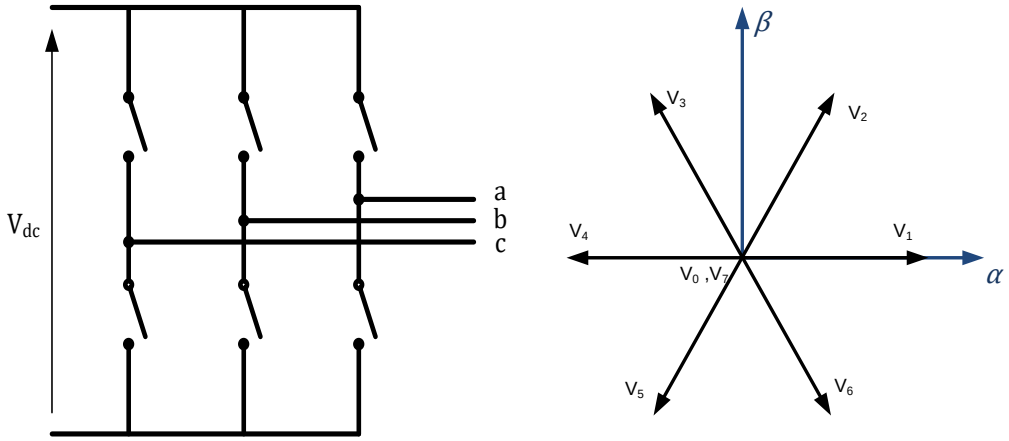


**(a)** **(b)**

**Figure 2-2 Two level voltage source inverters (a) Schematic diagram (b) output space voltage vectors**

**Table 2-1 Switching states for two-level VSI**

| | $V_0$ | $V_1$ | $V_2$ | $V_3$ | $V_4$ | $V_5$ | $V_6$ | $V_7$ |
|---|---|---|---|---|---|---|---|---|
| $S_a$ | 0 | 1 | 1 | 0 | 0 | 0 | 1 | 1 |
| $S_b$ | 0 | 0 | 1 | 1 | 1 | 0 | 0 | 1 |
| $S_c$ | 0 | 0 | 0 | 0 | 1 | 1 | 1 | 1 |

Therefore, the applied input voltage to the motor can be calculated as:

$$u_s = v_{s\alpha\beta} = V_{dc}\, T_{Cl}\, S_{abc} \tag{2.10}$$

where $V_{dc}$ is the DC link voltage. $T_{Cl}$ represents Clarke transformation.

$$T_{Cl} = \frac{2}{3}\begin{bmatrix} 0 & -\frac{\sqrt{3}}{2} & \frac{\sqrt{3}}{2} \\ 1 & -\frac{1}{2} & -\frac{1}{2} \end{bmatrix} \tag{2.11}$$

### 2.1.3 Stator flux estimation

The machine flux cannot easily be measured. Therefore, it is common to be estimated. The estimation can be accomplished using closed loop observer or in an open loop estimation manner. The former is more robust and accurate while the latter is simpler. Since the matrix $A$ of IM model is function of rotor speed as illustrated in equation 2.4, this results in a linear time varying system. As a result, the poles of the closed loop observer will be also time varying. Moreover, it will exhibit high oscillation at high speed (due to large imaginary part) [36]. In order to overcome this, it was proposed in [37] to use a closed loop observer with constant gain matrix. On the other hand, the open loop estimation depending on current equation [16], [22], [27], [34] or voltage equation [28], [29] is commonly reported in literature and results isn satisfactory performance. Therefore, open loop estimation will be adopted in this work. First, the rotor flux can be estimated from the rotor dynamics of IM governed by:

$$\psi_r + \tau_r \frac{d\psi_r}{dt} = L_m i_s \tag{2.12}$$

Here, stator current and rotor flux are expressed in rotor reference frame. Then using zero order hold (ZOH) discretization, the rotor flux can be rewritten as follows [34].

$$\psi_r^k = e^{\frac{-T_s}{\tau_r}} \psi_r^{k-1} + L_m \left(1 - e^{\frac{-T_s}{\tau_r}}\right) i_s \tag{2.13}$$

Knowing the rotor flux and current measurements, the discrete state equations can be used to predict stator flux one-step ahead. Then stator flux can be calculated at the $k+1$ sample from:

$$\psi_s^{k+1} = k_r \psi_r^{k+1} + L_\sigma i_s^{k+1} \tag{2.14}$$

It should be noted that the variables in (2.7) and (2.14) are expressed in stator reference frame. Therefore, the appropriate coordinate transformation should be considered as follows.

$$x^r = e^{-j\theta_r} x^s \tag{2.15}$$

where $x^s$ and $x^r$ are the variables in stator and rotor reference frame respectively. $\theta_r$ is the rotor angle.

In order to compensate for the time delay caused by calculation process [38], the variables at sample $k+2$ can be calculated using the variables at instant $k+1$ as follow:

$$x^{k+2} = A_d x^{k+1} + B_d u^{k+1} \tag{2.16}$$

$$\psi_s^{k+2} = k_r \psi_r^{k+2} + L_\sigma i_s^{k+2} \tag{2.17}$$

$$T^{k+2} = \frac{3}{2} n_p \left(\psi_s^{k+2} \times i_s^{k+2}\right) \tag{2.18}$$

### 2.1.4 Optimization

In this step, the predefined cost function $g$ is evaluated for all the possible voltage vectors given in Table 2-1 Switching states for two-level VSI. The minimum value is determined and its corresponding voltage vector should be applied for the next sample period as follows.

$$V_{sopt} = arg \min_{\{v_0,\ldots,v_7\}} g(V_s^{k+1}) \tag{2.19}$$

For PTC application, there are two commonly used objectives. These are torque ripple minimization and flux ripple minimization. The approaches for handling the objective functions and selecting the optimum voltage vector differentiate the algorithms used to solve this optimization problem.

## 2.2 Classification of Flux weighting factor selection methods

A cost function representing flux and torque error minimization should be designed to ensure fair optimization and to control the relative importance of each objective [26]. Since these objectives are of different nature (units and magnitudes), weighting factor should be assigned to each objective in order to guarantee fair optimization. Despite the simple and intuitive idea of MPC and its ability to easily handle nonlinearity and constrains, setting of weighting factors is not an easy task [15], [22], [26], [39], [40]. Moreover, it turns out that the values of these weighting factors depend on the operating point [22]. As a result, tedious offline tuning is required if the operating point changes. This motivates many researchers to propose several methods, which consider the weighting factor calculation as a part of MPC algorithm. Different methods reported in literature can be classified to offline and online calculation methods.

### 2.2.1 Offline methods

The simplest, yet time consuming, solution for weighting factor setting is aggregation of functions (AOF) where the individual cost functions are multiplied by weighting factors and added to form a single cost function. Then offline simulation, known also as parameters sweep, is used to design appropriate weights based on certain criteria or figure of merit. The work in [26] classifies different cost functions according to their importance and presents guidelines for offline calculation of the weights based on minimizing the root mean square error of the optimized parameters. Other figure of merits also proposed in literature like total harmonic distortion (THD) [34]. This method of calculating the weighting factors is the most common in literature and widely referred as the conventional method.

Another solution for weighting factor setting is to deal with the problem as a multi-objective optimization problem. Genetic algorithm was proposed in [41] for weighting factors design of multiple cost functions. Shunt active power filter was used as a case study with the goals of regulating DC bus voltage and controlling active and reactive powers. The concept of Pareto set was employed to design the weighting factors compromising different objectives.

The former two methods are offline design approaches. Consequently, if the operating point changes, the design process has to be repeated. To avoid such difficulty, several online approaches were reported.

### 2.2.2 Online methods

In these techniques, the weighting factors are either updated at each control sample or eliminated using mathematical manipulation. The dependence of the weighting factors

on the operating points was analytically demonstrated in [22]. FSC-MPC of induction motor (IM) was presented to minimize the torque ripple where mathematical relations between torque ripple, voltage vector, and the flux-weighting factor have been derived. Then, the weighting factor is calculated at each control sample to guarantee minimum torque deviation. Despite being complicated and highly parameter dependent, the results show clearly that the weighting factor updates its value online which has great influence on the quality of the generated torque. Nevertheless, this method has the drawback of dependence of weighting factor calculation on the operating point.

In [15], the multi-objective concept is used where the cost functions for torque and flux for all allowable voltage vectors have been evaluated. The resultant solutions of each cost function are sorted and ranked. Then, the voltage vector, which results in the highest average rank among the cost functions, is selected. The advantage of this method is that it avoids totally weighting factor calculation. Following the similar concept, fuzzy decision-making [FDM] was proposed to select the best voltage vector after evaluation of individual cost functions using membership function concept. This approach was successfully used for control of matrix converter in [40] and recently for predictive torque control of induction motor in [16], [34]. Recently, another technique is reported in literature based on Vlsekriterijuska Optimizacija I Komoromisno Resenje (VIKOR) method [29]. VIKOR is a multi-criteria decision-making method suitable for solving optimization problem with conflicting objective functions. Similar to [15], the individual cost functions of torque and flux deviations are evaluated. Then, the VIKOR method concept is utilized to assign an index to each allowable voltage vector. The voltage vector with the minimum index is selected as the optimal vector. For the

previously mentioned examples, only two cost functions were considered. However, multi-objective methods like FDM and VIKOR could be utilized for optimizing more than two cost functions.

A simple technique was presented in [17], [23] for model predictive flux control (MPFC) of induction motor. Based on mathematical model of the induction motor, the torque reference can be expressed in terms of the flux reference resulting in a new vector contains flux reference only. Since the two components of the resultant flux vector reference (direct and quadrature) are of the same nature, no weighting factor is required. Besides its simplicity, the method shows competing results at different operating conditions.

In the next few subsections, the details of five different weighting factor selection methods will be explained. Namely, the conventional, multi-objective ranking, fuzzy decision-making, VIKOR, weighting factor elimination methods are considered.

### 2.2.3 Conventional method (conv)

Weighting sum method is the most popular, which commonly referred in literature as the conventional method. In this method, the two cost functions are aggregated as follows.

$$g = \frac{|T^{ref} - T^{k+2}|}{T_{rated}} + K_{\psi} \frac{\left|\left\|\psi_s^{ref}\right\| - \left\|\psi_s^{k+2}\right\|\right|}{\|\psi_s\|_{rated}} \tag{2.20}$$

where $T^{ref}$ and $\psi_s^{ref}$ are the torque and stator flux references, respectively. $T_{rated}$ and $\|\psi_{rated}\|$ are the rated torque and rated stator flux magnitude, respectively. $K_{\psi}$ is the flux weighting factor. This factor determines the relative importance of flux error.

During the design process, $K_\psi$ should be carefully tuned in order to obtain good performance. One way to accomplish this is to choose a figure of merit like RMS torque and flux errors and choose a weighting factor compromising both [26]. Nevertheless, this task found to be tedious, since it has to be repeated if the operating point changes.

### 2.2.4 Multi-objective ranking method (ranking)

In this approach, each cost function is evaluated separately for all possible voltage vectors as follows [15].

$$g_1(V_s^{k+1}) = \left|T^{ref} - T^{k+2}\right| \tag{2.21}$$

$$g_2(V_s^{k+1}) = \left|\left\|\psi_s^{ref}\right\| - \left\|\psi_s^{k+2}\right\|\right| \tag{2.22}$$

The resultant values are sorted and ranked such that the highest rank corresponds to the least error and vice versa as follows.

$$g_1(V_s^{k+1}) \rightarrow r_1(V_s^{k+1}) \tag{2.23}$$

$$g_2(V_s^{k+1}) \rightarrow r_2(V_s^{k+1}) \tag{2.24}$$

A detailed calculations of the ranks $r_1(V_s^{k+1})$ and $r_2(V_s^{k+1})$ will be provided in next chapter. This ranking determines the relative quality of each voltage vector $(r_1, r_2)$ for each cost function $(g_1, g_2)$. Finally, an averaging of the two ranks associated with each voltage vector is calculated and used as a criterion to select the optimal voltage vector.

$$V_{sopt} = arg \min_{\{v_0,\ldots,v_7\}} \frac{r_1(V_s^{k+1}) + r_2(V_s^{k+1})}{2} \tag{2.25}$$

### 2.2.5 Multi-objective fuzzy decision method (FDM)

Similar to the ranking method described above, the individual cost functions are evaluated for all possible voltage vectors as follows [16], [34].

$$g_1(V_s^{k+1}) = (T^{ref} - T^{k+2})^2 \tag{2.26}$$

$$g_2(V_s^{k+1}) = \left(\left\|\psi_s^{ref}\right\| - \|\psi_s^{k+2}\|\right)^2 \tag{2.27}$$

The maximum and minimum, $g_i^{max}$ and $g_i^{min}$, among the resultant values are identified. Then, membership functions are evaluated for each possible voltage vector as follows.

$$\mu_1(V_s^{k+1}) = \left(\frac{g_1^{max} - g_1(V_s^{k+1})}{g_1^{max} - g_1^{min}}\right)^{k_1} \tag{2.28}$$

$$\mu_2(V_s^{k+1}) = \left(\frac{g_2^{max} - g_2(V_s^{k+1})}{g_2^{max} - g_2^{min}}\right)^{k_2} \tag{2.29}$$

$k_1$ and $k_2$ determine the priority of one cost function over the other, if $k_1 = k_2 = 2$, this results in quadratic membership function and gives equal priority for both torque and flux. At this stage, the possible values of each cost function are mapped into the range [0,1]. Thus, the two cost functions become compatible to each other. Since this process is repeated every sample, the relative importance can be updated according to the operating point for which flux and torque errors can vary. The best voltage vector is determined to maximize the decision function as follows.

$$\mu_D(V_s^{k+1}) = \mu_1(V_s^{k+1})\mu_2(V_s^{k+1}) \tag{2.30}$$

$$V_{sopt} = arg \max_{\{v_0,\ldots,v_7\}} \mu_D(V_s^{k+1}) \tag{2.31}$$

### 2.2.6 VIKOR method

VIKOR method is a multi-criteria decision-making method. Utilization of this method for PTC of IM was explained in [29] and can be summarized in the following steps. Firstly, the individual cost function for the torque and flux are calculated for all possible voltage vectors as follows.

$$g_1(V_s^{k+1}) = \left|T^{ref} - T^{k+2}\right| \tag{2.32}$$

$$g_2(V_s^{k+1}) = \left|\left\|\psi_s^{ref}\right\| - \left\|\psi_s^{k+2}\right\|\right| \tag{2.33}$$

Then minimum and maximum values for each objective are calculated. These represent the best and worst solutions respectively. Then, utility $S$ and a regret $R$ for each voltage vector can be defined as follows.

$$S(V_s^{k+1}) = w_T \frac{g_1^{max} - g_1(V_s^{k+1})}{g_1^{max} - g_1^{min}} + w_\phi \frac{g_2^{max} - g_2(V_s^{k+1})}{g_2^{max} - g_2^{min}} \tag{2.34}$$

$$R(V_s^{k+1}) = max\left[w_T \frac{g_1^{max} - g_1(V_s^{k+1})}{g_1^{max} - g_1^{min}}, w_\phi \frac{g_2^{max} - g_2(V_s^{k+1})}{g_2^{max} - g_2^{min}}\right] \tag{2.35}$$

$w_T$ and $w_\phi$ represent the weights associated to the torque and flux, respectively. For equal importance of torque and flux cost functions, $w_T$ and $w_\phi$are set equal to 0.5. Secondly, the minimum and maximum values of the utility and regret are calculated. Finally, the VIKOR index $Q$ is calculated for each voltage vector as follows.

$$Q(V_s^{k+1}) = v\left[\frac{S(V_s^{k+1}) - S^{min}}{S^{max} - S^{min}}\right] + (1 - v)\left[\frac{R(V_s^{k+1}) - R^{min}}{R^{max} - R^{min}}\right] \tag{2.36}$$

$v$ is called group utility factor and is set to 0.5. The voltage vector, which results in the minimum index, is representing the optimal solution.

$$V_{sopt} = \arg\min_{\{v_0,\ldots,v_7\}} Q(V_s^{k+1}) \tag{2.37}$$

### 2.2.7 Weighting factor elimination Method (WFE)

This method was presented recently in [17] and referred as model predictive flux control method. It aims at eliminating the flux weighting factor. The idea is based on using IM dynamic equation to relate the torque reference to the stator flux reference as follows.

$$T = \frac{3}{2}\, n_p \lambda\, L_m\, (\psi_r \times \psi_s) \tag{2.38}$$

$$T^{ref} = \frac{3}{2}\, n_p \lambda\, L_m\, (\psi_r \times \psi_s^{ref}) \tag{2.39}$$

$$\psi_s^{ref} = \left\|\psi_s^{ref}\right\|. \exp(j \angle \psi_s^{ref}) \tag{2.40}$$

$$\angle \psi_s^{ref} = \angle \psi_r + \arcsin\left(\frac{T^{ref}}{\frac{3}{2} n_p \lambda\, L_m \|\psi_r\| \left\|\psi_s^{ref}\right\|}\right) \tag{2.41}$$

where $\lambda = \frac{1}{L_s L_r - L_m^2}$

A new cost function is formed that represents the deviation between the reference and predicted stator flux vectors.

$$g(V_s^{k+1}) = \left|\psi_s^{ref} - \psi_s^{k+2}\right| \tag{2.42}$$

The last step is to select the voltage vector that minimizes the cost function as follows.

$$V_{sopt} = \arg \min_{\{v_0,\ldots,v_7\}} g(V_s^{k+1}) \tag{2.43}$$

Despite of various weighting factor selection methods reported in literature, there is a shortage in performance comparison among all of them. Only the performance of each method is compared to the conventional method (AOF). To the best of authors' knowledge, no attempt was reported in the literature to assess the performance of different weighting factor selection methods against each other. Therefore, a comparison study among the five above mentioned WFS methods is introduced in the next chapter.

## 2.3 Experimental setup

In this section, a detailed description of the developed experimental test bench will be introduced. Figure 2-3 demonstrates block diagram of the experimental setup.

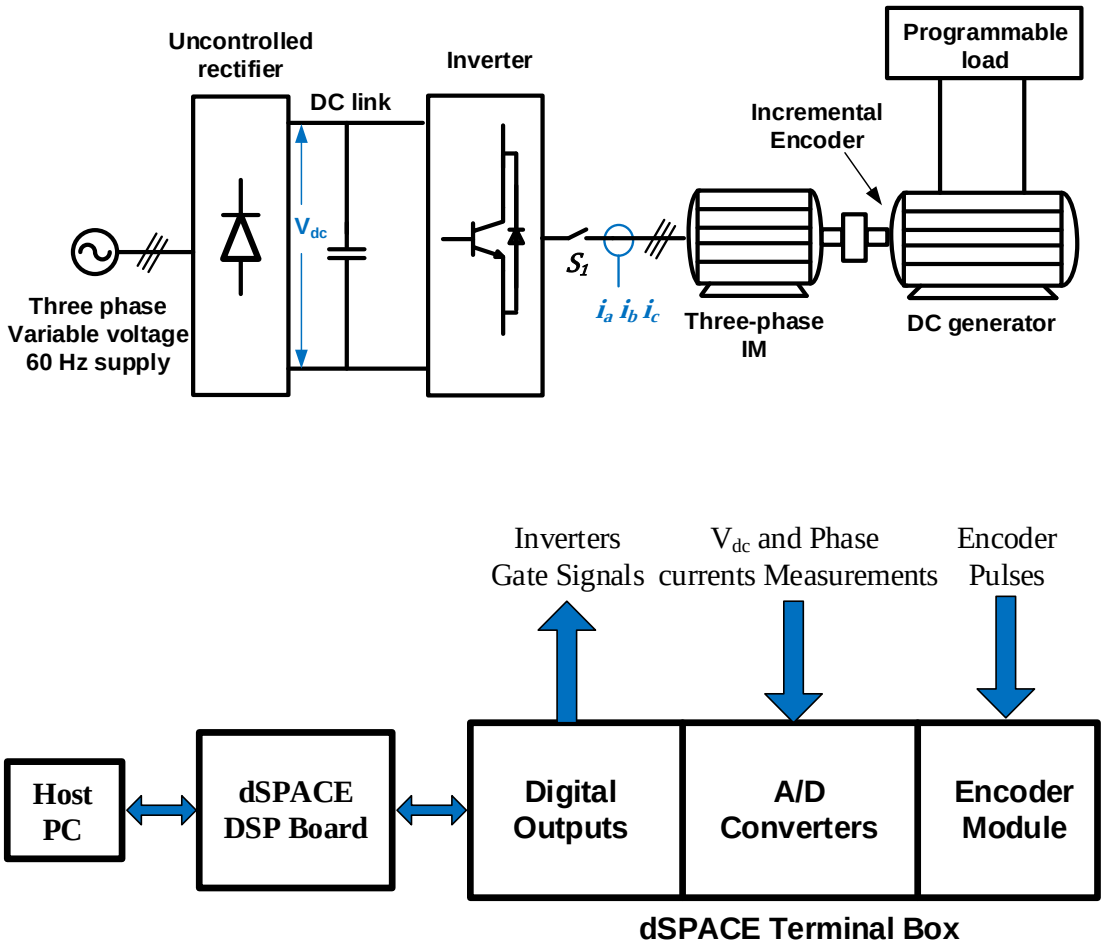


**Figure 2-3 Block diagram of the developed experimental setup**

The measured voltage and currents are sent to the controller platform terminal box along with the encoder signal. After conditioning this signal are transmitted to the DSP board where the control algorithm is executed.

The output of the controller are the inverter-gating signals which are generated from the digital outputs and are sent to the corresponding switches of the driving inverter. The measured signal can be monitored and recorded on the host PC. Figure 2-4 illustrates the physical setup.

### 2.3.1 Induction motor

A one KW, four poles squirrel cage induction motor from Leybold Didactic is used. The parameters of the motor are identified using the conventional no-load and locked rotor tests. The parameters are listed in Table 2-2.

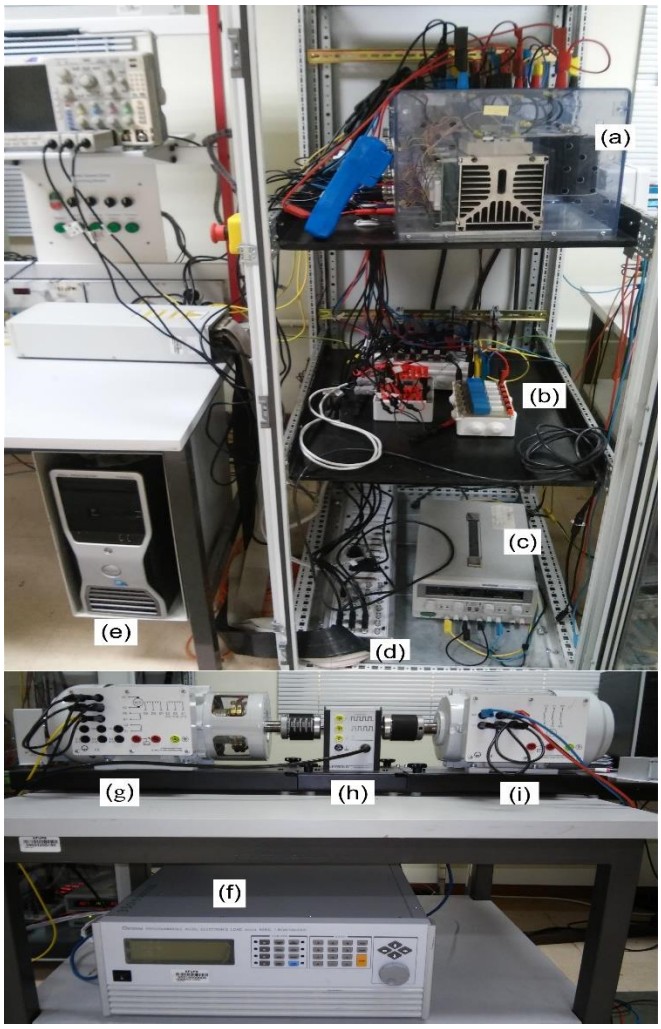


**Figure 2-4 Experimental setup (a) Semikron Inverter (b) LEM Sensors (c) ± 15V dc supply (d) dSPACE terminal box (e) Host PC (f) Chroma programmable load (g) DC generator (h) Incremental encoder (i) Induction motor**

**Table 2-2 Induction motor drive parameters**

| Parameter | Value | Parameter | Value |
|---|---|---|---|
| $P_r$ | 1 Kw | $T_{rated}$ | 5.5 N.m |
| $V_{rated}$ (ph) | 220 V | $\|\psi_s\|_{rated}$ | 0.8157 Wb |
| $I_{rated}$ | 2.2 A | $R_r$ | 6.0373 Ω |
| $N_{rated}$ | 1710 rpm | $L_r$ | 0.4577 H |
| $R_s$ | 8.15 Ω | $n_p$ | 2 |
| $L_s$ | 0.4577 H | $J$ | 0.07 Kg.m$^2$ |
| $L_m$ | 0.4372 H | $B$ | 0 N/rad/s |

**Table 2-3 Parameters of SEMIKRON inverter**

| Description | Parameter | Value |
|---|---|---|
| Maximum current | $I_{rms}$ | 30 A |
| Nominal DC link Voltage | $V_{dc}$ | 600 V |
| Maximum DC link Voltage | $V_{dcmax}$ | 750 V |
| Input AC voltage | $V_{in}$ | 400 V |

### 2.3.2 Inverter

**The controlled inverter is a three-phase 2L-VSI from SEMIKRON. The parameters of the inverter are listed in**

Table 2-3. The gating signal of the inverter is using 0/15 V logic

### 2.3.3 Loading mechanism

A 0.75 kW separately excited DC generator from Leybold Didactic is mechanically coupled to the motor. The terminal of the DC generator is connected to a programmable electronic load from CHROMA (Model 63802) with the parameters listed in Table 2-4.

**Table 2-4 DC operation characteristics of CHROMA programmable load**

| | |
|---|---|
| Model | 63802 |
| Power | 1800 W |
| Voltage range | 7.5 – 500 V |
| Current range | 0 – 18 A |

The programmable load is adjusted to constant current mode and by turning it on and off it can apply instant load to the generator, which will be reflected on the motor. Although the resultant load torque is smooth, the mechanism fails to apply rated load on the motor at low speed. Since the induced voltage on the DC generator terminal is very small at low speed, the programmable load becomes unable to draw the specified current and as a result only very low load torque can be realized at low speed operation points.

### 2.3.4 Measurements

Predictive torque control algorithm requires the measurements of the phase currents, DC link voltage and the mechanical speed. The DC link voltage and up to six phase motor currents are measured using LEM voltage and current sensors respectively Figure 2-5 .The speed is measured using a 1024 pulse per revolution incremental encoder from Leybold Didactic.

### 2.3.5 Control Platform

The control algorithm is implemented in real time using dSPACE platform. The dSPACE is equipped by A/D converters and encoder modules, which facilitate the acquirement and processing of the measures signals. On the other hand, digital outputs required for actuations (driving the inverters) using 0/5 V logic. Therefore, voltage level shifting circuit is designed and implemented to change the level of the actuation signals to the 0/15 V required for the inverter gating signals as shown in Figure 2-6.

**(a)** **(b)**

**Figure 2-5 Developed interface boards (a) Current measurement (b) Voltages measurement**

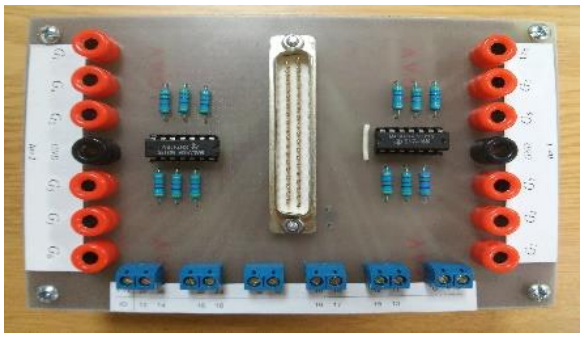

**Figure 2-6 Voltage level shifter from 0/5 to 0/15 V**

# CHAPTER 3

# Weighting Factor Selection Methods for PTC:

## Comparison study and Performance Improvement

The main steps of MPC algorithm is highlighted in chapter 2. In this chapter, more focus will be directed to the optimization step. Five methods recently reported in literature for design of flux weighting factor are assessed. The performance of predictive torque control (PTC) utilizing each of these methods will be evaluated considering torque ripple, flux ripple, current total harmonic distortion (THD) and average switching frequency as judging criteria. Moreover, an improvement to the multi-objective fuzzy decision method is introduced which result in reduced torque ripple.

## 3.1 PTC of Induction motor drive

Figure 3.1 illustrates the structure of PTC algorithm. The torque reference is generated from the outer speed control loop via a proportional integral (PI) controller. Flux reference is generated depending on the region of operation, constant torque, or field weakening. Based on the currents and voltage measurements and using suitable machine model, the machine flux is estimated. The machine model is then used for predicting the future torque and flux based on the measured and estimated states.

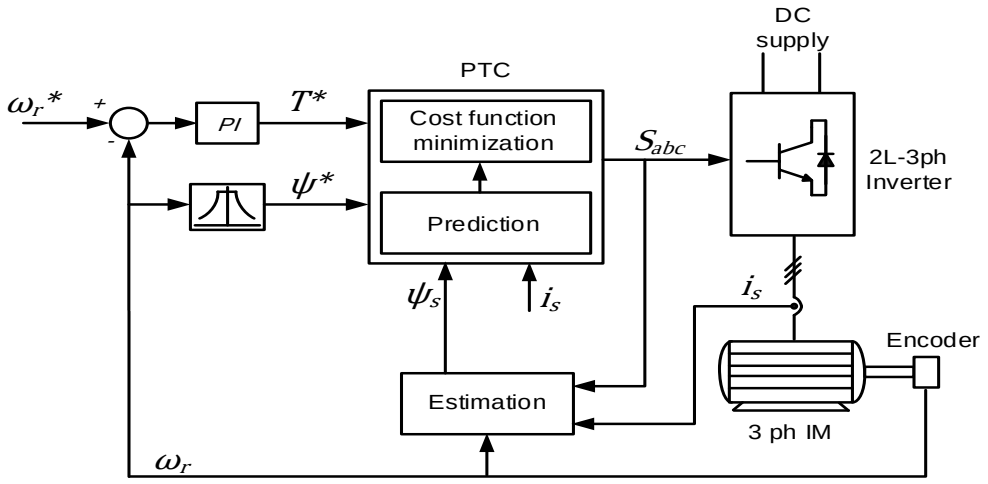


**Figure 3-1 Schematic diagram of PTC of induction motor**

Finally, an optimization step utilize the reference and predicted quantities to generate the optimal gating signal for the next control sample which will be applied to the two-level voltage source inverter (2L-VSI). As explained in the previous chapter, the cost function design is essential for the optimal voltage vector selection. Therefore, in the following section, the performance of PTC algorithm utilizing different weighting factor selection methods will be compared.

## 3.2 Performance Criteria

For the sake of comparison, different performance criteria will be considered to evaluate the performance of IM drive system when different weighting-factor selection methods are implemented as a part of PTC algorithm. These criteria include torque and flux ripples, current total harmonic distortion, and average switching frequency. These criteria can be defined as follows.

### 3.2.1 Torque and flux ripple

The torque and flux ripples can be calculated as:

$$X_{rip} = \frac{X_{max} - X_{avg}}{X_{rated}} \times 100 \quad (3.1)$$

where $X_{rip}$ stands for the torque or flux ripple. $X_{max}$ , $X_{avg}$ and $X_{rated}$ are the maximum, average and rated values, respectively.

### 3.2.2 Current total harmonic distortion

$$i_{THD} = 100 \times \sqrt{\left(\frac{I_{rms}}{I_{1rms}}\right)^2 - 1} \quad (3.2)$$

where $i_{THD}$ is the percentage current total harmonic distortion. $I_{rms}$ and $I_{1rms}$ are the root mean square values for the phase current and for the fundamental component respectively.

### 3.2.3 Average switching frequency

The average switching frequency is calculated by counting the total switching jumps $N$ over a fixed period of $d$ seconds [42]. Then the average frequency can be calculated as follows.

$$f_{av} = \frac{N}{n_s * d} \quad (3.3)$$

where $n_s$ represents the number of switches. In this work, $n_s = 6$ for two-level voltage source inverter (2L-VSI) and $d$ is set to 0.05 seconds.

## 3.3 Results and discussion

The previously explained methods for weighting factor selection for PTC are simulated using MATLAB/simulink environment. The machine parameters used in the simulation are listed in Table 3-1, and the designed controller parameters are given in Table 3-2. The PI gains of the outer speed loop are set based on pole placement technique.

Moreover, an anti-windup method is utilized to reduce the speed overshoot. The flux weighting factor of the conventional method is selected based several trials to compromise torque and flux ripples.

In order to evaluate the considered methods, steady state and dynamic responses of the system are examined with each method. In addition, a comparative study considering torque and flux ripples, current THD, and average switching frequency is carried out over a wide speed range.

**Table 3-1 Three phases induction motor drive parameters**

| Parameter | value | Parameter | Value |
|---|---|---|---|
| $P_r$ | 1 Kw | $T_{rated}$ | 5.5 N.m |
| $N_{rated}$ | 1710 rpm | $\|\psi_s\|_{rated}$ | 0.8157 Wb |
| $R_s$ | 8.15 Ω | $R_r$ | 6.0373 Ω |
| $L_s$ | 0.4577 H | $L_r$ | 0.4577 H |
| $L_m$ | 0.4372 H | $n_p$ | 2 |
| $J$ | 0.0034 Kg.m$^2$ | $B$ | 0 N/rad/s |

**Table 3-2 Controller parameters**

| Description | symbol | value |
|---|---|---|
| Simulation time | $T_{sim}$ | 2.5 µsec |
| PTC Sampling time | $T_s$ | 40 µsec |
| Speed loop sampling time | $T_{ss}$ | 5 msec |
| Flux weighting factor (conv) | $K_\psi$ | 7 |
| Proportional gain | $K_p$ | 0.2 |
| Integral gain | $K_i$ | 4.59 |
| Priority for torque (FDM) | $K_1$ | 2 |
| Priority for flux (FDM) | $K_2$ | 2 |
| Torque weighting factor (VIKOR) | $w_T$ | 0.5 |
| Flux weighting factor (VIKOR) | $w_\phi$ | 0.5 |

### 3.3.1 Dynamic response

The scenario used to start the IM from standstill to its rated speed is as follows. First, the flux is built to its rated value. Then at $t = 0.1$ sec, the speed command is applied. This pre-excitation process helps reducing the starting current [43]. Finally, at $t = 0.35$ sec, half the rated load (2.75 N.m) is applied. Figure 3-2 to Figure 3-6 illustrate the dynamic response of the IM drive system at both starting and loading for all the methods. Same PI controller gains for the outer speed loop are used with all methods. In addition, saturation and anti-windup are used to eliminate speed overshoot. Speed, torque, flux, and current responses for each method are presented. Analysis of different responses indicates that the online weighting factor calculation methods, shown in Figure 3-3 to Figure 3-6, successfully trace the flux and torque references and result in good dynamic speed response and load rejection. This response is close to that of the conventional method shown in Figure 3-2 where the flux-weighting factor is calculated after tedious offline simulation. It can be noted that the direction of the phase current in the conventional method is negative during the pre-excitation process while it is positive for the other methods. This can be explained as follows. During the pre-excitation process, only the magnitude of the stator flux is commanded while their no information about the direction since the speed command is zero during this period. As a result, it is up to the optimization process to select the optimal voltage vector satisfying this requirement. Consequently, different voltage vector can be selected according to the weighting factor selection (WFS) method used.

The performance of the different methods under step torque condition is illustrated in Figure 3-7 the test is performed by a sudden change in speed reference from 1000 to

1400 rpm at no-load, which leads to saturate the speed PI controller. Investigation of the responses of different methods in Figure 3-6 clearly indicates that all the methods have similar dynamic torque responses and the differences between them are insignificant. The previous tests prove that the dynamic response of the online WFS method is close to that of the conventional method. Therefore, the tedious offline calculation of the flux-weighting factor can be avoided without degrading the dynamic response of the PTC algorithm. In the next section, a comparison study based on the different criteria defined in section 3.2 is presented to reveal the characteristics of each method at steady state.

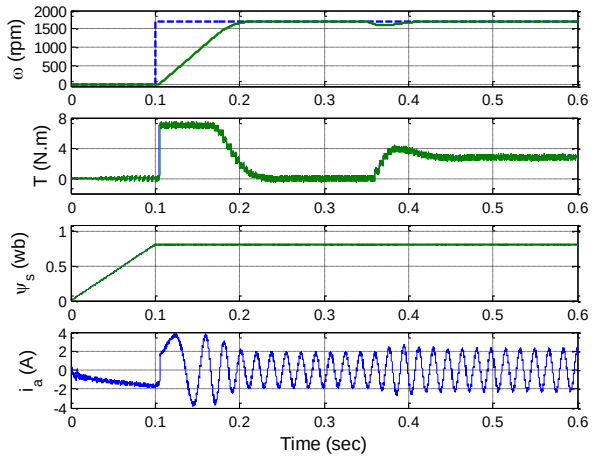


**Figure 3-2 Dynamic response for conventional method**

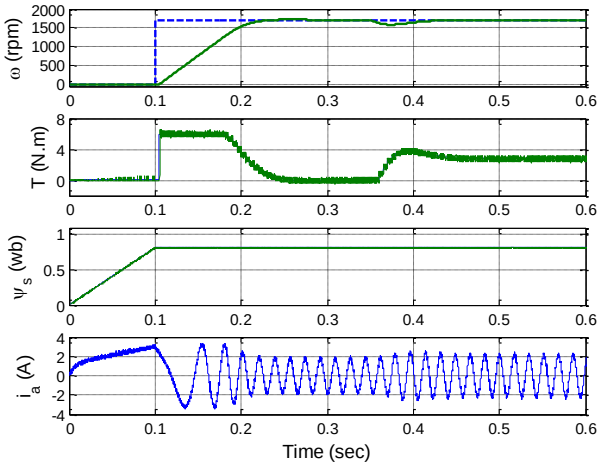


**Figure 3-3 Dynamic response for ranking method**

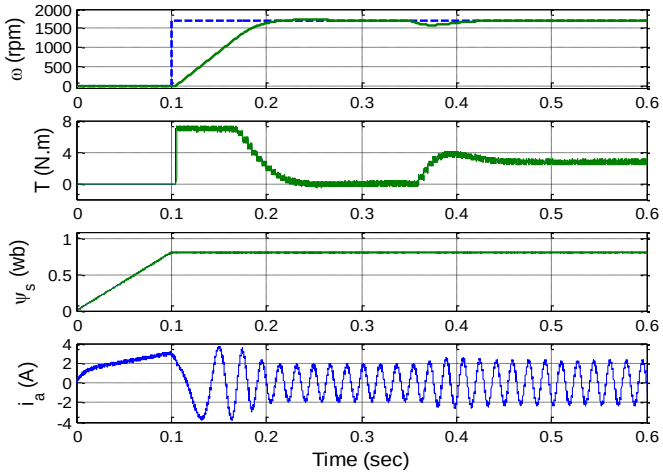


**Figure 3-4 Dynamic response for FDM method**

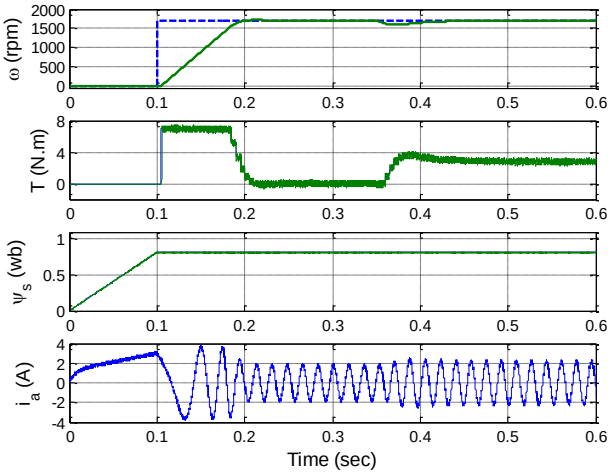


**Figure 3-5 Dynamic response for VIKOR method**

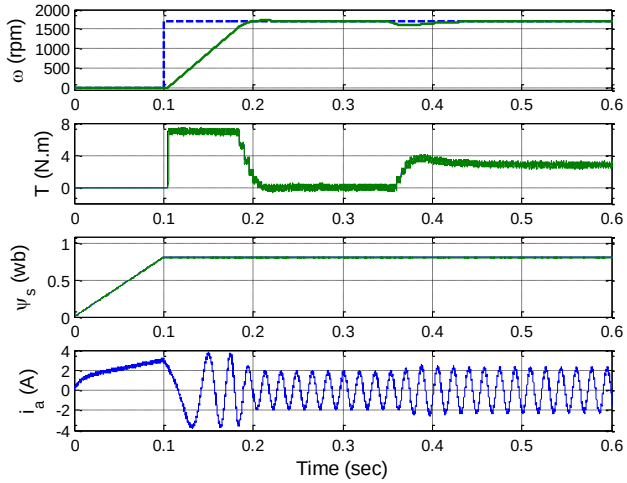


**Figure 3-6 Dynamic response for weighting factor elimination method**

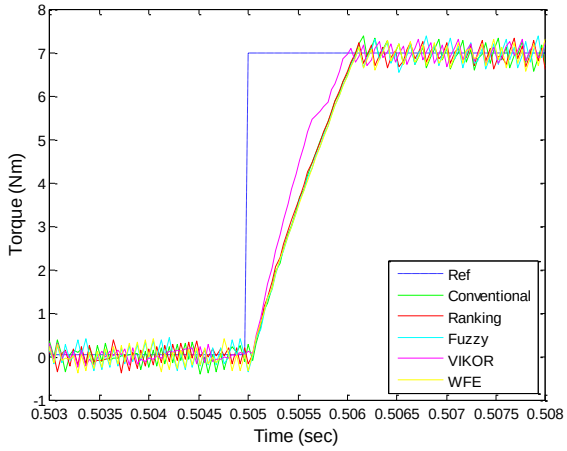


**Figure 3-7 Step response of torque command using different weighting factor design methods**

### 3.3.2 Steady state response

Figure 3-8 to Figure 3-12 illustrate the steady state responses for each method at the rated speed .At this operating point, the five methods have close performance except for the conventional and the ranking based methods, which are characterized by higher flux ripple compared to the other methods. This can be explained as follows. For the conventional method, a weighting factor compromising torque and flux ripple is selected. Definitely, higher value for the weighting factor can be assigned to improve the flux but it will result in worse torque ripple. On the other hand, the ranking method can result in two equally ranked voltage vectors. Since only one voltage vector should be applied, the one resulting in lower torque ripple is selected [15]. Therefore, for these cases, more weight is given to torque ripple over the flux ripple.

### 3.3.3 Comparison criteria

For further steady state performance comparison, the PTC of IM drive system is simulated using the considered methods for a wide speed range. The load is fixed at half rated load. At each speed, torque ripple, flux ripple, current total harmonic distortion,

and average switching frequency are calculated for the sake of comparison. Since studying at only one operating point can result in unfair comparison, different operating point is tested at different reference speeds. Table 3-3 and Table 3-4 show the values of different performance indices at reference speeds of 200, 800, and 1710 rpm respectively. These results represent low, medium, and rated speed, respectively. The results are also represented graphically in Figure 3-13 to Figure 3-16 for a wide speed range. During this simulation, the weighting factor for the conventional method is kept constant. This value was calculated to compromise flux and torque error at rated speed. The FDM and VIKOR methods are simulated for equal importance for the torque and flux cost functions by setting appropriate weights and priorities as indicated in Table 3-2.

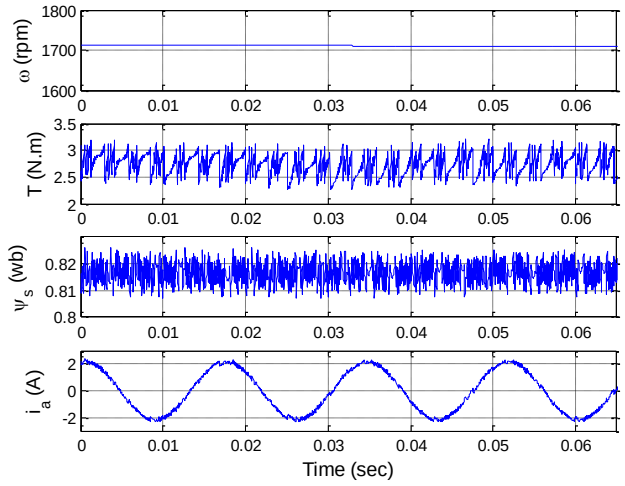


**Figure 3-8 Steady state response for conventional method**

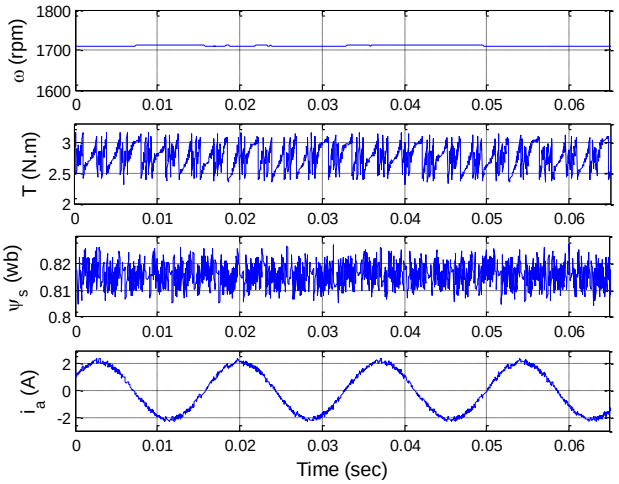


**Figure 3-9 Steady state response for ranking method**

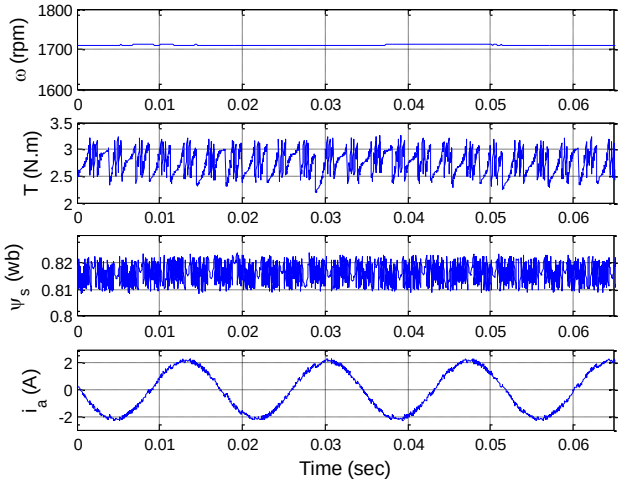


**Figure 3-10 Steady state response for FDM method**

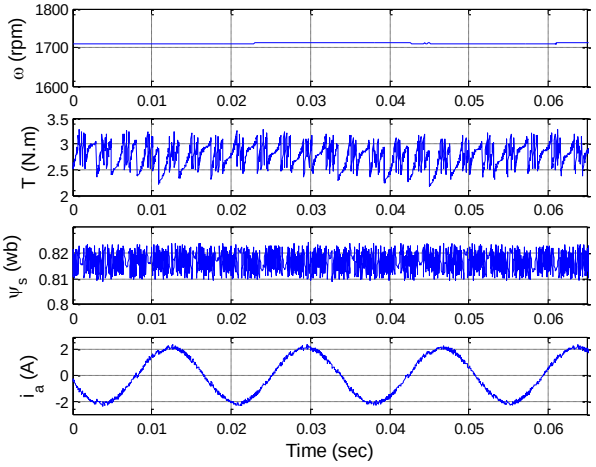


**Figure 3-11 Steady state response for VIKOR method**

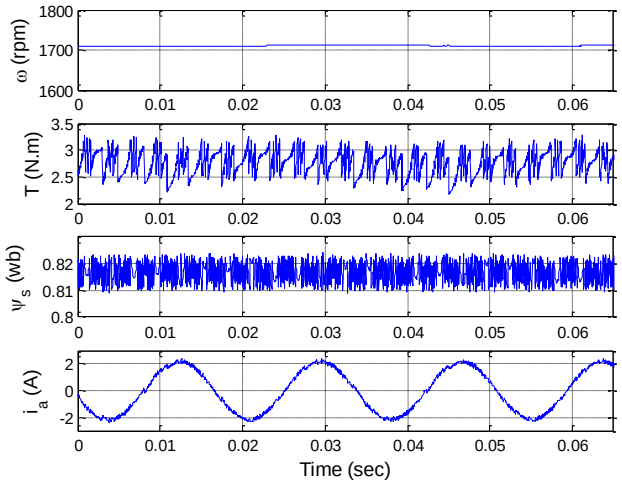


**Figure 3-12 Steady state response for weighting factor elimination method**

**Table 3-3 Different methods performance indecis (N=200 rpm)**

| Indices / Methods | $T_{rip}(\%)$ | $\psi_{rip}(\%)$ | THD (%) | $f_{av}\ (KHz)$ |
|---|---|---|---|---|
| Conventional | 9.1558 | 1.2178 | 6.27 | 2.05 |
| Ranking | 11.7412 | 1.4919 | 6.75 | 2.65 |
| FDM | 8.6000 | 0.9226 | 6.16 | 1.82 |
| VIKOR | 8.6869 | 0.9883 | 6.28 | 1.85 |
| WFE | 8.1520 | 1.0139 | 6.02 | 1.81 |

**Table 3-4 Different methods performance indecis (N=800 rpm)**

| Indices / Methods | $T_{rip}(\%)$ | $\psi_{rip}(\%)$ | THD (%) | $f_{av}\ (KHz)$ |
|---|---|---|---|---|
| Conventional | 8.7464 | 1.2145 | 6.2 | 5.3 |
| Ranking | 12.0033 | 1.4240 | 6.72 | 5.95 |
| FDM | 8.0154 | 0.9477 | 6.18 | 4.75 |
| VIKOR | 8.4423 | 0.9946 | 6.19 | 4.7 |
| WFE | 8.1705 | 0.9578 | 6.04 | 4.97 |

**Table 3-5 Different methods performance indecis (N=1710 rpm)**

| Indices / Methods | $T_{rip}(\%)$ | $\psi_{rip}(\%)$ | THD (%) | $f_{av}\ (KHz)$ |
|---|---|---|---|---|
| Conventional | 9.2145 | 1.2016 | 6.32 | 2.63 |
| Ranking | 8.8304 | 1.5049 | 6.57 | 2.63 |
| FDM | 9.6893 | 0.8896 | 6.4 | 2.55 |
| VIKOR | 9.4059 | 0.9660 | 6.4 | 2.57 |
| WFE | 8.3861 | 1.0121 | 6.04 | 2.57 |

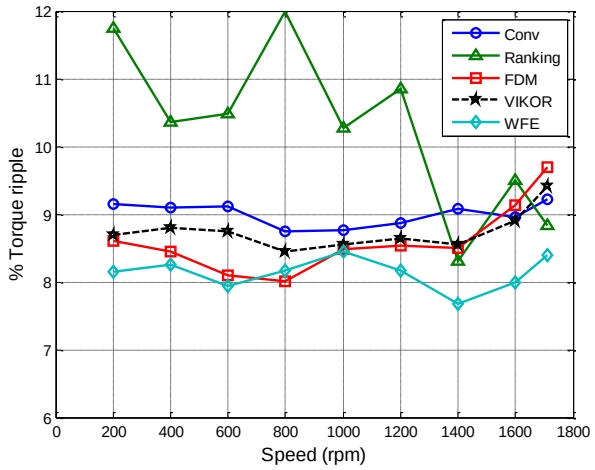


**Figure 3-13 Variation of torque ripple**

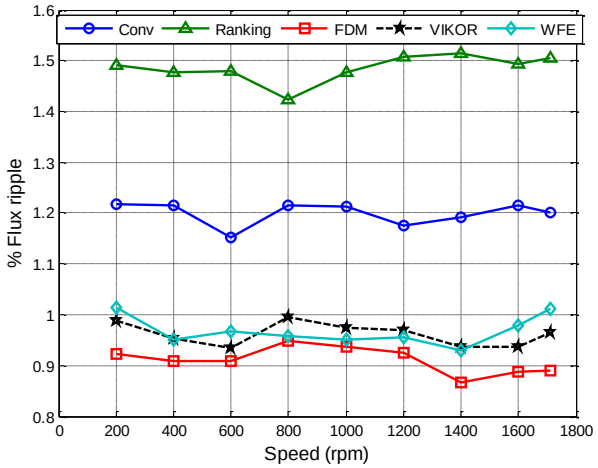


**Figure 3-14 Variation of flux ripple**

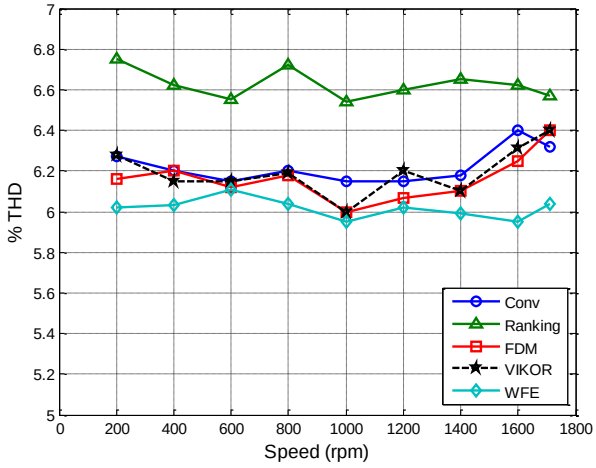


**Figure 3-15 Variation of current total harmonic distortion**

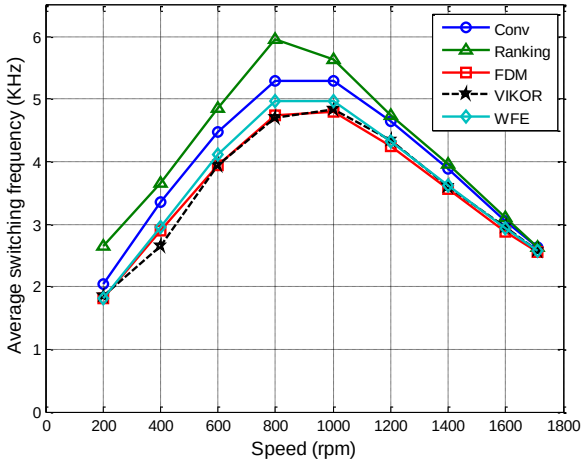


**Figure 3-16 Variation of average switching frequency**

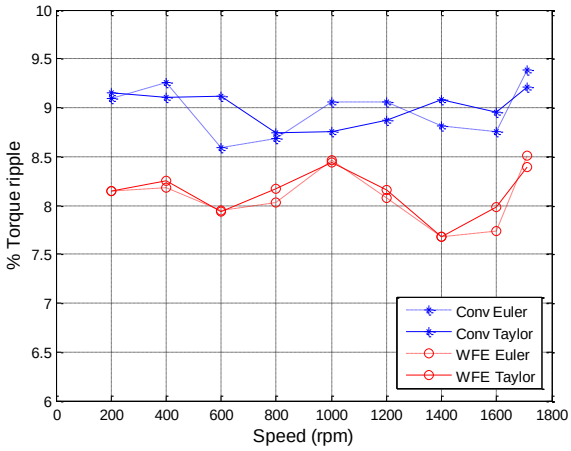


**Figure 3-17 Variation of torque ripple using Euler and Taylor discretization methods**

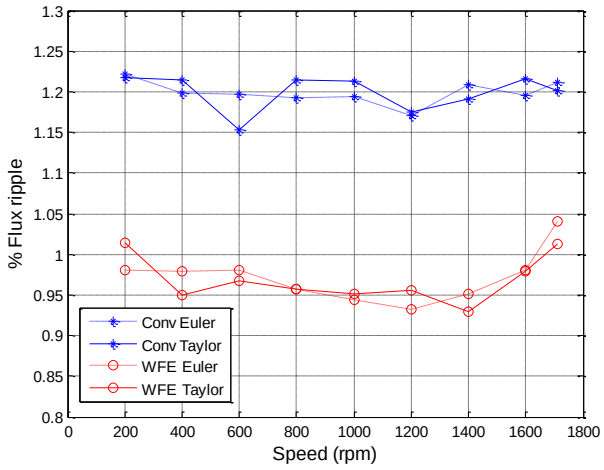


**Figure 3-18 Variation of flux ripple using Euler and Taylor discretization methods**

In order to investigate the effect of the discretization method on the steady state performance, PTC algorithm is simulated using Euler discretization method. The results of torque and flux ripple for two WFS methods are illustrated in Figure 3-17 and Figure 3-18 using Euler and Taylor second order discretization methods. Comparison of the responses of different WFS methods shows that the differences among the discretization methods are not significant

### 3.3.4 Discussion

Analysis of Table 3-3, Table 3-4, and Table 3-5 along with the results of Figure 3-13 to Figure 3-16 reveals the characteristics of each method, which can be highlighted in the following points:

- The ranking based method has the worst performance, if the overall speed range is considered. It has the highest torque and flux ripple. In addition, the torque ripple has a large variation at different speed points. Moreover, it also has the highest average switching frequency and current THD.

- The performance of FDM and VIKOR methods is superior to the conventional method since they have lower torque and flux ripples almost for all the speed range. Moreover, their average switching frequency is less than the conventional method while their performance is very close to that of the conventional method regarding the current THD.
- Weighting factor elimination (WFE) method is characterized by the smallest torque ripple and current THD and acceptable flux ripple. On the other hand, its average switching frequency is slightly higher than the FDM and VIKOR methods especially at medium speed range.
- FDM method results in the lowest flux ripple for all the speed range.

It should be noted that both FDM and VIKOR method could be tuned to give different performance by adjusting the relative importance of the torque and flux cost function using the priority factors. However, in this study, it was preferred to set equal importance for both torque and flux for fair comparison. Generally, these priority factors are similar to the flux-weighting factor for the conventional method. Although, they are much simpler to design, they could have a great influence on the overall performance.

Another important criterion considered for evaluation of different methods is the complexity of each method. The conventional method is definitely the simplest. The ranking based method needs additional sorting algorithm, which increases the complexity of the method. In addition, in some cases more than one voltage vector has the same average ranking. It was suggested to use additional criterion (by selecting the voltage vector resulting in minimum torque) to choose only one voltage vector at the end. This is another complication since this case occurs more than 20% of all samples

as observed in this study. The optimization step of WFE method is highly parameter dependent; as a result, it was proposed to use a full order flux observer to increase the robustness of the method. This definitely adds a complexity to the design and implementation of the method.

Based on the above discussion, the multi-objective based weighting factor method is superior to the conventional one. In particular, fuzzy decisions method (FDM) has the lowest flux ripple but it suffer of high torque ripple at some operating points. In the next section, a deep analysis of the FDM is given and a modification is proposed to reduce the torque ripple.

## 3.4 Improved multi-objective fuzzy decision based PTC

The salient feature of the proposed approach lies in its capability to avoid high torque ripple and eliminate the need of extra priority factors, which increase the complexity of the technique. In the proposed approach, the membership functions are normalized using the global optimal values. As a result, an efficient compromise solution between torque and flux ripples minimization is automatically achieved. Simulation study and experimental setup are used to validate the proposed method. Torque ripple, flux ripple, current total harmonic distortion, and average frequency are used as criteria for performance comparison to the conventional and fuzzy decision method discussed in the previous chapter. The results show considerable improvement in torque ripple with slightly increased flux ripple proving the simplicity and compromising ability of the proposed approach

### 3.4.1 Problem statement

Fuzzy predictive torque control (FPTC) was presented in [27] where priority factors for each cost function were assigned to reduce the high torque ripple inherently results from this method. By manipulating these priority factors, the torque and flux ripples can be controlled. This added extra complexity to the method since another procedure is needed to determine the best priority factors. For clarity, the procedure of this method is revisited. The procedure of FDM explained in previous chapter and repeated hereafter for the convenience of the reader. The individual cost functions are evaluated for all the possible voltage vectors as follows.

$$J_1(V_s^{k+1}) = (T^{ref} - T^{k+2})^2 \tag{3.3}$$

$$J_2(V_s^{k+1}) = \left(\left\|\psi_s^{ref}\right\| - \left\|\psi_s^{k+2}\right\|\right)^2 \tag{3.4}$$

Then $J_i^{max}$ and $J_i^{min}$ among the resultant values are calculated representing the maximum and minimum deviation from the references at the current sample. Here, $i = [1,2]$ for the two cost functions. Then membership functions, $\mu_1$ and $\mu_2$, are evaluated for each possible voltage vector.

$$\mu_1(V_s^{k+1}) = \left(\frac{J_1^{max} - J_1(V_s^{k+1})}{J_1^{max} - J_1^{min}}\right)^{k_1} \tag{3.5}$$

$$\mu_2(V_s^{k+1}) = \left(\frac{J_2^{max} - J(V_s^{k+1})}{J_2^{max} - J_2^{min}}\right)^{k_2} \tag{3.6}$$

where $k_1$ and $k_2$ determine the priority of one cost function over the other. At this stage, the possible values of each cost function are mapped into the range [0,1]. Thus, the two cost functions become compatible to each other. Since this process is repeated every sample, the relative importance can automatically updated according the operating

point. The best voltage vector is determined to maximize the decision function as follows.

$$\mu_D(V_s^{k+1}) = \mu_1(V_s^{k+1})\mu_2(V_s^{k+1}) \tag{3.7}$$

$$V_{sopt} = \arg \max_{\{v_0,\ldots,v_7\}} \mu_D(V_s^{k+1}) \tag{3.8}$$

It can be noted that the priority factors represent extra complexity for this method since an appropriate procedure is needed for their determination. For simplicity, equal values can be considered but this results in higher torque ripple compared to the conventional method [34][27].

The high torque ripple for equal priority factors can be explained as follows. Referring to Figure 3-19 (a), two successive calculations for flux membership function are illustrated. For the membership function calculation at sample $k$, the highest cost function is mapped to zero while the lowest cost function is mapped to one (red line). For the sample $k+1$, the process is repeated (blue line).

Notice that the highest cost function for the latter sample $J_{max}^{k+1}$ is mapped to zero even though the value of the cost function itself is close to the minimum value of the cost function of the previous sample $J_{min}^{k}$, which was mapped to one. Moreover, mapping the cost function $J_{max}^{k+1}$ to zero will exclude the corresponding voltage vector from the selection according to equations (3.7) and (3.8) whatever the value of the torque cost function is. Therefore, for some samples, voltage vector that can result in low torque ripple and relatively good flux ripple will be missed because it will lead to the highest flux ripple locally at the calculated sample.

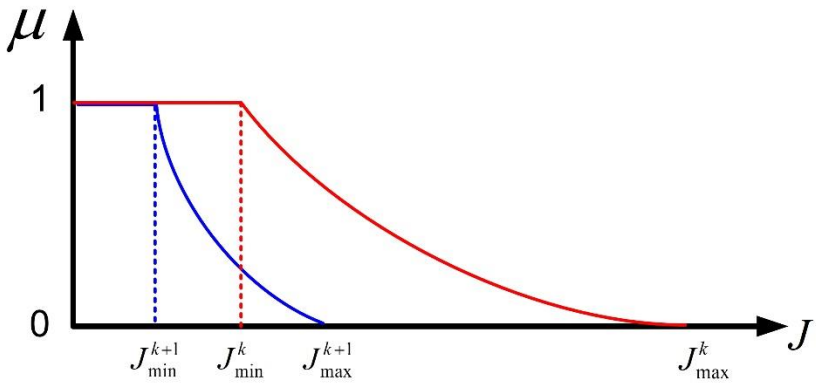


**(a)**

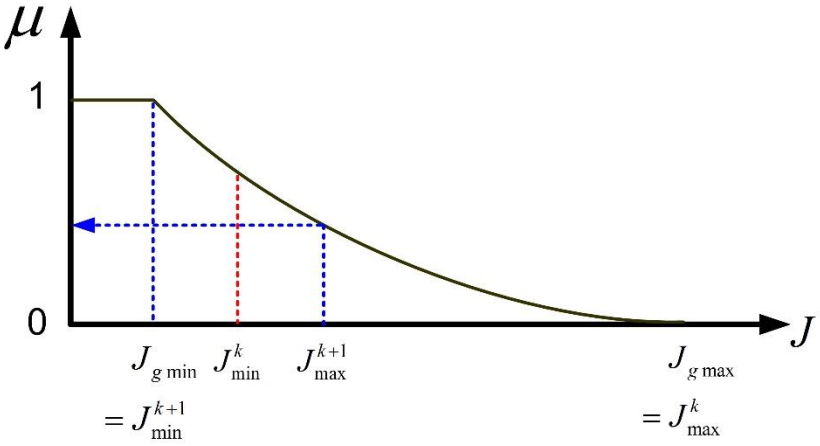


**(b)**

**Figure 3-19 Membership function used in PTC (a) FPTC (b) MFPTC**

This limits the effectiveness of this method to capture the optimal voltage vector. To avoid this problem, a modified fuzzy predictive torque control (MFPTC) is proposed as described below.

### 3.4.2 Proposed method

Based on the previous discussion, the following procedure is proposed to avoid missing some potential voltage vector. The mapping procedure of the maximum and minimum values of the cost function to one and zero, respectively, is modified. In the proposed procedure, the global minima and maxima are calculated and updated at each sample. The global values will be mapped to zero and one while any other values will be mapped

to the period ]0,1[. The resultant membership function is illustrated in Figure 3-19 (b). This will ensure that only the worst (maximum) cost function among all samples will be mapped to zero. As a results, the voltage vector truly compromises flux and torque cost functions could be selected. For example, $J_{max}^{k+1}$ in Figure 3-19 (b) is no longer mapped to zero. It has a certain value relative to the global maximum $J_{gmax}$. Actually, $J_{gmax}$ is the one mapped to zero in this case. This concept can be applied for both torque and flux cost functions. However, it was found after deep analysis that applying this to the flux cost function only, results in lower torque ripple. Similarly, the cost functions for torque and flux will be calculated as given in (4.1) and (4.2). Then the proposed method will be implemented as follows.

$$\mu_1(V_s^{k+1}) = \left(\frac{J_1^{max} - J_1(V_s^{k+1})}{J_1^{max} - J_1^{min}}\right)^2 \tag{3.9}$$

$$\mu_2^p(V_s^{k+1}) = \left(\frac{J_{2\,gmax} - J(V_s^{k+1})}{J_{2\,gmax} - J_{2\,gmin}}\right)^2 \tag{3.10}$$

$$\mu_D^p(V_s^{k+1}) = \mu_1(V_s^{k+1})\mu_2^p(V_s^{k+1}) \tag{3.11}$$

$$V_{sopt} = \arg \max_{\{v_0,\ldots,v_7\}} \mu_D^p(V_s^{k+1}) \tag{3.12}$$

where $J_{2\,gmax}$ and $J_{2\,gmin}$ are the global maxima and minima of the flux cost function which should be checked and updated at each sample period.

In order to illustrate the proposed method, a calculation example is presented in Table 3-6. Cost functions for torque and flux are calculated for the different seven voltage vectors. Then following the procedure of FPTC method, membership functions are calculated using equal priority factors ($k_1 = k_2 = 2$). Fuzzy based decision resulted

in selecting $V_0$ since it maximize $\mu_d$ as indicated by the underlined values in Table 3-6. Now, following the proposed method, the global minimum, and maximum are used to calculate $\mu_2^p$. The values used for $J_{2\,gmax}$ and $J_{2\,gmin}$ in this example are 7.1e-04 and 2.06e-12 $wb$ respectively. Fuzzy based decision resulted in selecting $V_6$ since it maximize $\mu_d^p$. By comparing the cost functions for torque and flux corresponding to $V_0$ and $V_6$, it will be noticed that the torque error for the FPTC is three times higher than that of MFPTC. On the other hand, the flux error for MFPTC is still very low. Another observation is that using FPTC, two voltage vectors will result in zero values for $\mu_d$. As a result, they will never be selected. This will be more severe if FPTC used to optimize three cost functions since three values in $\mu_d$ will equal zero, which corresponding to the maximum or the worst value of each membership function. This will limit the selection to only four vectors out of the available seven vectors of the 2L-VSI.

**Table 3-6 Calculation example for FPTC and MFPTC methods**

| VV | $J_1(Nm)$ | $J_2\,(Wb)$ | $\mu_1$ | $\mu_2$ | $\mu_D$ | $\mu_2^p$ | $\mu_D^p$ |
|---|---|---|---|---|---|---|---|
| 0 | 0.301 | 7.7e-6 | 0.758 | 0.9804 | 0.743 | 0.978 | 0.741 |
| 1 | 0.193 | 4.0e-4 | 0.856 | 0 | 0 | 0.188 | 0.161 |
| 2 | 1.722 | 2.3e-4 | 0.022 | 0.1721 | 0.003 | 0.444 | 0.010 |
| 3 | 2.021 | 3.8e-6 | 0 | 1.0000 | 0 | 0.989 | 0 |
| 4 | 0.433 | 2.1e-4 | 0.646 | 0.2322 | 0.150 | 0.495 | 0.320 |
| 5 | 0.046 | 1.0e-4 | 1.000 | 0.5751 | 0.575 | 0.737 | 0.737 |
| 6 | 0.104 | 5.1e-5 | 0.941 | 0.7748 | 0.729 | 0.860 | 0.809 |

### 3.4.3 Simulation results

In order to validate the proposed method, simulation using Matlab/Simulink is performed. The parameters used is the same one adopted before and listed in Table 3-1 and Table 3-2 except for the sample time, set to 50 $\mu sec$ for the sake of fair comparison with the experimental results introduced in the following section.

First, the starting characteristics of the classical multi-objective fuzzy decision method with equal priority factors and the proposed method are illustrated. The scenario used is to start the motor from standstill to its reference speed. First, the flux is built then at $t = 0.1$ sec, the speed command is applied. At $t = 0.35$ sec, load torque of 2 Nm is applied. Figure 3-20 and Figure 3-21 shows the response for speed, torque, flux, and current respectively from top to bottom. Both methods have similar dynamic response. The steady state response of torque, flux, and current at the same previous operating point is illustrated in Figure 3-22 and Figure 3-23. Comparing the upper figures clearly demonstrates that the torque ripple is considerably reduced in the proposed method without affecting the flux ripple.

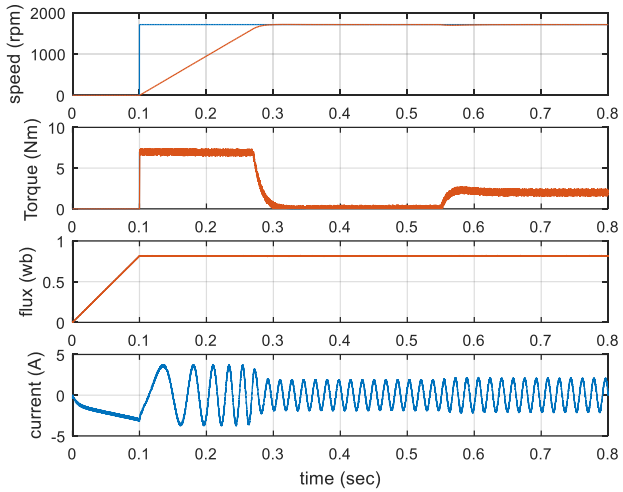


**Figure 3-20 Simulated starting and loading responses for FPTC method**

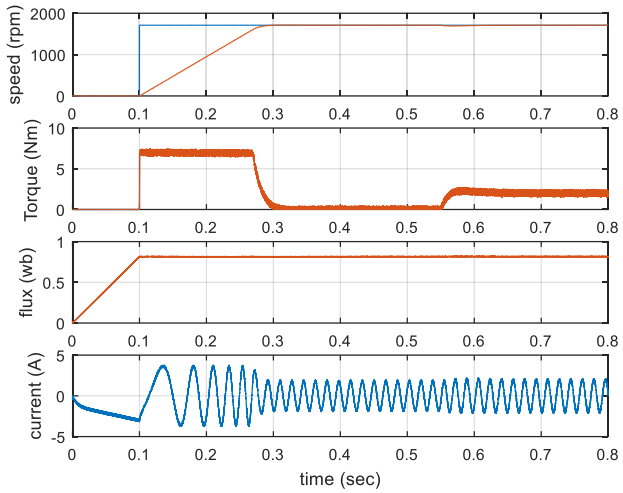


**Figure 3-21 Simulated starting and loading responses for MFPTC method**

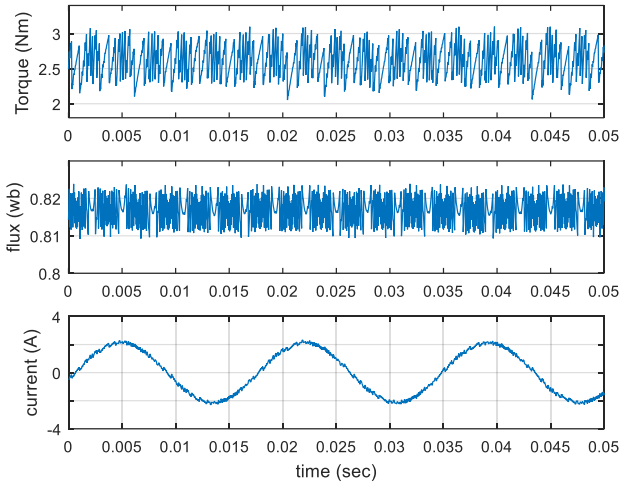


**Figure 3-22 Simulated steady state response at rated speed and 2 Nm load for FPTC method**

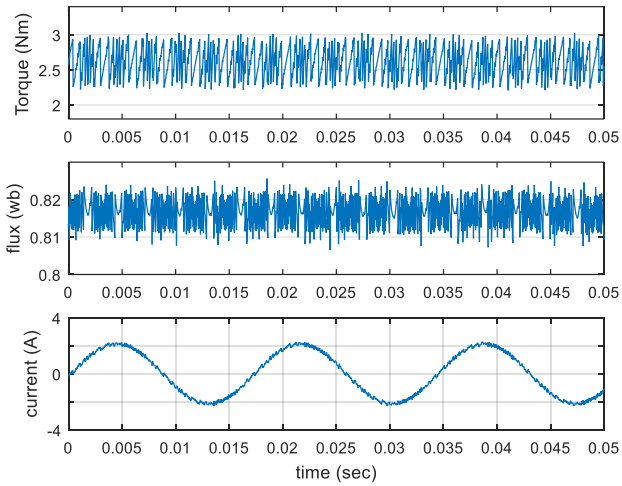


**Figure 3-23 Simulated steady state response at rated speed and 2 Nm load for MFPTC method**

### 3.4.4 Experimental Results

In order to validate the proposed method, the same previous tests are implemented using the developed experimental setup. dSPACE 1104 platform is for real time implementation. The execution time for the conventional method and for fuzzy decision based method are 37 and 43 $\mu sec$ respectively. Therefore, the sample time is set to 50 $\mu sec$ for all the methods. The same tests depicted in the simulation study are repeated. Figure 3-24 and Figure 3-25 illustrate the starting and loading response for FPTC and MFPTC methods respectively. As can be noted, the dynamic responses for both methods are similar and close to simulation results of Figure 3-20 and Figure 3-21. In addition, the steady state response is illustrated in Figure 3-26 and Figure 3-27. It is obvious that the torque ripple is reduced for the proposed method while the flux ripple is almost the same. This proves that the suggested modification can efficiently compromise between torque and flux ripple minimization.

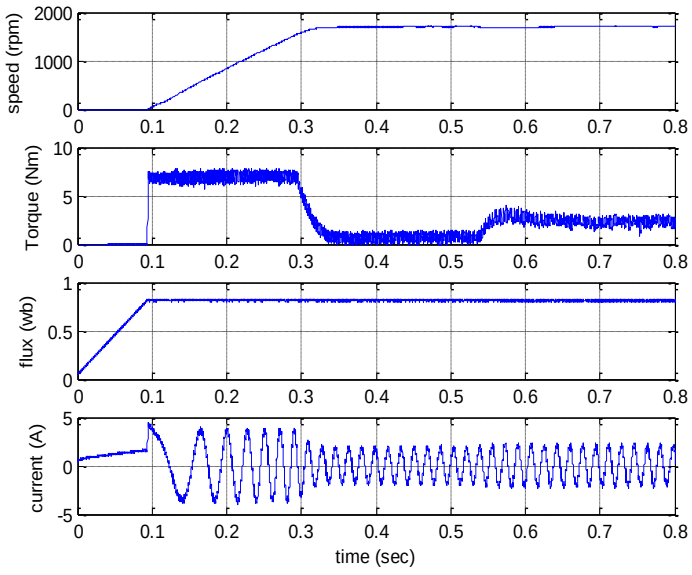


**Figure 3-24 Measured starting and loading responses for FPTC method**

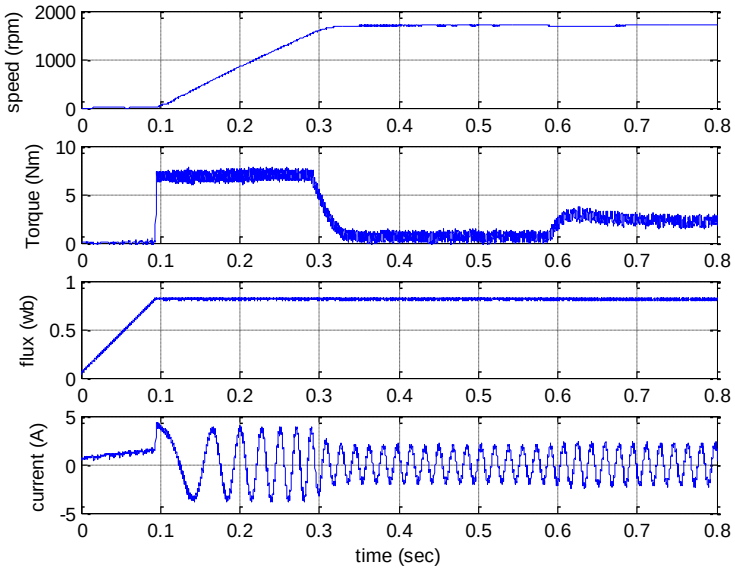


**Figure 3-25 Measured starting and loading responses for MFPTC method**

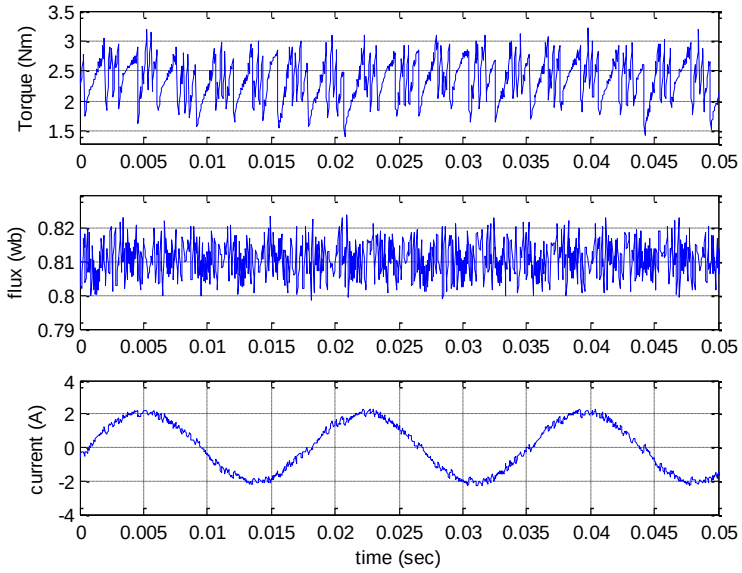


**Figure 3-26 Measured steady state response at rated speed and 2 Nm load for FPTC method**

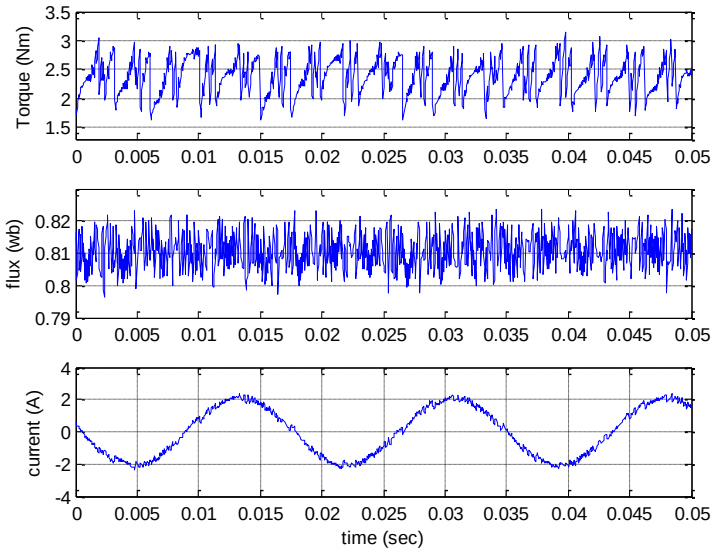


**Figure 3-27 Measured steady state response at rated speed and 2 Nm load for MFPTC method**

For further illustration, torque ripple, flux ripple, current total harmonic distortion (THD), and average switching frequency are used as comparison criteria among the conventional, multi-objective fuzzy decision, and the proposed method. Table 3-7 summarizes the results obtained at rated speed and 2 Nm load torque. The results demonstrate the ability of the proposed method to compromise between torque and flux ripple minimization. It can also be noted that there is a slight increase in flux ripple and current THD. The average switching frequency is so close for both methods and less than the conventional method.

**Table 3-7 performance Comparison at rated speed**

| Method | $T_{rip}(Nm)$ | $\psi_{rip}(wb)$ | $THD_{is}$ (%) | $f_{av}$ $(KHz)$ |
|---|---|---|---|---|
| Conventional | 0.8296 | 0.0151 | 4.28 | 2.2 |
| Fuzzy decision | 0.9181 | 0.0139 | 3.62 | 2.13 |
| Proposed method | 0.7978 | 0.0142 | 3.71 | 2.1 |

## 3.5 Conclusion

Flux weighting factor is an important design parameter in PTC of induction motor drive. Through this chapter five different methods recently reported in literature for weighting factor calculation are compared. The principles of each method were highlighted. Moreover deep analysis using torque ripple, flux ripple, current total harmonic distortion, and average switching frequency has been carried out at wide speed range.

It can be concluded that multi-objective based methods like fuzzy decision and VIKOR have a great potential and can facilitate the weighting-factor design process. Moreover, they still have the ability to give more importance to one cost function over the other. One the other hand, model predictive flux method can eliminate the weighting factor and yet results in good performance especially from the viewpoint of torque ripple and current total harmonic distortion compared to other methods. Generally, the weighting factor design is still an open problem. The reported methods in literature succeed to calculate the weighting factor and show good performance but with added complexity compared to the conventional method.

A modification for the multi-objective fuzzy decision making algorithm used to compute the flux-weighting factor is also proposed. The original method suffers from high torque ripple and needs extra priority factors, which increase the complexity of the technique. The reasons for this drawback are highlighted and a remedy is proposed by changing the way the membership function is calculated. The performance of the proposed method is validated experimentally and compared to the original multi-

objective method. The results demonstrate the effectiveness of the proposed method to select the voltage vector compromising between torque and flux ripple minimization.

# CHAPTER 4

# EFFICIENT PTC OF INDUCTION MOTOR DRIVE

This chapter introduces a simple and efficient predictive torque control (PTC) algorithm for induction motor (IM) drive. The proposed technique eliminates the need for flux weighting factor for the conventional PTC. Moreover, unlike the conventional method which needs to evaluate the cost function seven times each control sample, the proposed method needs only to test four voltage vectors (VVs) at each control sample which leads to a significant reduction in the computation time and switching frequency without sacrificing the performance. The effectiveness of the proposed method is demonstrated by both simulation and experimental results with comprehensive comparisons with the reported literature.

## 4.1 Limitation of PTC and review of reported solutions

Regardless the simplicity of FCS-MPC and its ability to handle nonlinearity and constrains, two main drawbacks are widely reported regarding its implementation [5]–[7]. In addition to the weighting factor selection problem discussed in details in previous chapters, the computation cost related to the prediction and optimization steps of the algorithm which grows rapidly if the number of admissible voltage vectors increases. This is typically the case for multi-phases and multi-level converters. Therefore, for these systems, even if a short prediction horizon is used, a long sampling period is unavoidable for the algorithm to select the optimal voltage vector among all the

available ones. Increasing the sampling period is reflected negatively on the quality of the controlled variable (torque, flux, and current).

Several solutions have been reported in literature to overcome these problems. For the reducing computation burden, mathematical techniques have been adopted to deal with long horizon prediction of multi-level inverters [44], [45]. Another trend is to try to use reduced number of voltage vectors for the prediction and optimization stages of PTC algorithm. In [46], it was suggested to use only four voltage vector among the available seven voltage vector of the two levels voltage source inverter (2L-VSI) for prediction and optimization. These four vectors are nominated at each control sample based on switching frequency reduction criterion. This method is characterized by noticeable reduction in the average switching frequency. However, the torque and flux ripple increased significantly compared to the conventional method. Similar idea is presented in [47] to use only three voltage vectors at each sample. These three vectors are selected based on the location of the stator flux vector and the sign of torque error. This technique results in reduction in the average switching frequency and renders good performance compared to the conventional method. In [48], the cost function was reformulated to include the difference between the reference and the candidate voltage vectors. Based on the location of the reference voltage, one zero and one active voltage vector are selected and evaluated. This method reduces the computation cost since the prediction needs to be executed only once to generate the reference voltage vector. It is more suitable for grid connected converters where the main control variable is the load current.

In this chapter, a simple yet an efficient PTC of three phase IM drive is proposed. The

proposed technique utilizes only four VVs at each control sample instead of the usual seven VVs used for 2L-VSI case. This not only results in reducing the computation burden and the average switching frequency but also maintains reduced values of torque and flux ripples. Moreover, the weighting factor elimination (WFE) method is used to eliminate the need for flux weighting factor design and update if the operating point changes.

The same steps of PTC explained in details in previous chapters are adopted. The only difference is how to design the cost function and number of iterations required for the optimization step, which will be demonstrated in the next section.

## 4.2 Proposed method

In this section, the superiority of the proposed method over the conventional one is discussed in terms of reducing the prediction and optimization steps and the weighting factor selection.

### 4.2.1 Reducing the computation burden

The 2L-VSI has seven different VVs to be evaluated in the conventional method. In the proposed method, a group of four VVs, $V_g$, will be evaluated each control sample and the optimal one will be selected. As a result, the computation burden of the prediction and optimization steps is reduced substantially. The group $V_g$ of the four VVs is updated each control sample based on the previous optimal VV and a predefined lookup table. Unlike [46], the proposed method is designed with two goals; reducing the switching frequency and maintaining good performance in terms of torque and flux ripples.

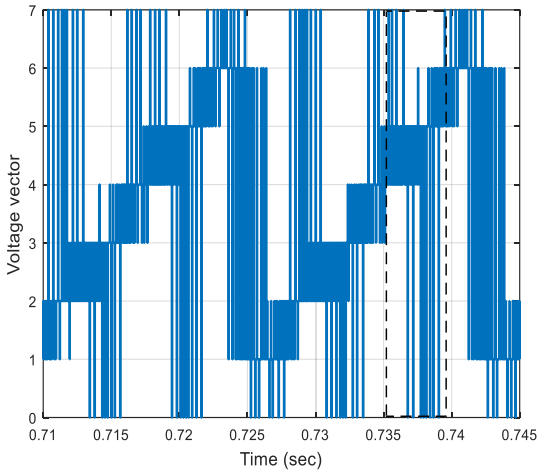


**(a)**

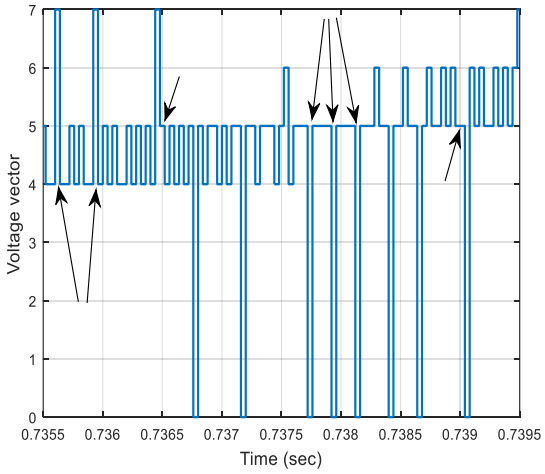


**(b)**

**Figure 4-1 Simulation of Switching vector selection for the conventional method at rated speed without load (a) Complete electrical cycle (b) Zoomed view**

The conventional PTC method is simulated and the optimal selected voltage vector at each sample is recorded Figure 4-1. From Figure 4-1 (a), it can be noted that there is a pattern where nonzero VVs are changing in a certain sequence. For example, the optimal VV changes between $V_1$ and $V_2$ in a period followed by that where $V_2$ or $V_3$ are always selected as the optimal VV and so on. Moreover, this pattern is repeated each electric cycle. In case, the zero voltage is selected to be the optimal VV, either $V_0$ or $V_7$ are selected based on reducing number of switches jump criterion. Final observation is illustrated in Figure 4-1 (b) which represents a zoomed view for the period highlighted

by the dashed rectangular in Figure 4-1 (a). If the previous VV was one of the zero VVs, there are two possibilities for the next optimal VV; either it returns to the last nonzero VV ($V_{NZ}$) or returns to a VV adjacent to $V_{NZ}$. These two cases are pointed at in Figure 4-1 (b) by arrows.

Based on the previous observations, the proposed method forms the candidate group $V_g$ based on the optimal VV of the previous sample $V_{old}$. If the previous VV is nonzero, $V_{old}$ will be used directly to select the candidate group. On the other hand, if $V_{old}$ is one of the zero VVs, $V_g$ will be selected based on $V_{NZ}$. Table 4-1 illustrates the voltage group formation based on either $V_{old}$ or $V_{NZ}$. After the candidate group $V_g$ is determined, the cost function will be evaluated for each of the four VVs included. This method will also result in reducing the average switching frequency since the VVs in the candidate group are different from the old VV by only one switch state as indicated in Table 4-1.

### 4.2.2 Cost function design

As discussed earlier, the design of the cost function and in particularly the flux weighting factor is not a trivial task since it greatly affects the overall performance of the motor [22], [26]. This will be even more obvious with the reduced number of voltage vectors.

**Table 4-1 Voltage group selection**

| $V_{old}$ OR $V_{NZ}$ | $V_g$ |
|---|---|
| $V_1$ | $[V_6\ V_1\ V_2\ V_0]$ |
| $V_2$ | $[V_1\ V_2\ V_3\ V_7]$ |
| $V_3$ | $[V_2\ V_3\ V_4\ V_0]$ |
| $V_4$ | $[V_3\ V_4\ V_5\ V_7]$ |
| $V_5$ | $[V_4\ V_5\ V_6\ V_0]$ |
| $V_6$ | $[V_5\ V_6\ V_1\ V_7]$ |

In order to avoid this complexity, the weighting factor elimination (WFE) method is used [49]. The procedure of this methods described in chapter two and repeated her for the convenience of the reader:

$$T = \frac{3}{2}\, n_p \lambda\, L_m\, (\psi_r \times \psi_s) \tag{4.1}$$

$$T^{ref} = \frac{3}{2}\, n_p \lambda\, L_m\, (\psi_r \times \psi_s^{ref}) \tag{4.2}$$

$$\psi_s^{ref} = \left\|\psi_s^{ref}\right\|.\exp(j\angle\psi_s^{ref}) \tag{4.3}$$

$$\angle\psi_s^{ref} = \angle\psi_r + \arcsin\left(\frac{T^{ref}}{\frac{3}{2} n_p \lambda\, L_m \|\psi_r^{k+2}\| \left\|\psi_s^{ref}\right\|}\right) \tag{4.4}$$

where $\lambda = \frac{1}{L_s L_r - L_m^2}$

A new cost function is formed that represents the deviation between the reference and predicted stator flux vectors.

$$g(V_s^{k+1}) = \left|\psi_s^{ref} - \psi_s^{k+2}\right| \tag{4.5}$$

The value of stator flux at step $k+2$ can be calculated as follows:

$$\psi_s^{k+2} = \psi_s^{k+1} + T_s\, (V_s^{k+1} - R_s\, i_s^{k+1}) \tag{4.6}$$

where $V_s^{k+1}$ represents one of the candidate VV. The last step is to select the VV that minimizes the cost function among the candidate group $V_g$ as follows:

$$V_{opt} = \arg\min_{\{V_g\}} g(V_s^{k+1}) \tag{4.7}$$

### 4.2.3 Proposed control algorithm

The proposed algorithm can be summarized in the following steps, which also illustrated in the flowchart shown in Figure 4-2.

Step 1: Initialize $V_{old} = 0, V_{NZ} = 1, V_{opt} = 0$

Step 2: Apply $V_{opt}$

Step 3: Measure stator current and DC link voltage and rotor speed

Step 4: Estimate rotor flux using

Step 5: Predict one step ahead using

Step 6: Compensate for calculation delay using

Step 7: Calculate reference stator flux vector

Step 8: Check if $V_{old}$ is zero or nonzero VV then use Table 4-1 to determine the candidate VV group $V_g$

Step 9: Update $V_{old}$ by value of $V_{opt}$

Step 10: If $V_{opt}$ is a nonzero VV update $V_{NZ}$

Step 11: Calculate the cost function four different times for each VV included in the selected $V_g$

Step 12: Determine the new optimal VV

The execution of the algorithm should continue repeating steps 2 to 12.

For the sake of comparison, the performance of the proposed method will be assessed in the following sections versus the conventional method and the reduced switching frequency (RSF) method reported in [46]. The latter aims to reduce the average switching frequency by limiting the selection of the optimal voltage vector to those with minimum number of switching jumps [13]. In this case, the conventional cost function is repeated only four times based on a preselected four VVs. These VVs are updated each control sample based on the previous optimal VV such that at most one of the three

states $(S_a, S_b, S_c)$ is allowed to change. For example if the previous optimal VV is (1,0,0), the four allowable VVs are (1,0,0), (1,1,0), (1,0,1), (0,0,0). This method leads to reduction in the computation burden and the average switching frequency. However, the torque and flux ripples deteriorate compared to the conventional method [46].

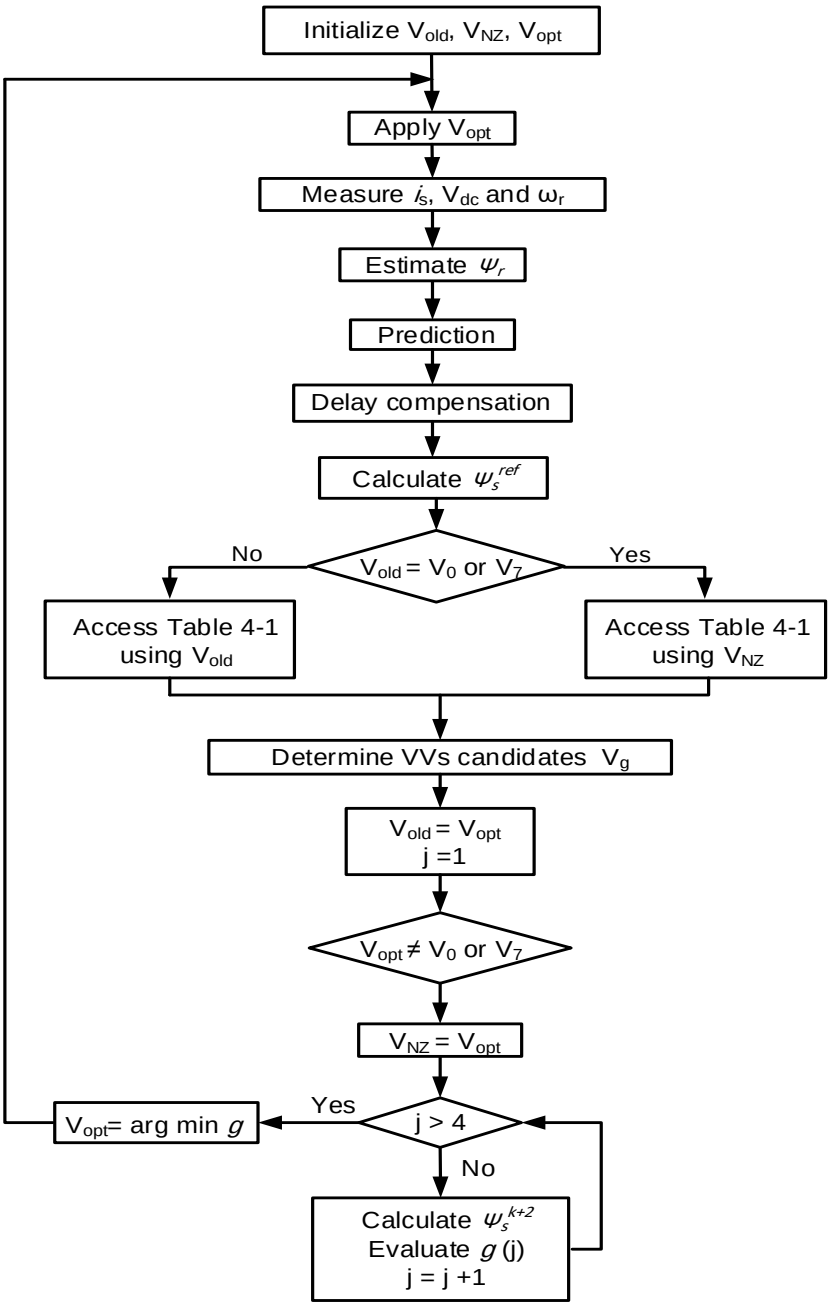


**Figure 4-2 Flowchart of the proposed method**

## 4.3 Simulation results

The proposed method is simulated using MATLAB Simulink environment. For the sake of comparison, the reduced switching frequency (RSF) [46] with one step prediction and the conventional method are also simulated using the same flux weighting factor. The same machine and controller parameters used as the previous chapters. Firstly, the flux is built to its rated value then the speed command is applied at $t = 0.1$ sec. Finally, at $t = 0.5$ sec, rated load is applied. The same PI controller gains for the outer speed loop is used for all methods. Figure 4-3 illustrates the dynamic response of the IM drive system for all methods where speed, torque, flux and phase current are presented. The responses shown in Figure 4-3 indicate that the proposed method has fast dynamic response and robustness against external load disturbance. It can also be noted that from the viewpoint of dynamics, the responses of all the methods are comparable.

## 4.4 Experimental Results

The developed test bench described earlier is used to validate the proposed method. The PTC algorithm is implemented in real time using dSPACE 1103 (1 GHz) platform. The sample time for all the algorithms is set to 40 $\mu$sec. The speed is measured using a 1024 pulse per revolution incremental encoder and a low pass filter is adopted to reduce the quantization error.

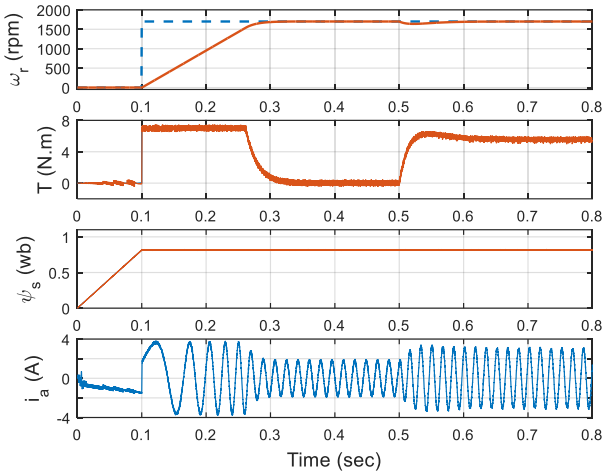


**(a)**

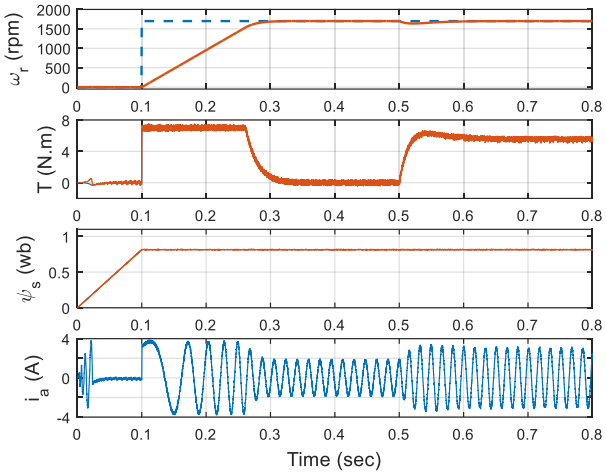


**(b)**

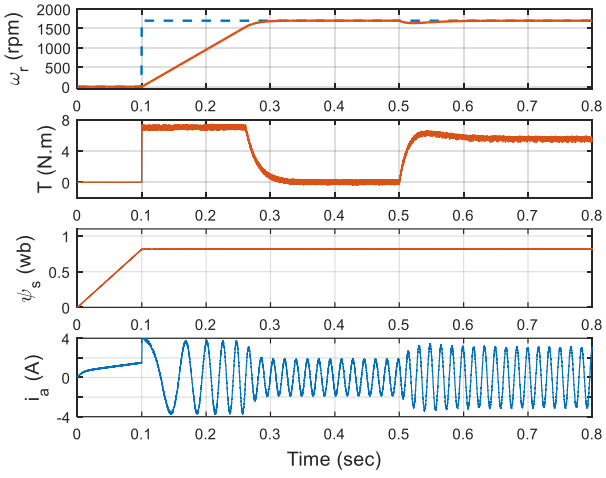


**(c)**

**Figure 4-3 Simulated starting and loading response (a) Conventional method (b) RSF method and (c) Proposed method**

### 4.4.1 Dynamic characteristics

Figure 4-4 shows the motor starting from standstill to the rated speed using the conventional and proposed methods. The same pre-excitation process depicted in the simulation section is used. Both the conventional method and the proposed method has similar starting responses. As it can be noted in Figure 4-4 decoupled control of torque and flux is achieved in the proposed method. This way, the same performance of the conventional method is maintained with simpler design of the cost function due to elimination of flux weighting factor.

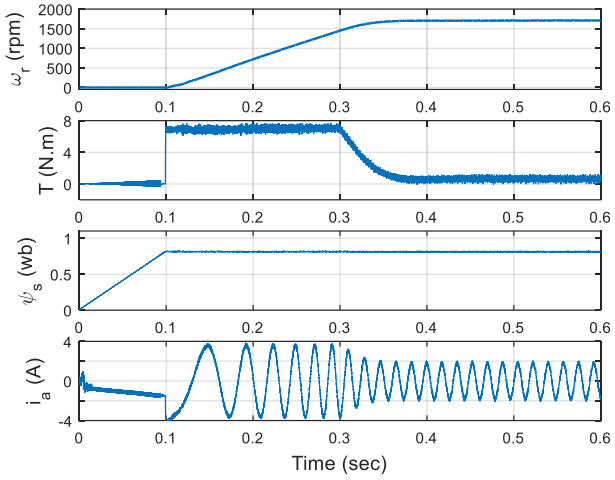


**(a)**

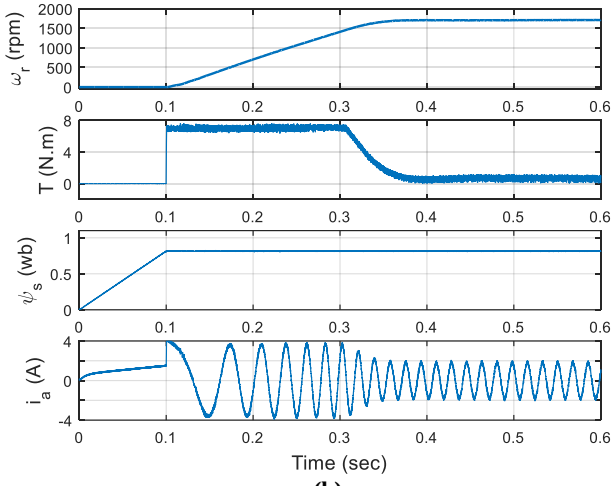


**(b)**

**Figure 4-4 Measured starting from zero to rated speed at no-load using (a) Conventional method (b) Proposed method**

In order to test the robustness against external load, the rated load is applied to the motor while running at rated speed. Figure 4-5 shows the sudden loading response for the conventional and the proposed method. The proposed method successfully regains its reference speed after a short transient period in a manner similar to the conventional method proving its robustness against load disturbance.

Finally, a speed reversal test is implemented. Figure 4-6 demonstrates the speed reversal from 1710 to -1710 rpm at no-load condition for the conventional, RSF [46], and the proposed methods respectively.

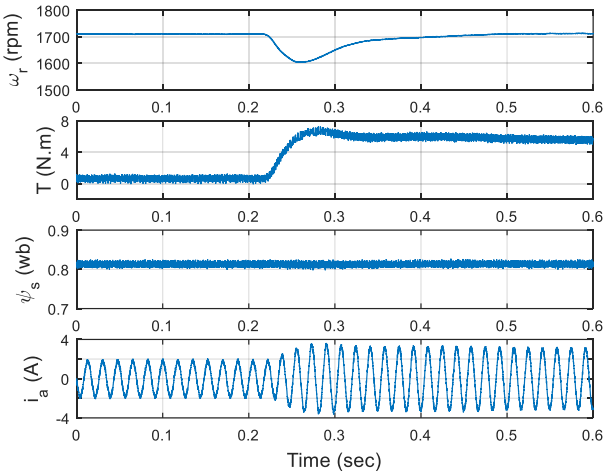


**(a)**

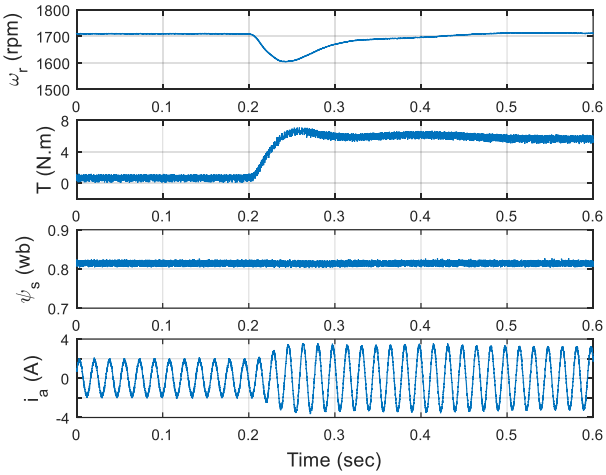


**(b)**

**Figure 4-5 Measured Sudden rated load response at rated speed using (a) Conventional method (b) Proposed method**

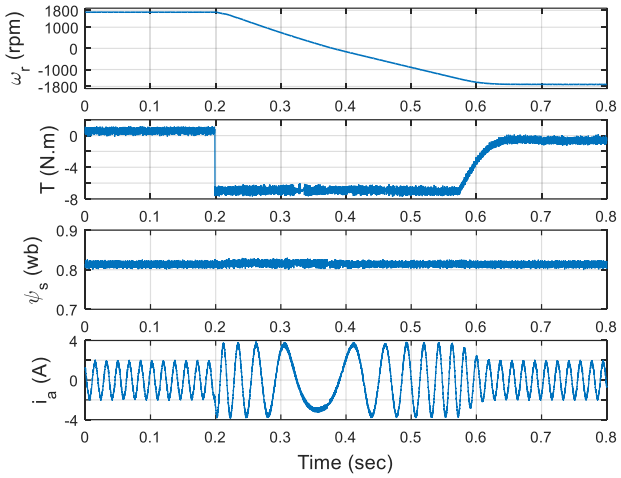


**(a)**

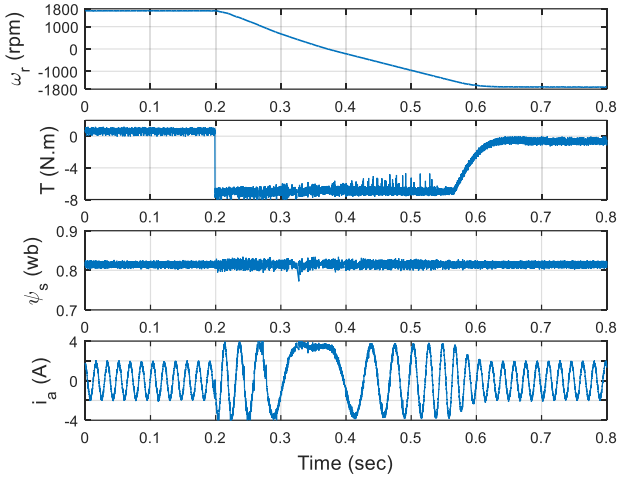


**(b)**

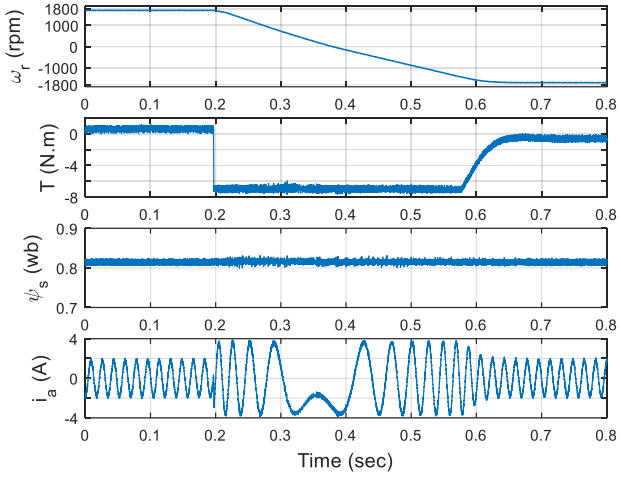


**(c)**

**Figure 4-6 Measured speed reversal response at 1710 rpm and no-load condition (a) Conventional method (b) RSF method(c) Proposed method**

For the proposed and conventional methods, it can be noted that the flux is fixed to its rated value during all the transient period proving the decoupled effect between flux and torque control. On the other hand, the flux ripple, torque ripple, and current distortion increase significantly with the RSF method. Similar response was reported in [46]. This indicates that the RSF cannot work properly at low speed high torque operating point where further tuning for the flux-weighting factor is required. The torque response for the proposed method is uniform. This is due to the weighting factor elemination method utilized in the proposed approach which automatically compromise between torque and flux errors

### 4.4.2 Steady state analysis

For further comparison among the three methods, deeper steady state analysis is presented. Figure 4-7 illustrates the low speed operation at 50 rpm and no-load condition. It can be clearly noticed that the RSF has the worst response with the highest torque ripple and most distorted current waveform. The proposed method has lower torque and flux ripple than the conventional method. In addition, the current waveform is uniform and sinusoidal unlike the distorted waveform, which can be observed in the RSF method current waveform.

In order to cover different operating points, the response of the three methods have been recorded at different speed and (2.5 Nm) load. Torque ripple, flux ripple, current THD, and average switching frequency are calculated and the results are listed in Table 4-2. Analysis of the third column in Table 4-2 clearly indicates that the proposed method is superior regarding the torque ripple for all the speed range.

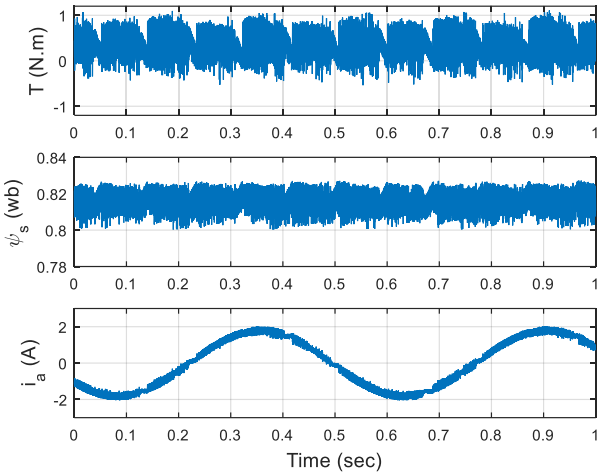


**(a)**

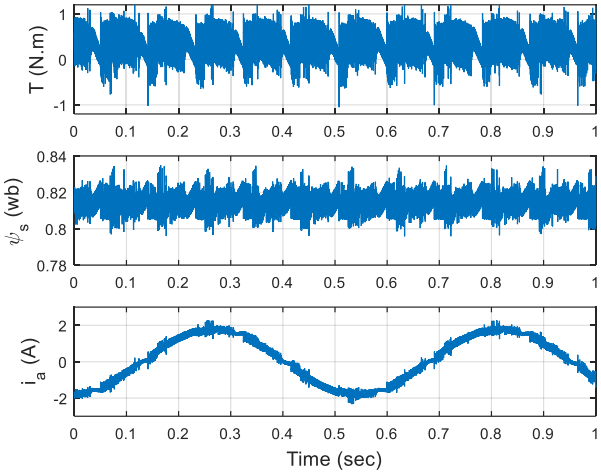


**(b)**

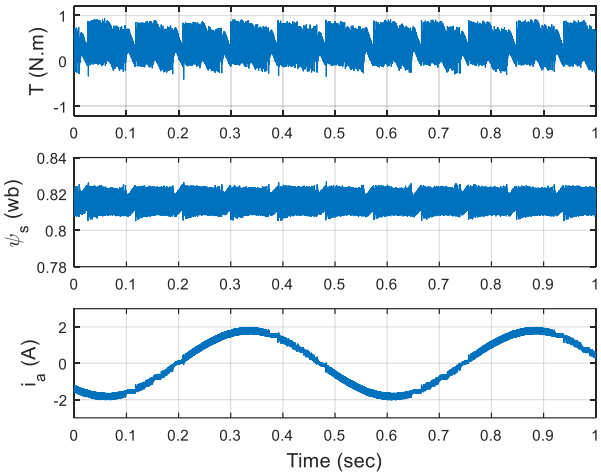


**(c)**

**Figure 4-7 Measured low speed response at 50 rpm and no-load condition (a) Conventional method (b) RSF method (c) Proposed method**

**Table 4-2 Performance comparison among three PTC methods at 2.5 Nm**

| $N\ (rpm)$ | Method | $T_{rip}\ (Nm)$ | $\psi_{rip}\ (wb)$ | $f_{av}\ (KHz)$ | $i_{THD}$ % |
|---|---|---|---|---|---|
| 300 | Conv | 0.813 | 0.012 | 4.24 | 6.93 |
| | RSF | 0.895 | 0.019 | 2.31 | 9.69 |
| | Proposed | 0.761 | 0.014 | 2.53 | 7.26 |
| 600 | Conv | 0.718 | 0.012 | 5.50 | 6.36 |
| | RSF | 0.789 | 0.017 | 2.89 | 9.91 |
| | Proposed | 0.621 | 0.015 | 4.13 | 6.99 |
| 1000 | Conv | 0.807 | 0.012 | 5.11 | 6.15 |
| | RSF | 0.775 | 0.018 | 3.52 | 10.38 |
| | Proposed | 0.646 | 0.013 | 4.44 | 6.64 |
| 1400 | Conv | 0.724 | 0.012 | 3.76 | 6.42 |
| | RSF | 0.711 | 0.014 | 3.34 | 8.59 |
| | Proposed | 0.573 | 0.013 | 3.49 | 6.63 |
| 1710 | Conv | 0.703 | 0.013 | 2.67 | 7.21 |
| | RSF | 0.665 | 0.012 | 2.66 | 7.21 |
| | Proposed | 0.618 | 0.011 | 2.54 | 6.95 |

The flux ripple of the proposed method is comparable to the conventional method and shows a slight increase at some operating speed. It is still much lower than the flux ripple measure for RSF method. As expected from the algorithm design of the proposed and RSF methods, both of them have lower average switching frequency compared to the conventional method as can be observed from the measured average switching frequency in Table 4-2. Although there is a little increase in the average switching frequency of the proposed method compared to RSF, the reduction of the torque and flux ripples is quite evident. It can be also noted that proposed method has a little higher THD values compared to the conventional method. This can be expected due to the reduced average switching frequency of the proposed method. It is well known that THD and switching frequency are inversely proportional to each other [50].

**Table 4-3 Performance comparison for the thee PTC method at Rated Speed (1710 rpm) and rated load torque (5.58 Nm)**

| | $T_{rip}\ (Nm$ | $\psi_{rip}\ (Wb)$ | $f_{av}\ (KHz)$ | $i_{THD}\ \%$ |
|---|---|---|---|---|
| Conventional | 0.629 | 0.0135 | 2.70 | 4.41 |
| RSF | 0.602 | 0.0122 | 2.66 | 4.54 |
| Proposed | 0.549 | 0.0140 | 2.78 | 4.38 |

**Table 4-4 Computation times for different PTC methods**

| Method | Pred &opt ($\mu$sec) | Total ($\mu$sec) |
|---|---|---|
| Conventional | 1.9 | 10.3 |
| RSF | 1.23 | 9.51 |
| Proposed | 1.56 | 9.87 |

On the other hand, the RSF method has the worst current THD since its deteriorated flux response is reflected on the current waveform this can be observed clearly also from Figure 4-7 (b) at low speed operating point.

Due to hardware limitation, the rated torque can not be applied at low speed. Therefore, the same comparison criteria are calculated and listed in Table 4-3 when the motor is running at rated speed and rated load condition. From Table 4-3 it can be noted that proposed method has the lowest torque ripple. The proposed method has the lowest current THD among the three method.

Finally, the average execution time of the three method is recorded in

Table 4-4. Since the methods differ only in the prediction and optimization steps, only the sum of prediction and optimization steps and total execution times are reported. The RSF method has the shortest execution time since it needs to repeat the prediction and optimization steps four times only. The conventional method has the longest execution time as expected with seven iteration required to finish the prediction and optimization steps. Although proposed method needs only four iteration for prediction

and optimization, it has longer execution time compared to the RSF method. This is due to the time required for reference flux vector calculation, which is necessary for eliminating the need for flux weighting factor. Even though the execution time is still less than that of the conventional method as indicated in Table 4-4. Actually, about 18 % reduction in the execution time can be achieved using the proposed method compared to the conventional one.

# CHAPTER 5

# Modeling and Parameter Identification of Six phase Induction motor

Application of MPC in higher order induction motor drives is one of the main objectives of this work. Since the structure of the six-phase machines is quite different from the three-phase ones, a detailed description about modeling and parameter identifications is provided in this chapter. The stator leakage mutual inductance is a commonly neglected in six-phase IM models. An accurate parameter identification method is considered to separate the stator leakage mutual inductance and rotor leakage inductance.

## 5.1 Background

The potential of multiphase machines was demonstrated since sixties of the last century. They are characterized by reduced current and torque harmonics, reduced current magnitude per phase, reduced dc link current harmonics, high reliability and high power to volume ratio [32], [51], [52]. The last two decades witness a growing interest in multiphase machines. Their advantages make them suitable for electric/hybrid vehicles, aerospace applications and ship propulsion. Recently, it is also utilized in power generation in particular wind energy conversion systems[53]–[57].

Multiphase machines can be realized as induction or synchronous machines [32]. The stator of multiphase machines consists of $n$ distributed phase windings. Although odd

prime number of phases (5, 7, 11, …) are common [58]–[62], industry prefers the use of number of phases $n = 3k$ where $(k = 2,3,4, ...)$ [51], [63], [64]. In the latter cases, the stator windings can be considered as multiple three-phase windings. This facilitates the design and control of these machines as it manufactured utilizing the stator of existing three-phase machines. Moreover, using suitable modelling method, well established control methods like field oriented control (FOC) and direct torque control (DTC) can be adopted after some necessary modifications [32], [51].

Similar to three-phase machines, multiphase induction machines are the most commonly used and investigated in literature [51], [63] because of its robustness, lower cost and less maintenance. Among different designs of multiphase machines, the five and six phases are the widely used in different applications. As mentioned earlier, number of stator slots required for five-phase machines design and manufacture is not common for commercial three phase ones. So, to realize five-phase winding either special stator lamination should be manufactured [65] or in some cases on-shelf three phase stator winding can be used leaving a number of stator slots empty which of course will affect the magnetic motive force (MMF) distribution in the airgap. On the other hand, design and implementation of six-phase windings are much easier. Only number of pole pairs may be required to be changed in order to realize the required phase shifts between different distributed phases [66]. Based on the phase shift between the two three phase sets of the six-phase machines, they can be classified as symmetric and asymmetric for phase shifts of 60 and 30 degree respectively [67] as illustrated in Figure 5-1.

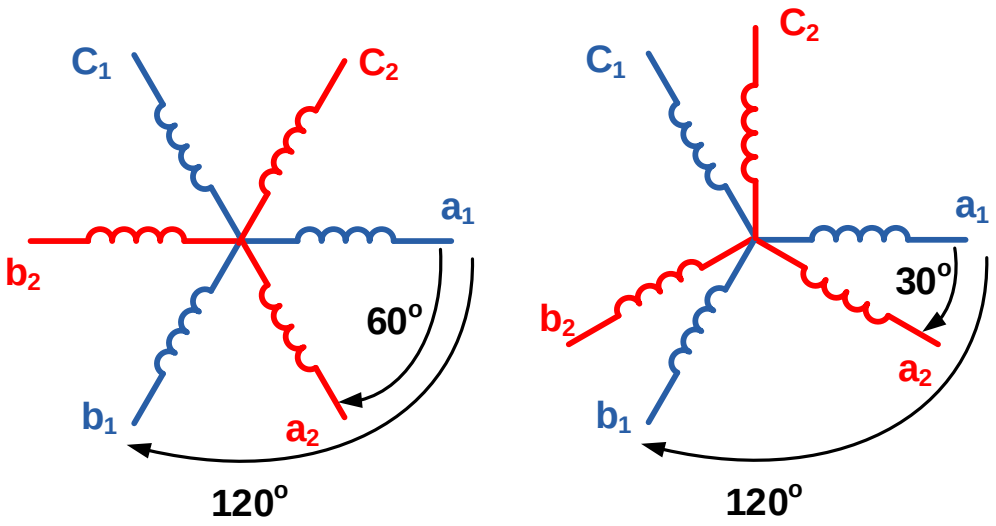


**Figure 5-1 Spatial distribution of stator winding in (a) Symmetric (b) Asymmetric six-phase IM**

The asymmetric six-phase IM has the advantage of lower airgap MMF distribution compared to the symmetric one [66]. Therefore, the resultant torque harmonic in particular the fifth and seven harmonic is reduced for asymmetric six-phase IM. Based on the previous discussion, asymmetric six-phase induction motor will be considered through this work.

## 5.2 Modeling of six-phase induction motor drive

The construction of six-phase IM is similar to the three-phase one. They have the same rotor and stator core just different phase windings. As a result, the same mathematical modelling principles of the three-phase machines applies for the six-phase under the common assumption of sinusoidal winding distribution, constant airgap and neglecting saturation and core losses [63].

### 5.2.1 Six-phase induction motor

Many attempts have been reported for modelling of multi-phase machines in general or for specific type or number of phases [68]–[76]. Two different modelling approaches can be distinguished; double d-q model and voltage space decomposition (VSD).

Double d-q model method

In this approach the machine is represented by two stator circuits and the rotor is assumed to be equivalent to three-phase wound rotor [72]–[74]. Figure 5-2 illustrates the single-phase equivalent circuit in the stationary reference frame. It can be noted that the stator leakage mutual inductance is included even it is common to be neglected in literature for the sake of simplicity.

First two separate decoupling transformations applied to the two winding sets of the six-phase machine considering the $30^o$ phase shift between the two sets.

$$T_1 = \frac{2}{3}\begin{bmatrix} 1 & -\frac{1}{2} & -\frac{1}{2} \\ 1 & \frac{\sqrt{3}}{2} & -\frac{\sqrt{3}}{2} \end{bmatrix} \tag{5.1}$$

$$T_2 = \frac{2}{3}\begin{bmatrix} \frac{\sqrt{3}}{2} & -\frac{\sqrt{3}}{2} & 0 \\ \frac{1}{2} & \frac{1}{2} & -1 \end{bmatrix} \tag{5.2}$$

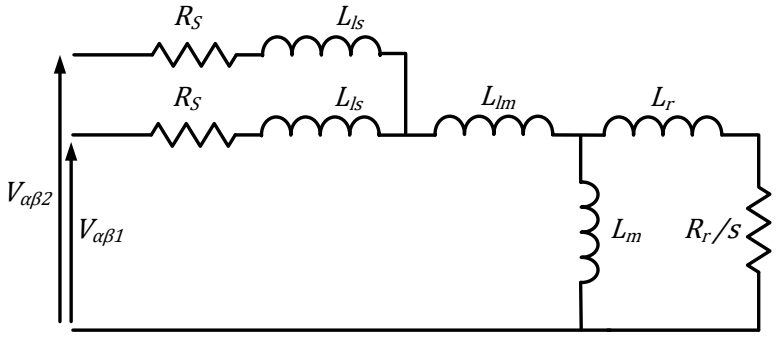


**Figure 5-2 Equivalent circuit of six-phase IM using d-q model approach**

Then the new variables can be computed as

$$x_{\alpha\beta 1} = T_1\, x_{a_1 b_1 c_1} \tag{5.3}$$

$$x_{\alpha\beta 2} = T_1\, x_{a_2 b_2 c_2} \tag{5.4}$$

where $x$ represents any quantities like voltage, current or flux. $(a_1 b_1 c_1)$ and $(a_2 b_2 c_2)$ are the three phases of the first and second sets respectively as shown in Figure 5-1. Based on the equivalent circuit of Figure 5-2, the machine model can be represented in the stationary reference frame as follows:

$$\left.\begin{aligned} v_{s1} &= R_s\, i_{s1} + p\, \lambda_{s1} \\ v_{s2} &= R_s\, i_{s2} + p\, \lambda_{s2} \\ 0 &= R_r\, i_r + p\, \lambda_r - j\, \omega_r\, \lambda_r \end{aligned}\right\} \tag{5.5}$$

$$\left.\begin{aligned} \lambda_{s1} &= L_{ls}\, i_{s1} + L_{lm}\,(i_{s1} + i_{s2}) + L_m(i_{s1} + i_{s2} + i_r) \\ \lambda_{s2} &= L_{ls}\, i_{s2} + L_{lm}\,(i_{s1} + i_{s2}) + L_m(i_{s1} + i_{s2} + i_r) \\ \lambda_r &= L_{lr}\, i_r + + L_m(i_{s1} + i_{s2} + i_r) \end{aligned}\right\} \tag{5.6}$$

$$T_e = \frac{3}{2}\frac{P}{2}\frac{L_m}{L_r}\left(\lambda_r \times (i_{s1} + i_{s2})\right) \tag{5.7}$$

where $v_{si} = [v_{\alpha si}\ v_{\beta si}]^T$, $i_{si} = [i_{\alpha si}\ i_{\beta si}]^T$, $\lambda_{si} = [\lambda_{\alpha si}\ \lambda_{\beta si}]^T$, $\lambda_r = [\lambda_{\alpha r}\ \lambda_{\beta r}]^T$, $i_r = [i_{\alpha r}\ i_{\beta r}]^T$ and $i = [1,2]$. $R_s$ and $R_r$ are stator and rotor resistances, respectively. $L_{ls}$ and $L_{lr}$ are stator and rotor leakage inductances, respectively. $L_m$ is the mutual inductance and $L_{lm}$ is stator leakage mutual inductance. $\omega_r$ is electrical rotor speed. $j = \begin{bmatrix} 0 & -1 \\ 1 & 0 \end{bmatrix}$.

Voltage space decomposition (VSD) method

The double d-q methods suffers from the coupling between the two transformed planes $(\alpha\beta_1)$ and $(\alpha\beta_2)$. This complicated the analysis and controller design for the six-phase

IM. In order to overcome this drawback the VSD was presented in [75]. This method is not based on physical interpretation like the double d-q method. It is a mathematical transformation aims to transform the variable in the original spaces to six dimension orthogonal spaces. The new spaces forms three decoupled planes commonly referred as $(\alpha-\beta)$, $(x-y)$ and $(z_1-z_2)$. Besides being decoupled, it can be proved that only $(\alpha-\beta)$ plane is involved in the electromagnetic conversion [75]. This greatly simplifies the analysis and control of the motor as the equivalent circuit representing the variables mapped to this plane is similar to that of the three-phase machine. The transformation matrix used for VSD can be expressed as follows:

$$T_6 = \frac{1}{3}\begin{bmatrix} 1 & \cos(4\theta) & \cos(8\theta) & \cos(\theta) & \cos(5\theta) & \cos(9\theta) \\ 0 & \sin(4\theta) & \sin(8\theta) & \sin(\theta) & \sin(5\theta) & \sin(9\theta) \\ 1 & \cos(8\theta) & \cos(4\theta) & \cos(5\theta) & \cos(\theta) & \cos(9\theta) \\ 0 & \sin(8\theta) & \sin(4\theta) & \sin(5\theta) & \sin(\theta) & \sin(9\theta) \\ 1 & 1 & 1 & 0 & 0 & 0 \\ 0 & 0 & 0 & 1 & 1 & 1 \end{bmatrix} \tag{5.8}$$

where $\theta$ represents the angular displacement between the two three-phase sets. For asymmetric six phase IM, $\theta = 30^o$. Then the transformation matrix can be represented as follows:

$$T_6 = \frac{1}{3}\begin{bmatrix} 1 & -\frac{1}{2} & -\frac{1}{2} & \frac{\sqrt{3}}{2} & -\frac{\sqrt{3}}{2} & 0 \\ 0 & \frac{\sqrt{3}}{2} & -\frac{\sqrt{3}}{2} & \frac{1}{2} & \frac{1}{2} & -1 \\ 1 & -\frac{1}{2} & -\frac{1}{2} & -\frac{\sqrt{3}}{2} & \frac{\sqrt{3}}{2} & 0 \\ 0 & -\frac{\sqrt{3}}{2} & \frac{\sqrt{3}}{2} & \frac{1}{2} & \frac{1}{2} & -1 \\ 1 & 1 & 1 & 0 & 0 & 0 \\ 0 & 0 & 0 & 1 & 1 & 1 \end{bmatrix} \tag{5.9}$$

Then the new transformed variables can be obtained as:

$$\begin{bmatrix} X_\alpha \\ X_\beta \\ X_x \\ X_y \\ X_{z1} \\ X_{z2} \end{bmatrix} = T_6 \begin{bmatrix} X_{a1} \\ X_{b1} \\ X_{c1} \\ X_{a2} \\ X_{b2} \\ X_{c2} \end{bmatrix} \tag{5-10}$$

Where $X$ can represents voltage, current or flux linkage variables. Applying this transformation to the original variables the following model is obtained.

$$\left.\begin{aligned} v_{\alpha\beta s} &= R_s\, i_{\alpha\beta s} + p\, \lambda_{\alpha\beta s} \\ v_{xy} &= R_s\, i_{xy} + p\, \lambda_{xy} \\ v_{z1z2} &= R_s\, i_{z1z2} + p\, \lambda_{z1z2} \\ 0 &= R'_r\, i_r + p\, \lambda_r - j\, \omega_r\, \lambda_r \end{aligned}\right\} \tag{5.11}$$

$$\left.\begin{aligned} \lambda_{\alpha\beta s} &= (L_{ls} + L'_{lm} + L'_m)\, i_{\alpha\beta s} + L'_m\, i_r) \\ \lambda_{xy} &= L_{ls}\, i_{xy} \\ \lambda_{z1z2} &= L_{ls}\, i_{z1z2} \\ \lambda_r &= L'_m\, i_{\alpha\beta s} + (L'_{lr} + L'_m)\, i_r \end{aligned}\right\} \tag{5.12}$$

$$T_e = \frac{3}{2}\frac{P}{2}\frac{L'_m}{L'_r}\left(\lambda_r \times i_{\alpha\beta s}\right) \tag{5.13}$$

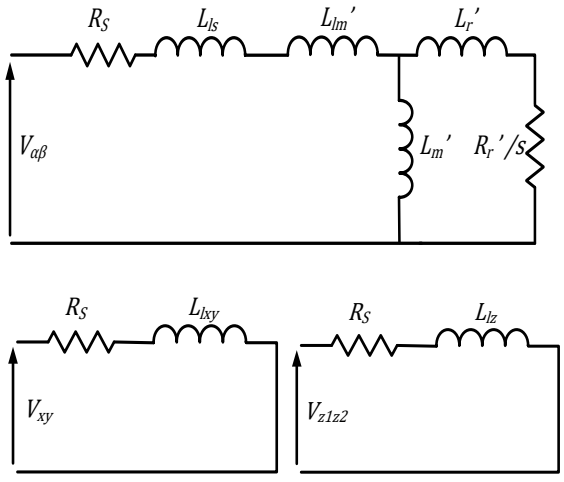


**Figure 5-3 Equivalent circuits of six-phase IM using VSD approach**

where $v_{\alpha\beta s} = [v_{\alpha s}\ v_{\beta s}]^T, v_{xy} = [v_x\ v_y]^T,\ v_{z1z2} = [v_{z1}\ v_{z2}]^T\ \ i_{\alpha\beta s} = [i_{\alpha s}\ i_{\beta s}]^T,\ i_r = [i_{\alpha r}\ i_{\beta r}]^T,\ \ i_{xy} = [i_x\ i_y]^T,\ \ i_{z1z2} = [i_{z1}\ i_{z2}]^T,\ \ \lambda_{\alpha\beta s} = [\lambda_{\alpha s}\ \lambda_{\beta s}]^T,\ \ \lambda_r = [\lambda_{\alpha r}\ \lambda_{\beta r}]^T,\ \lambda_{xy} = [\lambda_x\ \lambda_y]^T, \lambda_{z1z2} = [\lambda_{z1}\ \lambda_{z2}]^T$. In order to maintain equivalence between the double d-q and VSD methods, the following relations holds [63],[77].

$$\left.\begin{aligned} L_{lm} &= 2\,L'_{lm} \\ L_m &= 2\,L'_m \\ L_r &= 2\,L'_r \\ R_r &= 2\,R'_r \end{aligned}\right\} \tag{5.14}$$

The equivalent circuits representing the six-phase IM using VSD are illustrated in Figure 5-3.

### 5.2.2 Six-phase voltage source inverter

In order to drive the six-phase IM, two 2L-VSI are required. The two inverters can either be connected in series [78] or connected in parallel to the dc link. The latter is the most common in literature and is adopted through this work. Figure 5-4 illustrates the schematic of the connection of the two inverters used. As it can be noted, the system now consists of six states. As a result, there are 64 ($2^6$) possible output voltage vectors.

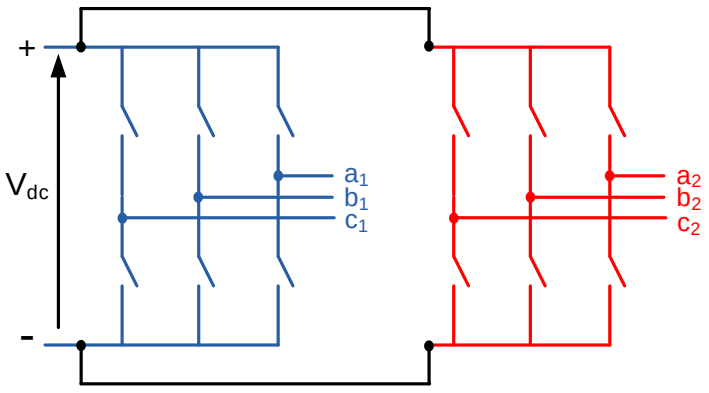


**Figure 5-4 Schematic diagram for inverters used for driving the six-phase IM**

The switching state of each leg of the inverter is defined as $S_i$, where $S_i = 1$ if the upper switch is ON and $S_i = 0$ if the upper switch is OFF. Defining the switching state as a vector $[S] = [S_{a1}\ S_{b1}\ S_{c1}\ S_{a2}\ S_{b2}\ S_{c2}]^T$. The output voltage of the inverter can be calculated as follows:

$$\begin{bmatrix} v_{a1} \\ v_{b1} \\ v_{c1} \\ v_{a2} \\ v_{b2} \\ v_{c2} \end{bmatrix} = \frac{V_{dc}}{3} \begin{bmatrix} 2 & -1 & -1 & 0 & 0 & 0 \\ -1 & 2 & -1 & 0 & 0 & 0 \\ -1 & -1 & 2 & 0 & 0 & 0 \\ 0 & 0 & 0 & 2 & -1 & -1 \\ 0 & 0 & 0 & -1 & 2 & -1 \\ 0 & 0 & 0 & -1 & -1 & 2 \end{bmatrix} [S] \tag{5.15}$$

By applying the VSD method. The mapping of the inverter output voltages to the new subspaces can be realized using $T_6$ as follows.

$$\begin{bmatrix} v_{\alpha} \\ v_{\beta} \\ v_{x} \\ v_{y} \\ v_{z1} \\ v_{z2} \end{bmatrix} = T_6 \begin{bmatrix} v_{a1} \\ v_{b1} \\ v_{c1} \\ v_{a2} \\ v_{b2} \\ v_{c2} \end{bmatrix} \tag{5.16}$$

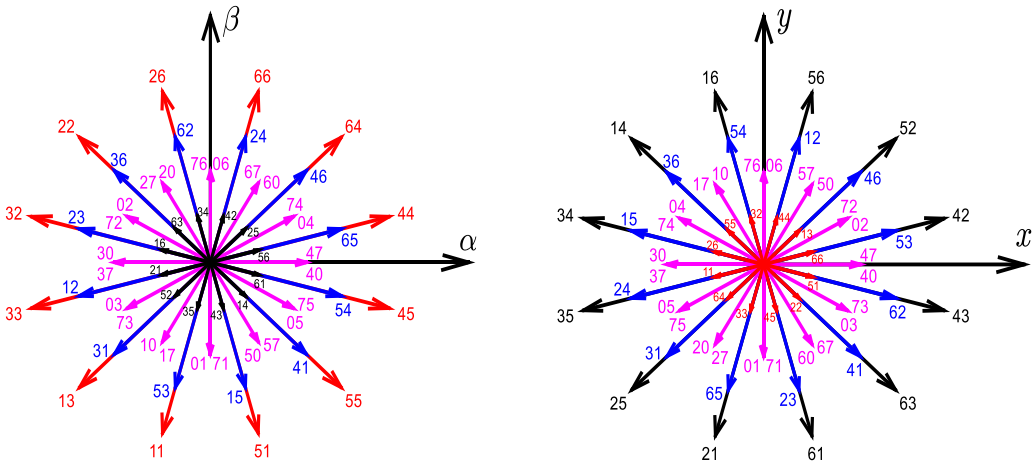


**Figure 5-5 Mapping of voltage space vectors to $\alpha\beta$ and $xy$ subspaces for six-phase inverter**

If the two neutral points of the two three-phase sets of the IM are isolated, the currents in $Z_1 - Z_2$ plane is zero. Therefore, the mapping to this subspace is not of importance and can be neglected. Figure 5-5 demonstrates the mapping of different voltage vectors (VVs) to $\alpha\beta$ and $xy$ subspaces where the associated numbers is the decimal conversion of the binary number define by the value of each switch ($S_{a1}\ S_{b1}\ S_{c1}\ S_{a2}\ S_{b2}\ S_{c2}$). It can be noted that the large VVs in $\alpha\beta$ plane are mapped to small VVs in the $xy$ plane and vice versa.While the medium and large-medium VVs have the same magnitude in both subspace but with different directions.

## 5.3 Parameter identification of six-phase induction motor

The next step towards developing the six-phase drive system is the parameter identification of the motor. The parameter identification for three-phase machine is well established using standard test and some empirical formula if needed to separate rotor parameters [79]. On the other hand, parameters identification of multi-phase machines is relatively new. Many efforts have been devoted to accurately identify the parameters of multi-phase machines [65], [77], [80]–[83]. The most common is to use the VSD equivalent circuit and performing certain tests in different subspaces. Stator leakage mutual inductance is commonly neglected to simplify this process. Recently, an accurate parameters identification method is introduced in [77] where the effect of the stator leakage mutual inductance and rotor circuit effect for zeros subspace excitation is considered. This method is adopted through this work and the procedures explained in [77] are described in the following subsections.

The stator resistance is determined using dc test and found to be equal to 2.8 Ω. In order to take the effect of ac current the stator resistance value modified as follows.

$$R_s = 2.8 * 1.1 = 3.1\ \Omega \tag{5.17}$$

The six-phase voltage source inverter described earlier is used for supplying the six-phase motor based on the conditions of each test. The frequency is fixed at 60 Hz. The voltage applied in $\alpha - \beta$ subspace in open loop manner while a PI controller is used to regulate the $xy$ currents at zero. This reduces the inherent symmetries in the machine and the converter [79]. For each test, all phases and voltages waveforms are recorded using the oscilloscope. Then using MATLAB, fast Fourier transform extracts the fundamental components of voltages and currents and the corresponding angles. For each test, the calculations of resistances and inductances are made for each phase separately then the average value of all phases is considered.

### 5.3.1 Standard no-load and locked rotor tests

In this test, the six-phase voltage source inverter is used to apply balanced asymmetric six phase voltage to the six-phase machine where only $\alpha - \beta$ subspace is exited. The results of these tests can be expressed as follows referring to the equivalent circuit of VSD method Figure 5-3 and using the standard assumptions.

$$L_{nl} = L'_{ls} + L'_{lm} + L'_m \tag{5.18}$$

$$L_{locked} = L'_{ls} + L'_{lm} + L'_{lr} \tag{5.19}$$

$$R_{locked} = R_s + R'_r \tag{5.20}$$

The inductance and resistance for the standard no-load and locked rotor test can be obtained as follows

$$L = \frac{V_1}{\omega I_1}\sin(\theta) \tag{5.21}$$

$$R = \frac{V_1}{\omega I_1}\cos(\theta) \tag{5.22}$$

where $V_1$ and $I_1$ are the fundamental components for the voltage and current respectively. $\theta$ is the phase shift between the fundamental of the voltage and current for the same phase.

### 5.3.2 X-Y subspace test

This tests aims to identify the stator leakage inductance by exiting only $x - y$ subspace. This can be accomplished by interchanging phases ($b_1 - C_1$ and $a_2 - b_2$) [79]. By changing the phases order, only $x - y$ subspace will be exited (notice the sequence in the third and fourth rows in $T_6$ Equation 5.9). Similarly, Equation 5.21 can be used to calculate the inductance, which is equivalent to stator leakage inductance Equation 5.12.The results obtained from the previous tests are summarized in Table 5-1

**Table 5-1 Parameters obtained from standard and x-y subspace tests**

| Parameter | Value |
|---|---|
| $L_{nl}$ | $136\ mH$ |
| $L_{locked}$ | $19.19\ mH$ |
| $R_{locked}$ | $5.04\ \Omega$ |
| $L_{xy} = L_{ls}$ | $2.05\ mH$ |
| $R_r$ | $1.94\ \Omega$ |

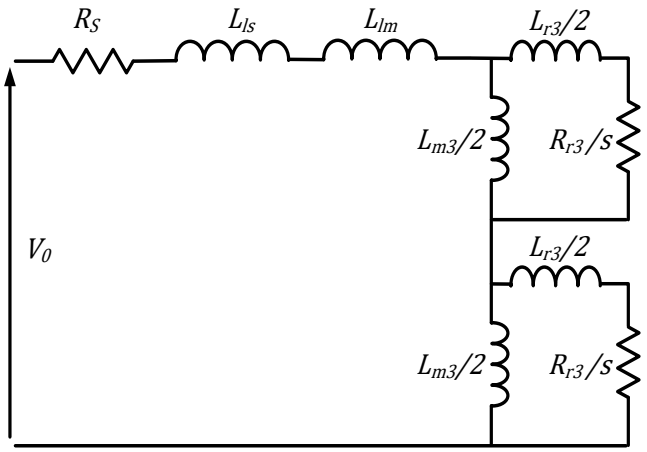


**Figure 5-6 Equivalent circuit of six-phase IM under zero-sequence excitation**

### 5.3.3 Zero sequence test

This test can be performed by connecting one of the three phase set in parallel then connect them to a single-phase AC voltage. Even with zero sequence excitation, the rotor circuit effect cannot be neglected [79]. The third harmonic component of the airgap flux will be of pulsating nature. Therefore, an equivalent circuit similar to the single-phase induction motor is suggested to represent the six-phase machine under zero sequence excitation Figure 5-6.

After some mathematical manipulation, the equivalent zero-sequence resistance and reactance can be represented as follows.

$$R_z = R_s + \frac{R_{r3}(\omega\, K_{m31}\, L_{m1})^2}{R_{r3}^2+\omega^2(L_{lr3}+K_{m31}L_{m1})^2} \tag{5.23}$$

$$X_z = \omega\left(L_{ls} + L_{lr} + \frac{K_{m31}L_{m1}\left(R_{r3}^2+\omega^2 L_{lr3}(L_{lr3}+K_{m31}L_{m1})\right)}{R_{r3}^2+\omega^2(L_{lr3}+K_{m31}L_{m1})^2}\right) \tag{5.24}$$

Where the magnetizing inductance for the third harmonic $L_{m3}$ is expressed in terms of the fundamental magnetizing inductance $L_{m1} = L_m$ as follows.

$$L_{m3} = K_{m31}\, L_{m1} \tag{5.25}$$

The third harmonic rotor resistance and rotor leakage inductance can be calculated as follows.

$$\left.\begin{aligned} R_{r3} &= C_{31}\, R_{r1} \\ L_{lr3} &= C_{31} L_{lr1} \end{aligned}\right\} \tag{5.26}$$

where

$$C_{31} = \left(\frac{K_{skew1}\, K_{w3}}{K_{w1}\, K_{skew3}}\right)^2 \tag{5.27}$$

$K_{skew(i)}$ and $K_{w(i)}$ are the skew and winding factors of harmonic order $i$ respectively. The skew factor can be calculated as follows.

$$K_{skew(i)} = \left(\frac{\sin\left(\frac{i\,\delta}{2}\right)}{\frac{i\,\delta}{2}}\right) \tag{5.28}$$

where $\delta$ is the rotor skew angle which can be considered equal to one stator slot angle. The measured zero-sequence resistance and inductance along with the required coefficients are summarized in Table 5-2. Details calculations of these parameters can be found in the appendix.

The final step in the parameter identification procedure is to separate different inductances namely $L_{lm}$ , $L_m$ and $L_{lr}$.

**Table 5-2 Summary of zero-sequence test**

| Parameter | Value |
|---|---|
| $R_z$ | 3.29 Ω |
| $X_z$ | 8.7 $mH$ |
| $K_{skew1}$ | 0.9886 |
| $K_{skew3}$ | 0.9 |
| $K_{w1}$ | 0.9659 |
| $K_{w3}$ | 0.707 |
| $C_{31}$ | 0.646 |

**Table 5-3 Parameters of six-phase IM**

| Parameters | Value |
|---|---|
| $R_s$ | 3.1 $\Omega$ |
| $R'_r$ | 1.94 $\Omega$ |
| $L_{ls}$ | 2.05 $mH$ |
| $L'_{lm}$ | 10.4 $mH$ |
| $L'_m$ | 123.4 $mH$ |
| $L'_{lr}$ | 6.6 $mH$ |

Equations (5.18), (5.19), (5.23) and (5.24) can be solved instantaneously to get the values of these inductances along with the value of the coefficient $K_{m31}$. Summary of the all the identified parameters of the six-phase machine are listed in Table 5-3

# CHAPTER 6

# PREDICTIVE CURRENT CONTROL OF SIX-PHASE INDUCTION MOTOR

In this chapter, the application of predictive current control (PCC) on asymmetric six-phase IM will be discussed. Based on the equivalent circuits developed in the previous chapter, a discrete model is derived. In addition, the estimation and cost function design are explained in details. Finally, PCC algorithm will be applied to the six-phase induction motor and its performance will be examined using simulation and experimental setup.

## 6.1 Background

Naturally, the first step towards the closed loop control of multiphase machines was to extend the well-established approaches used for three-phase machines like FOC and DTC [84]–[90]. This can be accomplished by utilizing the VSD model for which $\alpha\beta$ subspace results in a model similar to that of the three phase one after using Clark transformation. Although the flux and torque components references can be successfully tracked, the stator current for multiphase machines suffers from high distortion if the classical FOC or DTC methods are typically implemented. This is due to the circulating $xy$ current components. Although these components do not contribute in torque generation, they can increase the copper loss and decrease the efficiency [91]–[95].

Therefore, extra control loops have to be added to regulate the $xy$ current components either to zero or to certain reference values for certain applications [53], [54]. Besides FOC and DTC, other control method like sliding mode, intelligent and nonlinear controllers [96], [97] also implemented successfully for six-phase IM drives.

The success MPC based controller achieved in three-phase machines, motivated the researchers lately to implement it for multiphase machines [31], [60]–[62], [98]–[104].

## 6.2 Proposed PCC

One of the main advantages of FCS-MPC is that no modulation is required. This will facilitate the design of controller especially with the large number of VVs available for multiphase machines which requires sophisticated PWM control techniques [67]. The following subsections will discuss in details the implementation of predictive current control for asymmetric six-phase IM drive system, which have similar steps like those discussed for three phase IM in previous chapters as illustrated in Figure 6-1.

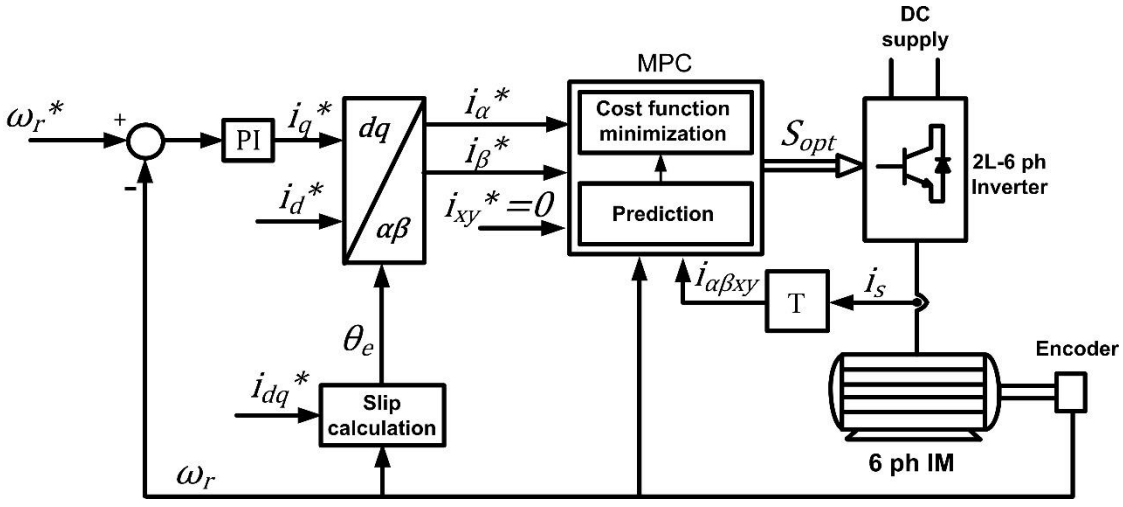


**Figure 6-1 Schematic diagram for PCC of six-phase IM**

### 6.2.1 Prediction step

Based on the developed model using VSD method equation (5-11) and (5-12), the six-phase IM model can be represented as follows:

$$\begin{bmatrix} v_{\alpha s} \\ v_{\beta s} \\ 0 \\ 0 \end{bmatrix} = \begin{bmatrix} R_s & 0 & 0 & 0 \\ 0 & R_s & 0 & 0 \\ 0 & \omega_r L_m & R_r & \omega_r L_r \\ -\omega_r L_m & 0 & -\omega_r L_r & R_r \end{bmatrix} \begin{bmatrix} i_{\alpha s} \\ i_{\beta s} \\ i_{\alpha r} \\ i_{\beta r} \end{bmatrix} + \begin{bmatrix} L_s & 0 & L_m & 0 \\ 0 & L_s & 0 & L_m \\ L_m & 0 & L_s & 0 \\ 0 & L_m & 0 & L_s \end{bmatrix} . p \begin{bmatrix} i_{\alpha s} \\ i_{\beta s} \\ i_{\alpha r} \\ i_{\beta r} \end{bmatrix} \quad (6.1)$$

$$\begin{bmatrix} v_{xs} \\ v_{ys} \end{bmatrix} = \begin{bmatrix} R_s & 0 \\ 0 & R_s \end{bmatrix} \begin{bmatrix} i_{xs} \\ i_{ys} \end{bmatrix} + \begin{bmatrix} L_{ls} & 0 \\ 0 & L_{ls} \end{bmatrix} . p . \begin{bmatrix} i_{xs} \\ i_{ys} \end{bmatrix} \quad (6.2)$$

where $L_s = L_{ls} + L'_{lm} + L'_m$ and $L_r = L_{lr} + L'_m$. Considering stator currents as the state variables and using first Euler method for discretization the prediction can be accomplished as follows [100].

$$X(k+1) = A(k)\, X(k) + BU(k) + C(k) \quad (6.3)$$

where $X = \left[ i_{\alpha s} \;\; i_{\beta s} \;\; i_x \; i_y \right]^T$, $U(k) = \left[ v_{\alpha s} \; v_{\beta s} \;\; v_x \; v_y \right]^T$ which can be synthesized from the switching states and dc link voltage as illustrated in Equation (5-15) and (5-16). Matrices $A$ and $B$ can be calculated as follows.

$$A = I + T_s \begin{bmatrix} -a_1 & a_2\, \omega_r & 0 & 0 \\ -a_2\, \omega_r & -a_1 & 0 & 0 \\ 0 & 0 & -a_3 & 0 \\ 0 & 0 & 0 & -a_3 \end{bmatrix} \quad (6.4)$$

$$B = T_s \begin{bmatrix} b1 & 0 & 0 & 0 \\ 0 & b1 & 0 & 0 \\ 0 & 0 & b1 & 0 \\ 0 & 0 & 0 & b1 \end{bmatrix} \quad (6.5)$$

where $c_1 = L_s\, L'_r - L'^2_m$ , $a_1 = \frac{R_s\, L'_r}{c_1}$ , $a_2 = \frac{L'^2_m}{c_1}$ , $a_3 = \frac{R_s}{L_{ls}}$ , $b_1 = \frac{L'_r}{c_1}$. Matrix $C$ lumps all the unmeasurable quantities (rotor variables). The unmeasurable variables can be

estimated in an open or closed loop manner [58]. For simplicity, matrix $C$ will be estimated based on the past values of the measured variables [31], [100], [103]. All unmeasured quantities are lumped together and estimated at each sample based on the current and past values of measured states and assuming zero initial conditions as follows.

$$C(k) = X(k) - \big(A(k)\, X(k-1) + BU(k-1)\big) \tag{6.6}$$

In order to compensate for the time delay caused by calculation process [38], the variables at sample $k+2$ can be calculated using the variables at instant $k+1$ as follows.

$$X(k+2) = A(k)\, X(k+1) + BU(k+1) + C(k+1) \tag{6.7}$$

$$C(k+1) = X(k+1) - \big(A(k)\, X(k) + BU(k)\big) \tag{6.8}$$

where the same matrix $A(k)$ is used assuming the value of rotor speed will not change for small sample time.

### 6.2.2 Optimization step

The target of the controller is to track the flux and torque producing components $i_\alpha$ and $i_\beta$ and at the same time limit $i_x$ and $i_y$ to the minimum value, ideally zero, in order to reduce stator copper loss. Therefore, the cost function used is as follows.

$$g(V_s^{k+1}) = |i_\alpha^* - i_\alpha(k+2)| + \left|i_\beta^* - i_\beta(k+2)\right| + K_1\, |i_x^* - i_x(k+2)| +$$

$$K_1 \left|i_y^* - i_y(k+2)\right| \tag{6.9}$$

Where $i_\alpha^*$ and $i_\beta^*$ are the reference currents which can be generated as illustrated in Figure 6-1. The reference currents $i_x^*$ and $i_y^*$ are set to zero. $K_1$ is a weighting factor which controls the relative importance of $xy$ plane components compared to $\alpha\beta$ plane components. Based on several simulation trials it is set to 0.2 in this work. Finally, the optimal VV can be selected as follows.

$$V_{sopt} = arg \min_{\{v_0,\ldots,v_n\}} g(V_s^{k+1}) \tag{6.10}$$

Referring to Figure 5-5, there are 48 non-redundant active VV that can be obtained from the inverter. Therefore the prediction and optimization steps have to be repeated 49 times (48 active VVs and one zero VV). In order to reduce the computation cost, the large VVs in $\alpha\beta$ plane will be used. Those VVs when maps to $xy$ plane they becomes small VVs resulting in the smallest $xy$ current components. By this way the prediction and optimization steps need to be repeated 13 times only.

## 6.3 Simulation results

The proposed PCC algorithm is simulated using MATLAB Simulink environment. The motor parameters used are the one obtained from the parameter identification and listed in Table 5-3 while the PI controller and other specifications are shown in Table 6-1. The sample time is set to $40\mu sec$.

Figure 6-2 illustrates the starting response of the motor from standstill to 1000 rpm. Speed, direct axis current, quadrature axis current, the two controlled currents ($i_\alpha$, $i_x$) and phase current are shown in Figure 6-2 from up to bottom respectively. It can noted that the motor has fast dynamic response and the PCC successfully tracks the reference

flux and torque producing currents $i_\alpha, i_\beta$ plane and minimizing the current components in $i_x, i_y$ plane.

**Table 6-1 Simulation parameters**

| Parameters | Value |
|---|---|
| $T_s$ | 40 $\mu sec$ |
| $T_{sim}$ | 2 $\mu sec$ |
| $V_{dc}$ | 220 $V$ |
| $K_p$ | 0.37 |
| $K_i$ | 5.1 |
| $K_1$ | 0.2 |

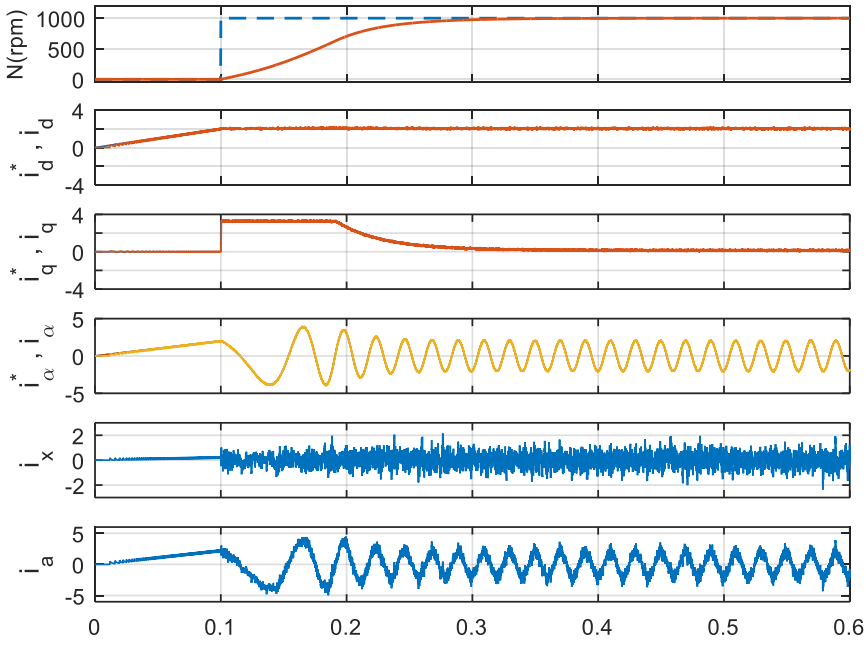


**Figure 6-2 Simulated starting response of six-phase IM using PCC method**

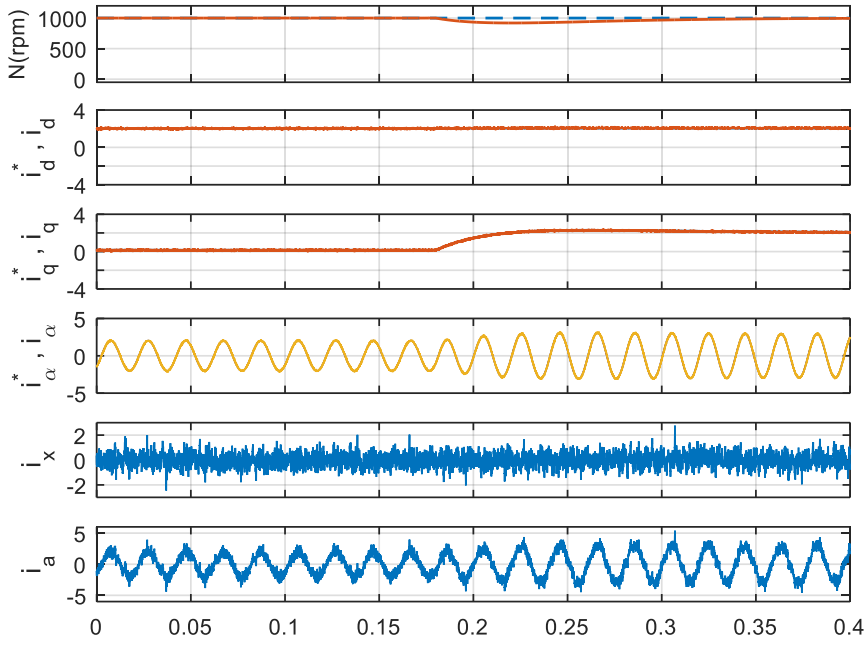


**Figure 6-3 simulated sudden load response of six-phase IM using PCC method**

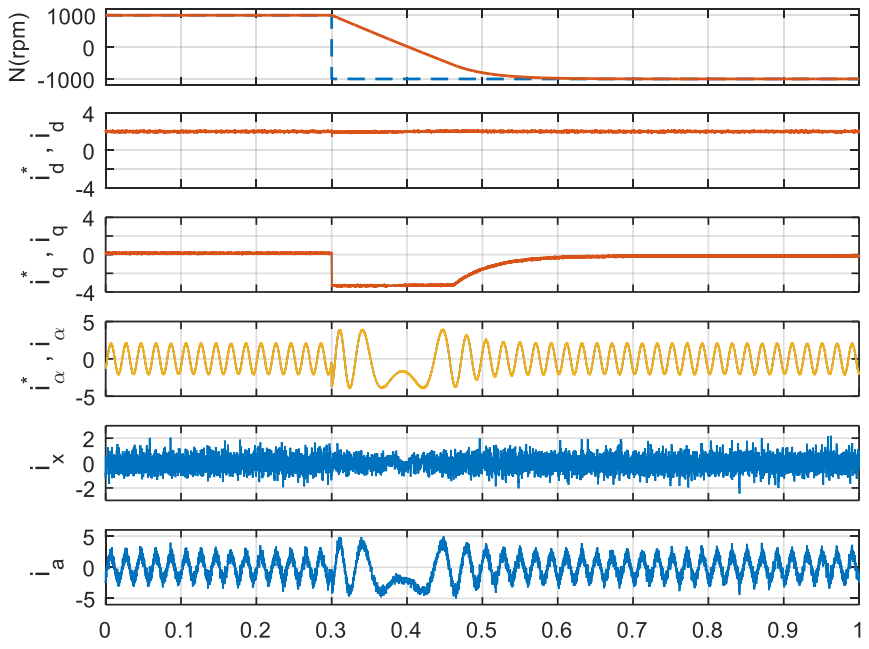


**Figure 6-4 Simulated speed reversal of six-phase IM from 1000 to -1000 rpm at no-load condition**

Figure 6-3 shows the response of the motor under sudden load of 4 Nm. It is evident from the speed response that the controller is robust against external disturbance. Moreover, the direct and quadrature component of the current are totally decoupled assuring fast transient response. Figure 6-4 shows speed reversing test for the motor. Again the PCC show fast dynamic response and decoupled direct and quadrature currents.

## 6.4 Experimental setup

A 1 KW three-phase motor is rewound to form six poles asymmetric six-phase induction motor as shown in Figure 6-5. Table 6-2 lists the ratings of the new motor. A detailed description of the tests used for motor parameter identification discussed in details in chapter 5.

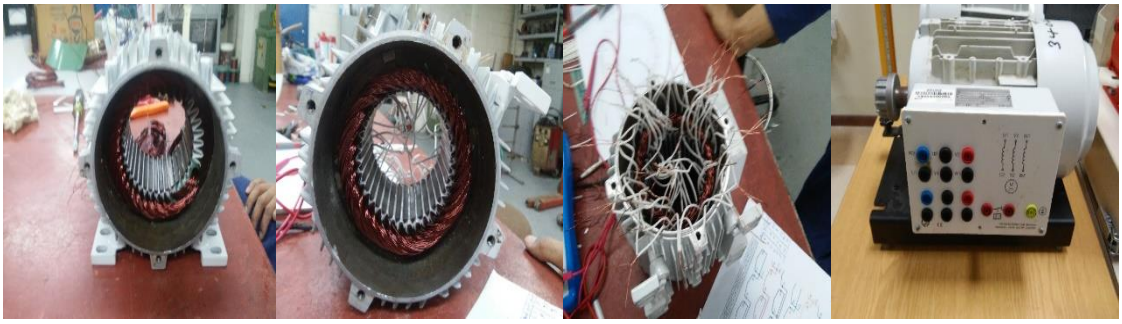

**Figure 6-5 Different stages of winding the six-phase induction motor**

**Table 6-2 Rating of the new wound six-phase induction motor**

| | |
|---|---|
| Rated Power | 1 Kw |
| Rated Current | 2.2 A |
| Rated Phase Voltage | 110 V |
| Frequency | 60 Hz |
| Number of poles | 6 |
| Rated speed | 1140 $rpm$ |

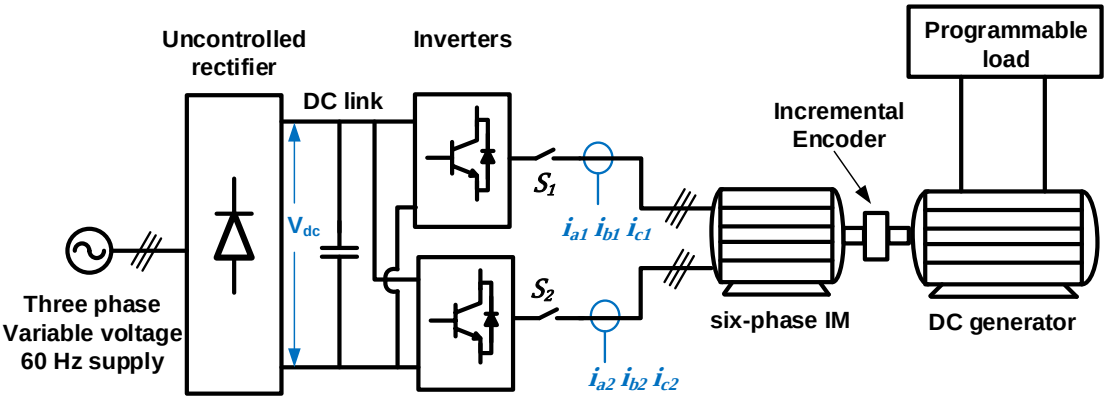


**Figure 6-6 Schematic diagram for six phases IM drive system**

Figure 6-6 demonstrates block diagram of the experimental setup. The two inverters are connected in parallel to the rectifier. Therefore, for six-phase operation both $S_1$ and $S_2$ should be closed. The measured voltage and currents are sent to the controller platform terminal box along with the encoder signal. After conditioning this signal are transmitted to the DSP board where the control algorithm is executed. dSPACE 1103 platform and the same interface circuits utilized with three phase controller implementation are used here.

## 6.5 Experimental results

In order to validate the proposed controller, the same tests illustrated in the simulation section are repeated using the experimental test bench. The same parameters used for the simulation are utilized for the experimental study. The average execution time using only 13 VVs is found to equal 16 $\mu sec$. Therefore, the sampled time is set to 40 $\mu sec$. Figure 6-7 shows measured phase current of the six-phase IM. The upper curves of Figure 6-7 illustrate the first phase currents for each three-phase set $(i_{a1}, i_{a2})$ with a phase shift of $30^o$. The lower curves illustrate two current of the same three-phase set $(i_{a1}, i_{b1})$ with a phase shift of $120^o$.

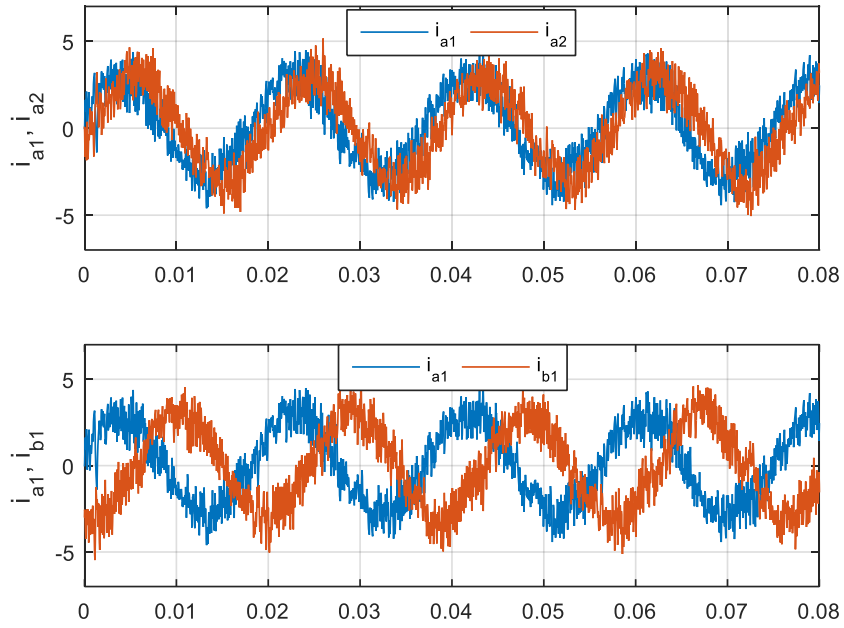


**Figure 6-7 Measured currents of six-phase IM at 1000 rpm and 4 Nm**

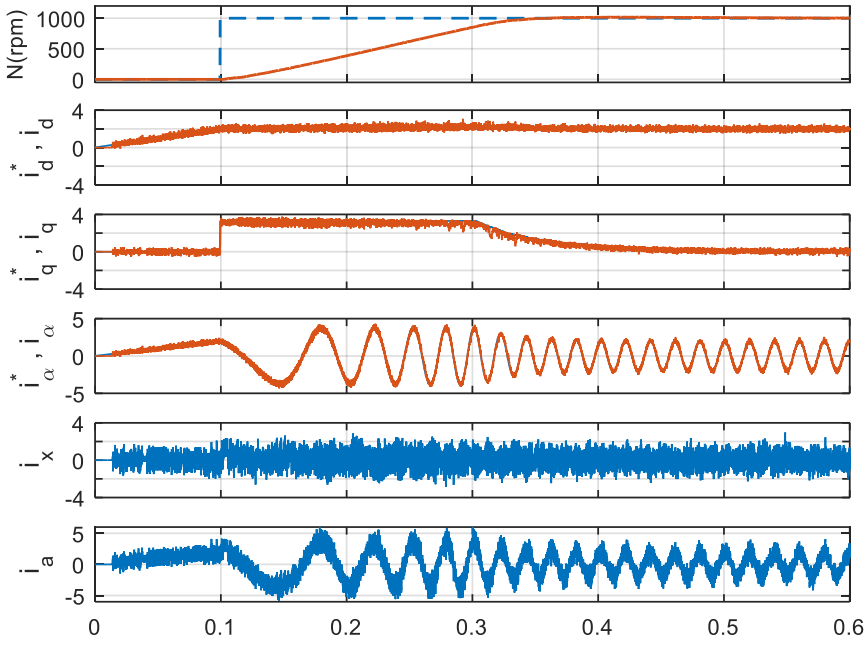


**Figure 6-8 Measured starting response of six-phase IM using PCC method**

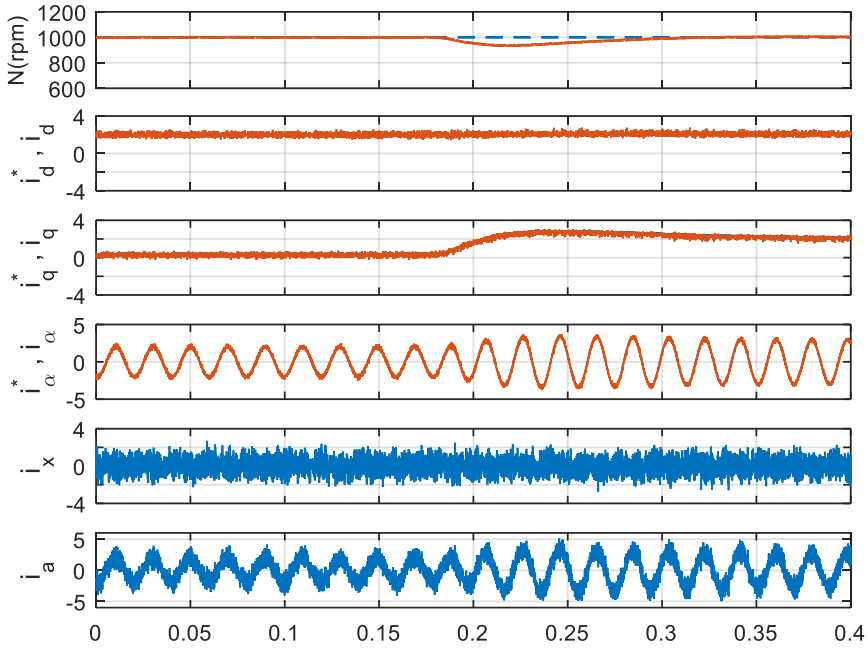


**Figure 6-9 Measured sudden load response of six-phase IM using PCC method**

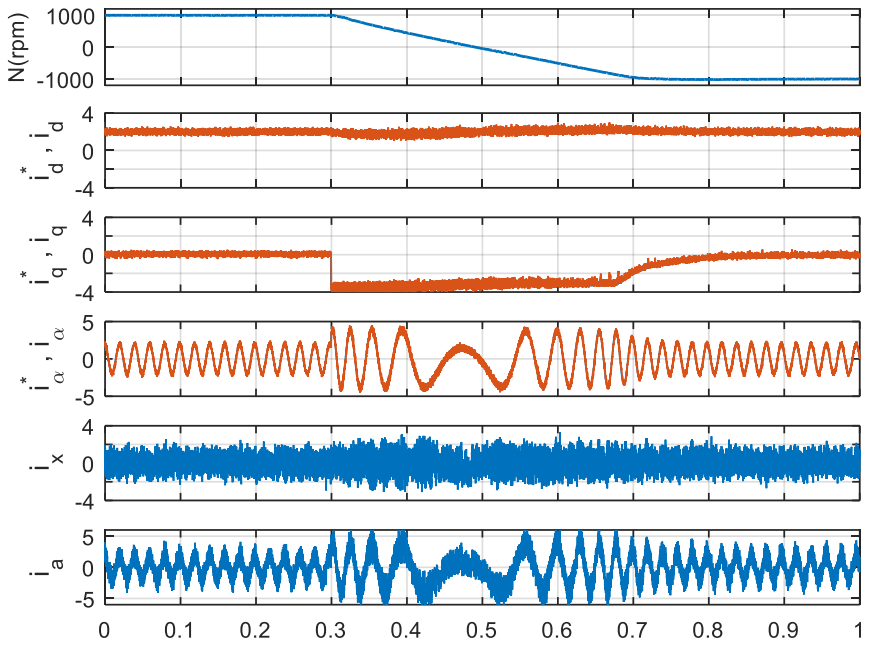


**Figure 6-10 Measured speed reversal of six-phase IM from 1000 to -1000 rpm at no-load condition**

Figure 6-8 to Figure 6-10 show the starting, loading and reversing tests performed on the six-phase IM respectively. These results are close to those of the simulation study Figure 6-2 to Figure 6-4. This demonstrates that the PCC can efficiently drive the six-phase motor under different operating conditions maintaining high decoupling between flux and torque producing current components which results in fast speed dynamic response.

# CHAPTER 7

# CONCLUSION AND FUTURE WORK

## 7.1 Conclusions

The Model predictive based controllers have a high potential in electric drives and power electronics applications. This is evident from the increased number of publications addressing MPC for electric drives for the last few years.

In this thesis, two major challenges for the application of MPC in electric drive are discussed. The first is the problem of simple and accurate design of flux weighting factor for PTC algorithm. The performance of predictive torque control utilizing five different methods reported in literature are compared based on different figures of merits like torque ripple, flux ripple, current THD and average switching frequency. The multi-objective based approaches are found to be superior to the conventional weighting sum design method. Moreover, a modification for multi-objective fuzzy decision based is introduced. This modification solve the high torque ripple characterize the original method reported in literature as illustrated by simulation and experimental results.

The second problem handled in this work is the commonly reported challenge of high computational burden of PTC algorithm. An efficient PTC algorithm characterized by its simplicity and short execution time is proposed. This accomplished by eliminating the flux weighting factor and using only four voltage vectors during the optimization step. The proposed method is validated experimentally at different operating method.

Moreover, its performance is assessed against the conventional and reduced switching frequency algorithms reported in literature. The obtained results proves that the advantages of the algorithm does not comes in cost of the performance.

In addition, the application of MPC in multi-phase machines is investigated. An experimental test bench consisting of asymmetric six-phase induction motor, voltage source inverter and the necessary interface circuits is built. Predictive current control is implemented in real time for driving the six-phase motor using DSP board. Regardless the complicity of system represented in the circulated current components of $(xy)$plane and large number of admissible voltage vectors, the PCC simply succeeds in controlling the speed and currents effectively. Different operating conditions like, starting, sudden loading and speed reversal are tested. The obtained simulation and experimental results shows complete decoupling between the flux and torque producing current components and fast speed dynamic response.

## 7.2 Future work

As mentioned earlier application of MPC based controllers in electric drives is a rich topic with many challenges and open questions, which represent opportunities for future work. Among these challenges:

- Developing predictive speed control of three-phase induction motor. This one of the first motivation of using MPC in electrical drives aiming to get rid of the cascaded structure required for speed control. This can be accomplished by including the speed error as a part of the cost function in the optimization process. Unfortunately, this complicates the PTC algorithm by adding extra

weighting factor for the speed. Moreover, disturbance estimation becomes crucial since there is no external PI controller. In addition, problems regarding speed measurement noise are also reported in literature.

- Using long prediction horizon for MPC algorithm. Most of the reported algorithm reported in literature are based on one-step prediction. It is well known that increasing the prediction horizon will enhance the performance but with extra computation cost. Many mathematical optimization solutions have been reported in literature to solve this issue but it is still an open question.
- Developing of predictive torque control of multiphase machines. Most of the reported MPC algorithm for multi-phase machines are predictive current control (PCC) based. It is well known that the dynamic of the torque and flux is better if PTC is utilized instead of PCC. It is believed that PTC is avoided for multi-phase machines to simplify the design since there will be two weighting factors in the cost function one for the flux and the other for $(xy)$ currents. The design of these cost function is really challenging.
- Investigate the predictive control under faulty condition. The high reliability of multi-phase machines are one of their distinguished features as they can still operate if one phase opens. If this happen the model of the system differs completely based on which phase or phases are opened. This is challenging for MPC since it totally depend on the model of the system for prediction and optimal voltage selection.
- Developing sensorless speed control and nonlinear control of multiphase machines. The multi-phase machine are relatively new. So many of the well-

established theories for three-phase machine can be extended to the multi-phase counterparts with necessary modifications. This open the area for possible contributions.

# References


[1] I. Takahashi and T. Noguchi, “A New Quick-Response and High-Efficiency Control Strategy of an Induction Motor,” *IEEE Trans. Ind. Appl.*, vol. IA-22, no. 5, pp. 820–827, 1986.

[2] J. H. Lee, “Model predictive control: Review of the three decades of development,” *Int. J. Control. Autom. Syst.*, vol. 9, no. 3, pp. 415–424, 2011.

[3] C. E. García, D. M. Prett, and M. Morari, “Model predictive control: Theory and practice—A survey,” *Automatica*, vol. 25, no. 3, pp. 335–348, 1989.

[4] S. Vazquez, J. I. Leon, L. G. Franquelo, J. Rodriguez, H. a. Young, A. Marquez, and P. Zanchetta, “Model predictive control: A review of its applications in power electronics,” *IEEE Ind. Electron. Mag.*, vol. 8, no. 1, pp. 16–31, 2014.

[5] J. Rodriguez, M. P. Kazmierkowski, J. R. Espinoza, P. Zanchetta, H. Abu-Rub, H. A. Young, and C. A. Rojas, “State of the Art of Finite Control Set Model Predictive Control in Power Electronics,” *IEEE Trans. Ind. Informatics*, vol. 9, no. 2, pp. 1003–1016, 2013.

[6] F. Wang, X. Mei, J. Rodriguez, and R. Kennel, “Model Predictive Control for Electrical Drive Systems-An Overview,” *Ces Trans. Electr. Mach. Syst.*, vol. 1, no. 3, pp. 219–230, 2017.

[7] S. Vazquez, J. Rodriguez, M. Rivera, L. G. Franquelo, and M. Norambuena, “Model Predictive Control for Power Converters and Drives: Advances and Trends,” *IEEE Trans. Ind. Electron.*, vol. 64, no. 2, pp. 935–947, 2017.

[8] R. Kennel, S. Member, A. Linder, and L. M, “Generalized Predictive Control ( GPC ) - Ready for Use in Drive Applications ?,” pp. 1839–1844, 1839.

[9] A. Linder and R. Kennel, “Model Predictive Control for Electrical Drives,” *Power Electron. Spec. Conf. 2005. PESC ’05. IEEE 36th*, pp. 1793–1799, 2005.

[10] S. Mariethoz and M. Morari, “Explicit Model-Predictive Control of a PWM Inverter With an <emphasis emphasistype=‘italic’>LCL</emphasis> Filter,” *IEEE Trans. Ind. Electron.*, vol. 56, no. 2, pp. 389–399, 2009.

[11] J. Rodriguez, J. Pontt, C. A. C. A. Silva, P. Correa, P. Lezana, P. Cortes, and U. Ammann, “Predictive Current Control of a Voltage Source Inverter,” *IEEE Trans. Ind. Electron.*, vol. 54, no. 1, pp. 495–503, 2007.

[12] F. Wang, Z. Zhang, A. Davari, J. Rodríguez, and R. Kennel, “An experimental assessment of finite-state Predictive Torque Control for electrical drives by considering different online-optimization methods,” *Control Eng. Pract.*, vol. 31, pp. 1–8, 2014.

[13] M. Preindl and S. Bolognani, “Maximum Torque Per Ampere Operation,” *IEEE Trans. Ind. Informatics*, vol. 9, no. 4, pp. 1912–1921, 2013.

[14] T. Geyer, G. Papafotiou, and M. Morari, “Model Predictive Direct Torque Control — Part I : Concept , Algorithm , and Analysis,” *IEEE Trans. Ind. Electron.*, vol. 56, no. 6, pp. 1894–1905, 2009.

[15] C. A. Rojas, J. Rodriguez, F. Villarroel, J. R. Espinoza, C. A. Silva, and M. Trincado, “Predictive Torque and Flux Control Without Weighting Factors,” *IEEE Trans. Ind. Electron.*, vol. 60, no. 2, pp. 681–690, 2013.

[16] C. A. Rojas, S. Kouro, M. Perez, F. Villarroel, and S. A. Cadetech, “Multiobjective Fuzzy Predictive Torque Control of an Induction Machine fed by a 3L-NPC Inverter,” *IEEE Int. Symp. Predict. Control Electr. Drives Power Electron.*, pp. 21–26, 2015.

[17] Y. Zhang and H. Yang, “Model-Predictive Flux Control of Induction Motor Drives With Switching Instant Optimization,” *IEEE Trans. Energy Convers.*, vol. 30, no. 3, pp. 1113–1122, 2015.

[18] J. C. Ramirez Martinez, R. M. Kennel, and T. Geyer, “Model predictive direct current control,” *Ind. Technol. (ICIT), 2010 IEEE Int. Conf.*, pp. 1808–1813, 2010.

[19] J. M. Retif, L.-S. Xuefang, and F. Morel, “Predictive Current Control for an Induction Motor,” *Power Electron. Spec. Conf. 2008. PESC 2008. IEEE*, pp. 3463–3468, 2008.

[20] D. G. Holmes and D. Martin, “Implementation of a direct digital predictive current controller for single and three phase voltage source inverters,” *IAS ’96. Conf. Rec. 1996 IEEE Ind. Appl. Conf. Thirty-First IAS Annu. Meet.*, vol. 2, pp. 906–913, 1996.

[21] P. Cortés, J. Rodríguez, D. Quevedo, and C. Silva, “Predictive current control strategy with imposed load current spectrum,” *EPE-PEMC 2006 12th Int. Power Electron. Motion Control Conf. Proc.*, vol. 23, no. 2, pp. 252–257, 2007.

[22] S. A. Davari, D. A. Khaburi, and R. Kennel, “An improved FCS-MPC algorithm for an induction motor with an imposed optimized weighting factor,” *IEEE Trans. Power Electron.*, vol. 27, no. 3, pp. 1540–1551, 2012.

[23] Y. Zhang and H. Yang, “Two-Vector-Based Model Predictive Torque Control Without Weighting Factors,” *IEEE Trans. Power Electron.*, vol. 31, no. 2, pp. 1381–1390, 2016.

[24] F. Wang, S. Li, X. Mei, W. Xie, J. Rodriguez, and R. Kennel, “Model Based Predictive Direct Control Strategies for Electrical Drives: An Experimental Evaluation of PTC and PCC Methods,” *IEEE Trans. Ind. Informatics*, vol. 3203, no. c, pp. 1–1, 2015.

[25] J. Rodríguez, R. M. Kennel, J. R. Espinoza, M. Trincado, C. a. Silva, and C. a. Rojas, "High-performance control strategies for electrical drives: An experimental assessment," *IEEE Trans. Ind. Electron.*, vol. 59, no. 2, pp. 812–820, 2012.

[26] P. Cortes, S. Kouro, B. La Rocca, R. Vargas, J. Rodriguez, J. I. Leon, S. Vazquez, and L. G. Franquelo, "Guidelines for weighting factors design in Model Predictive Control of power converters and drives," *IEEE Int. Conf. Ind. Technol.*, pp. 1–7, 2009.

[27] C. A. Rojas and J. Rodriguez, "Multiobjective Fuzzy-Decision-Making Predictive Torque Control for an InductionMotor Drive," *IEEE Trans. Power Electron.*, vol. 32, no. 8, pp. 6245–6260, 2017.

[28] V. P. Muddineni, S. R. Sandepudi, and A. K. Bonala, "Finite control set predictive torque control for induction motor drive with simplified weighting factor selection using TOPSIS method," *IET Electr. Power Appl.*, vol. 11, no. 5, pp. 749–760, 2017.

[29] V. P. Muddineni, A. K. Bonala, and S. R. Sandepudi, "Enhanced weighting factor selection for predictive torque control of induction motor drive based on VIKOR method," *IET Electr. Power Appl.*, vol. 10, no. 9, pp. 877–888, 2016.

[30] S. A. Davari, "Predictive Direct Angle Control of Induction Motor," *IEEE Trans. Ind. Electron.*, vol. 63, no. 8, pp. 5276–5284, 2016.

[31] F. Barrero, M. R. Arahal, R. Gregor, S. Toral, and M. J. Durán, "A proof of concept study of predictive current control for VSI-driven asymmetrical dual three-phase AC machines," *IEEE Trans. Ind. Electron.*, vol. 56, no. 6, pp. 1937–1954, 2009.

[32] E. Levi, "Multiphase electric machines for variable-speed applications," *IEEE Trans. Ind. Electron.*, vol. 55, no. 5, pp. 1893–1909, 2008.

[33] J. Holtz, "The dynamic representation of AC drive systems by complex signal flow graphs," *Proc. 1994 IEEE Int. Symp. Ind. Electron.*, pp. 1–6, 1994.

[34] C. A. Rojas and J. Rodriguez, "Multiobjective Fuzzy Predictive Torque Control of an Induction Motor Drive," in *International Power Electronics Drive Systems and Technologies Conference (PEDSTC2015)*, 2015, no. February, pp. 3–4.

[35] C. A. Rojas, J. I. Yuz, M. Aguirre, and J. Rodriguez, "A comparison of discrete-time models for model predictive control of induction motor drives," in *2015 IEEE International Conference on Industrial Technology (ICIT)*, 2015, pp. 568–573.

[36] G. C. Verghese and S. R. Sanders, "Observers for flux estimation in induction machines," *IEEE Trans. Ind. Electron.*, vol. 35, no. 1, pp. 85–94, 1988.

[37] Z. Yongchang and Z. Zhengming, "Speed sensorless control for three-level

inverter-fed induction motors using an Extended Luenberger Observer," *2008 IEEE Veh. Power Propuls. Conf. VPPC 2008*, pp. 1–5, 2008.

[38] P. Cortes, J. Rodriguez, C. Silva, and A. Flores, "Delay Compensation in Model Predictive Current Control of a Three-Phase Inverter," *IEEE Trans. Ind. Electron.*, vol. 59, no. 2, pp. 1323–1325, 2012.

[39] T. J. Vyncke, S. Thielemans, T. Dierickx, R. Dewitte, M. Jacxsens, and J. a. Melkebeek, "Design choices for the prediction and optimization stage of finite-set model based predictive control," *Preced. 2011 - Work. Predict. Control Electr. Drives Power Electron.*, pp. 47–54, 2011.

[40] F. Villarroel, J. R. Espinoza, C. A. Rojas, J. Rodriguez, M. Rivera, and D. Sbarbaro, "Multiobjective Switching State Selector for Finite-States Model Predictive Control Based on Fuzzy Decision Making in a Matrix Converter," *IEEE Trans. Ind. Electron.*, vol. 60, no. 2, pp. 589–599, 2013.

[41] P. Zanchetta, "Heuristic Multi-Objective Optimization for Cost Function Weights Selection in Finite States Model Predictive Control," *2011 IEEE Work. Predict. Control Electr. Drives Power Electron.*, pp. 70–75, 2011.

[42] Y. Zhang and H. Yang, "Generalized Two-Vector-Based Model-Predictive," *IEEE Trans. Power Electron.*, vol. 30, no. 7, pp. 3818–3829, 2015.

[43] Y. Zhang, J. Zhu, Z. Zhao, W. Xu, and D. G. Dorrell, "An Improved Direct Torque Control for Three-Level Sensorless drive," *IEEE Trans. Power Electron.*, vol. 27, no. 3, pp. 1502–1513, 2012.

[44] T. Geyer, "Computationally efficient model predictive direct torque control," *IEEE Trans. Power Electron.*, vol. 26, no. 10, pp. 2804–2816, 2011.

[45] T. Geyer and D. E. Quevedo, "Multistep finite control set model predictive control for power electronics," *IEEE Trans. Power Electron.*, vol. 29, no. 12, pp. 6836–6846, 2014.

[46] F. Wang, Z. Zhang, A. Davari, J. Rodríguez, and R. Kennel, "An experimental assessment of finite-state Predictive Torque Control for electrical drives by considering different online-optimization methods," *Control Eng. Pract.*, vol. 31, pp. 1–8, 2014.

[47] M. Habibullah, D. D.-C. Lu, D. Xiao, and M. F. Rahman, "A Simplified Finite-State Predictive Direct Torque Control for Induction Motor Drive," *IEEE Trans. Ind. Electron.*, vol. 63, no. 6, pp. 3964–3975, 2016.

[48] C. Xia, S. Member, T. Liu, T. Shi, and Z. Song, "A Simplified Finite-Control-Set Model-Predictive Control for Power Converters," *IEEE Trans. Ind. Informatics*, vol. 10, no. 2, pp. 991–1002, 2014.

[49] Y. Zhang and H. Yang, "Model Predictive Control of Induction Motor Drives : Flux Control versus Torque Control," vol. 0, no. 2, pp. 86–91, 2015.

[50] T. Geyer, “A comparison of control and modulation schemes for medium-voltage drives: Emerging predictive control concepts versus PWM-based schemes,” *IEEE Trans. Ind. Appl.*, vol. 47, no. 3, pp. 1380–1389, 2011.

[51] E. Levi, R. Bojoi, F. Profumo, H. A. Toliyat, and S. Williamson, “Multiphase induction motor drives – a technology status review,” *IET Electr. Power Appl.*, vol. 1, no. 4, p. 489, 2007.

[52] G. K. Singh, “Multi-phase induction machine drive research — a survey,” vol. 61, pp. 139–147, 2002.

[53] E. Levi, “Advances in converter control and innovative exploitation of additional degrees of freedom for multiphase machines,” *IEEE Trans. Ind. Electron.*, vol. 63, no. 1, pp. 433–448, 2016.

[54] I. Zoric, M. Jones, and E. Levi, “Arbitrary Power Sharing Among Three-Phase Winding Sets of Multiphase Machines,” *IEEE Trans. Ind. Electron.*, vol. 65, no. 2, pp. 1128–1139, 2017.

[55] F. Barrero and M. J. Duran, “Recent Advances in the Design, Modeling, and Control of Multiphase Machines - Part II,” *IEEE Trans. Ind. Electron.*, vol. 63, no. 1, pp. 459–468, 2016.

[56] F. Barrero and M. J. Duran, “Recent advances in the design, modeling, and control of multiphase machines - Part I,” *IEEE Trans. Ind. Electron.*, vol. 63, no. 1, pp. 449–458, 2016.

[57] E. Levi, F. Barrero, and M. Duran, “Multiphase Machines and Drives - Revisited,” *IEEE Trans. Ind. Electron.*, vol. 63, no. 1, pp. 1–1, 2015.

[58] C. Martin, M. R. Arahal, F. Barrero, and M. J. Duran, “Five-Phase Induction Motor Rotor Current Observer for Finite Control Set Model Predictive Control of Stator Current,” *IEEE Trans. Ind. Electron.*, vol. 63, no. 7, pp. 4527–4538, 2016.

[59] R. S. Arashloo, M. Salehifar, J. L. R. Martinez, and V. Sala, “Fault-tolerant model predictive control of five-phase permanent magnet motors,” *IECON 2013 - 39th Annu. Conf. IEEE Ind. Electron. Soc.*, no. 1, pp. 2857–2862, 2013.

[60] M. J. Duran, J. A. Riveros, F. Barrero, H. Guzman, and J. Prieto, “Reduction of Common-Mode Voltage in Five-Phase Induction Motor Drives Using Predictive Control Techniques,” *Ind. Appl. IEEE Trans.*, vol. 48, no. 6, pp. 2059–2067, 2012.

[61] M. Jones, M. Duran, E. Levi, S. Toral, J. Riveros, and F. Barrero, “Variable-Speed Five-Phase Induction Motor Drive Based on Predictive Torque Control,” *IEEE Trans. Ind. Electron.*, vol. 60, no. 8, pp. 1–1, 2012.

[62] H. Guzman, M. J. Duran, F. Barrero, B. Bogado, and S. Toral, “Speed Control of Five-Phase Induction Motors With Integrated Open-Phase Fault Operation Using

Model-Based Predictive Current Control Techniques," *IEEE Trans. Ind. Electron.*, vol. 61, no. 9, pp. 4474–4484, 2014.

[63] R. Bojoi, F. Farina, F. Profumo, and A. Tenconi, "Dual-Three Phase Induction Machine Drives Control-A Survey," *IEEJ Trans. Ind. Appl.*, vol. 126, no. 4, pp. 420–429, 2006.

[64] K. S. Khan, "Comparative analysis of multiphase machines," *Master Sci.*, 2008.

[65] A. G. Yepes, J. a Riveros, J. Doval-Gandoy, F. Barrero, Ó. Lopez, B. Bogado, M. Jones, and E. Levi, "Parameter Identification of Multiphase Induction Machines With Distributed Windings—Part 1: Sinusoidal Excitation Methods," *IEEE Trans. Energy Convers.*, vol. 27, no. 4, pp. 1056–1066, Dec. 2012.

[66] A. S. Abdel-Khalik, A. M. Massoud, and S. Ahmed, "A Senior Project-Based Multiphase Motor Drive System Development," *IEEE Trans. Educ.*, vol. 59, no. 4, pp. 307–318, 2016.

[67] D. Glose, R. Kennel, and S. Member, "Carrier-Based Pulse Width Modulation for Symmetrical Six-Phase Drives," vol. 30, no. 12, pp. 6873–6882, 2015.

[68] J. Figueroa, J. Cros, and P. Viarouge, "Generalized transformations for polyphase phase-modulation motors," *IEEE Trans. Energy Convers.*, vol. 21, no. 2, pp. 332–341, 2006.

[69] M. Zabaleta, E. Levi, and M. Jones, "Modelling Approaches for an Asymmetrical Six-Phase Machine," *Isie*, 2016.

[70] A. R. Munoz and T. A. Lipo, "Dual stator winding induction machine drive," vol. 36, no. 5, pp. 1369–1379, 2000.

[71] D. Hadiouche, H. Razik, and A. Rezzoug, "On the modeling and design of dual-stator windings to minimize circulating harmonic currents for VSI fed AC machines," *IEEE Trans. Ind. Appl.*, vol. 40, no. 2, pp. 506–515, 2004.

[72] G. Renukadevi and K. Rajambal, "Generalized d-q Model of n-Phase Induction Motor," vol. 6, no. 9, pp. 1066–1075, 2012.

[73] R. H. Nelson and P. C. Krause, "Induction machine analysis for arbitrary displacement between multiple winding sets," *IEEE Trans. Power Appar. Syst.*, vol. PAS-93, no. 3, pp. 841–848, 1974.

[74] T. A. Lipo, "A d-q model for six phase induction machines," *Int. Conf. on Electrical Machines (ICEM)*. pp. 860–867, 1980.

[75] Z. Yifan and T. a. Lipo, "Space Vector PWM Control of Dual Three-phase Induction Machine Using Vector Space Decomposition," *IEEE Trans. Ind. Appl.*, vol. 31, no. 5, pp. 1100–1109, 1995.

[76] E. A. Klingshirn, "High phase order induction motors - part I - description and

theoretical considerations," *IEEE Trans. Power Appar. Syst.*, vol. PAS-102, no. 1, pp. 47–53, 1983.

[77] H. S. Che, A. S. Abdel-khalik, S. Member, and E. Levi, "Parameter Estimation of Asymmetrical Six - phase Induction Machines using Modified Standard Tests," vol. 64, no. 8, pp. 6075–6085, 2017.

[78] H. S. Che, E. Levi, M. Jones, W. Hew, N. A. Rahim, and S. Member, "Current Control Methods for an Asymmetrical Six-Phase Induction Motor Drive," *IEEE Trans. Power Electron.*, vol. 29, no. 1, pp. 407–417, 2014.

[79] IEEE Machinery Committee, *IEEE Standard Test Procedure for Polyphase Induction Motors and*, vol. 2004, no. November. 2004.

[80] J. A. Riveros, A. G. Yepes, F. Barrero, J. Doval-Gandoy, B. Bogado, O. Lopez, M. Jones, and E. Levi, "Parameter identification of multiphase induction machines with distributed windingspart 2: Time-domain techniques," *IEEE Trans. Energy Convers.*, vol. 27, no. 4, pp. 1067–1077, 2012.

[81] A. S. Abdel-Khalik, M. I. Daoud, S. Ahmed, A. A. Elserougi, and A. M. Massoud, "Parameter identification of five-phase induction machines with single layer windings," *IEEE Trans. Ind. Electron.*, vol. 61, no. 10, pp. 5139–5154, 2014.

[82] H. S. Che, A. S. Abdel-khalik, S. Member, and E. Levi, "Parameter Estimation of Asymmetrical Six - phase Induction Machines using Modified Standard Tests," *Ieee Trans. Ind. Electron.*, vol. 64, no. 8, pp. 6075–6085, 2017.

[83] H. S. Che, A. S. Abdel-Khalik, O. Dordevic, and E. Levi, "Parameter Estimation of Asymmetrical Six-Phase Induction Machines Using Modified Standard Tests," *IEEE Trans. Ind. Electron.*, vol. 64, no. 8, pp. 6075–6085, 2017.

[84] M. B. R. Correa, C. B. Jacobina, C. R. da Silva, A. M. N. Lima, and E. R. C. da Silva, "Vector and scalar modulation for six-phase voltage source inverters," *IEEE 34th Annu. Conf. Power Electron. Spec. 2003. PESC '03.*, vol. 2, pp. 562–567, 2003.

[85] X. Kestelyn, E. Semail, and J. P. Hautier, "Multi-phase system supplied by SVM VSI: A new fast algorithm to compute duty cycles," *EPE J. (European Power Electron. Drives Journal)*, vol. 14, no. 3, pp. 25–31, 2004.

[86] G. K. Singh, D. K. P. Singh, K. Nam, and S. K. Lim, "A simple indirect field-oriented control scheme for multiconverter-fed induction motor," *IEEE Trans. Ind. Electron.*, vol. 52, no. 6, pp. 1653–1659, 2005.

[87] R. Bojoi, F. Farina, G. Griva, F. Profumo, and A. Tenconi, "Direct Torque Control for Dual Three-Phase Induction Motor Drives," *IEEE Trans. Ind. Appl.*, vol. 41, no. 6, pp. 1627–1636, 2005.

[88] P. Sanjeevikumar, G. Grandi, J. O. Ojo, and F. Blaabjerg, "Direct vector

controlled six-phase asymmetrical induction motor with power balanced space vector PWM multilevel operation," *Int. J. Power Energy Convers.*, vol. 7, no. 1, pp. 57–63, 2016.

[89] J. K. Pandit, M. V. Aware, R. Nemade, and E. Levi, "Direct Torque Control Scheme for a Six-Phase Induction Motor with Reduced Torque Ripple," *IEEE Trans. Power Electron.*, vol. 32, no. 9, pp. 1–1, 2016.

[90] R. Bojoi, M. Lazzari, F. Profumo, and A. Tenconi, "Digital field oriented control for dual three-phase induction motor drives," *Ind. Appl. Conf. 2002. 37th {IAS} Annu. Meet. Conf. Rec.*, vol. 2, no. 3, pp. 818--825 vol.2, 2002.

[91] C. S. Lim, E. Levi, M. Jones, N. A. Rahim, and W. P. Hew, "A comparative study of synchronous current control schemes based on FCS-MPC and PI-PWM for a two-motor three-phase drive," *IEEE Trans. Ind. Electron.*, vol. 61, no. 8, pp. 3867–3878, 2014.

[92] M. Jones, S. N. Vukosavic, D. Dujic, and E. Levi, "A synchronous current control scheme for multiphase induction motor drives," *IEEE Trans. Energy Convers.*, vol. 24, no. 4, pp. 860–868, 2009.

[93] R. Bojoi, F. Profumo, and a. Tenconi, "Digital synchronous frame current regulation for dual three-phase induction motor drives," *IEEE 34th Annu. Conf. Power Electron. Spec. 2003. PESC '03.*, vol. 3, pp. 1475–1480, 2003.

[94] R. Bojoi, A. Tenconi, F. Profumo, G. Griva, and D. Martinello, "Complete analysis and comparative study of digital modulation techniques for dual three-phase {AC} motor drives," *Power Electron. Spec. Conf. 2002. pesc 02. 2002 {IEEE} 33rd Annu.*, vol. 2, pp. 851--857 vol.2, 2002.

[95] R. Bojoi, F. Farina, M. Lazzari, F. Profumo, and A. Tenconi, "Analysis of the asymmetrical operation of dual three-phase induction machines," *IEMDC 2003 - IEEE Int. Electr. Mach. Drives Conf.*, vol. 1, pp. 429–435, 2003.

[96] S. M. J. Rastegar Fatemi, N. R. Abjadi, J. Soltani, and S. Abazari, "Speed sensorless control of a six-phase induction motor drive using backstepping control," *IET Power Electron.*, vol. 7, no. 1, pp. 114–123, 2014.

[97] M. A. Fnaiech, F. Betin, G. A. Capolino, and F. Fnaiech, "Fuzzy logic and sliding-mode controls applied to six-phase induction machine with open phases," *IEEE Trans. Ind. Electron.*, vol. 57, no. 1, pp. 354–364, 2010.

[98] R. Gregor, F. Barrero, S. L. Toral, M. J. Durán, M. R. Arahal, J. Prieto, and J. L. Mora, "Predictive-space vector PWM current control method for asymmetrical dual three-phase induction motor drives," *IET Electr. Power Appl.*, vol. 4, no. 1, p. 26, 2010.

[99] R. Gregor, F. Barrero, S. Toral, M. R. Arahal, J. Prieto, and M. J. Durán, "Enhanced Predictive Current Control Method for the Asymmetrical Dual – three

Phase Induction Machine," *IEEE Trans. Ind. Electron.*, vol. 56, no. 6, pp. 312–319, 2009.

[100] F. Barrero, J. Prieto, E. Levi, R. Gregor, S. Toral, M. J. Durán, and M. Jones, "An enhanced predictive current control method for asymmetrical six-phase motor drives," *IEEE Trans. Ind. Electron.*, vol. 58, no. 8, pp. 3242–3252, 2011.

[101] M. J. Duran, J. Prieto, F. Barrero, and S. Toral, "Predictive Current Control of Dual Three-phase Drives using Restrained Search Techniques," *Ind. Electron. IEEE Trans.*, vol. 58, no. 99, pp. 3253–3263, 2010.

[102] O. Gonzalez, M. Ayala, J. Rodas, R. Gregor, and M. Rivera, "Predictive Current Control with Kalman Filter Observer for a Five-Phase Induction Machine operating a Fixed Switching Frequency," no. 1, pp. 1–6.

[103] I. Gonzalez-Prieto, M. J. Duran, J. J. Aciego, C. Martin, and F. Barrero, "Model Predictive Control of Six-phase Induction Motor Drives Using Virtual Voltage Vectors," *IEEE Trans. Ind. Electron.*, vol. 65, no. 1, pp. 27–37, 2017.

[104] F. Barrero, J. Prieto, E. Levi, R. Gregor, S. Toral, M. J. Durán, and M. Jones, "An enhanced predictive current control method for asymmetrical six-phase motor drives," *IEEE Trans. Ind. Electron.*, vol. 58, no. 8, pp. 3242–3252, 2011.

# Appendix

### Winding design for asymmetric six-phase induction motor

A three phase, 220V, 1 KW, 36 slot, 4 poles is used for winding a six- phase one.

Slot angle can be calculated as: $\alpha = \frac{360}{S} * \frac{P}{2}$

$$\alpha = \frac{360}{36} * 2 = 20^o$$

Number of poles have to change to 6 then:

$$\alpha = \frac{360}{36} * 3 = 30^o$$

$30^o$ → 1 slots

$120^o$ → 4 slots

$180^o$ → 6 slots (pole pitch)

$$q = \frac{36}{6*6} = 1 \quad \text{(Slots per pole per phase)}$$

Chording of one slot is implemented during the rewinding. Thus the coil pitch is $\frac{5}{6}$ of the pole pitch and equal to 5 slots.

Pitch angle $\beta = \frac{\pi}{6}$

Rotor skew angle $\delta = \alpha$

The pitch, distribution and winding factor for harmonic of order $i$ can be calculated as follows:

$$K_{pi} = \cos\left(\frac{i\beta}{2}\right)$$

$$K_{di} = \frac{\sin\left(\frac{iq\alpha}{2}\right)}{q\sin\left(\frac{i\alpha}{2}\right)}$$

$$K_{wi} = K_{pi} * K_{di}$$

$$K_{p1} = 0.9659 \qquad K_{d1} = 1 \qquad K_{w1} = 0.9659$$

$$K_{p3} = 0.707 \qquad K_{d3} = 1 \qquad K_{w3} = 0.707$$

The skew factor for harmonic of order $i$ can be calculated as follows:

$$K_{skew(i)} = \frac{\sin\left(\frac{i\delta}{2}\right)}{\frac{i\delta}{2}}$$

$$K_{skew(1)} = 0.9886 \qquad K_{skew(3)} = 0.9$$

$$C_{31} = \left(\frac{K_{skew(1)} * K_{w3}}{K_{skew(3)} * K_{w1}}\right)^2 = 0.646$$

.

The same current rating (same conductor cross section) of the three phase machine will be maintained. For the same power rating the voltage rating, have to be half of that of

the three-phase machine. Therefore, the phase voltage rating of the six-phase induction motor is $220\ V$.

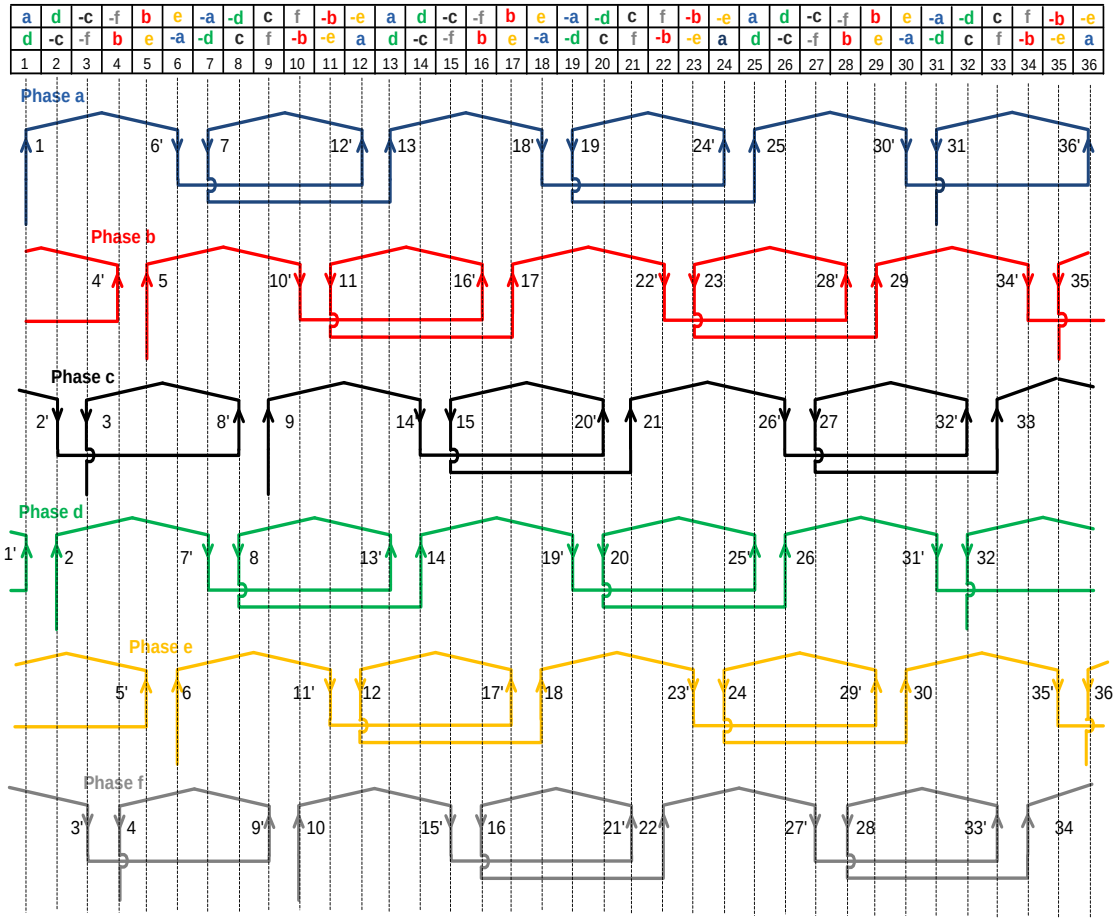


**Schematic of coils connections for different phases of the developed asymmetric six-phase induction motor**

# Vitae


| | |
|---|---|
| Name | : Mohamed Mamdouh Mohamed Saad El Shormbably |
| Nationality | : Egyptian |
| Date of Birth | : 4/12/1985 |
| Email | : m_mamdouh_5@hotmail.com |
| Address | : Tanta, Egypt |
| Academic Background | : **M.Sc. (Mechatronic and Robotic)** |
| | September 2012 |
| | Egypt Japan University of Science and Technology |
| | Alexandria, Egypt |
| | **B.Sc. (Electrical Power and Machines)** |
| | July 2007 |
| | Faculty of Engineering Tanta University |
| | Tanta, Egypt |